



DEVELOPMENT OF SURFACTANT ADDED POLYVINYL ALCOHOL AND TITANIUM  
DIOXIDE COMPOSITE FILMS



By

MISS Sirinan RATCHAWONG

A Thesis Submitted in Partial Fulfillment of the Requirements  
for Master of Engineering (CHEMICAL ENGINEERING)

Department of CHEMICAL ENGINEERING

Graduate School, Silpakorn University

Academic Year 2019

Copyright of Graduate School, Silpakorn University

การพัฒนาแผ่นฟิล์มพอลิไวนิลแอลกอฮอล์และไทเทเนียมไดออกไซด์คอมโพสิตด้วย  
การเติมสารลดแรงตึงผิว



วิทยานิพนธ์นี้เป็นส่วนหนึ่งของการศึกษาตามหลักสูตรวิศวกรรมศาสตรมหาบัณฑิต  
สาขาวิชาวิศวกรรมเคมี แผน ก แบบ ก 2 ระดับปริญญามหาบัณฑิต  
ภาควิชาวิศวกรรมเคมี  
บัณฑิตวิทยาลัย มหาวิทยาลัยศิลปากร  
ปีการศึกษา 2562  
ลิขสิทธิ์ของบัณฑิตวิทยาลัย มหาวิทยาลัยศิลปากร

DEVELOPMENT OF SURFACTANT ADDED POLYVINYL ALCOHOL AND  
TITANIUM DIOXIDE COMPOSITE FILMS



A Thesis Submitted in Partial Fulfillment of the Requirements  
for Master of Engineering (CHEMICAL ENGINEERING)

Department of CHEMICAL ENGINEERING

Graduate School, Silpakorn University

Academic Year 2019

Copyright of Graduate School, Silpakorn University

Title                      Development of surfactant added polyvinyl alcohol and titanium  
                                 dioxide composite films

By                            Sirinan RATCHAWONG

Field of Study            (CHEMICAL ENGINEERING)

Advisor                    Sirirat Wacharawichanant

---

Graduate School Silpakorn University in Partial Fulfillment of the Requirements for the Master  
of Engineering

.....Dean of graduate school  
(Associate Professor Jurairat Nunthanid, Ph.D.)

Approved by

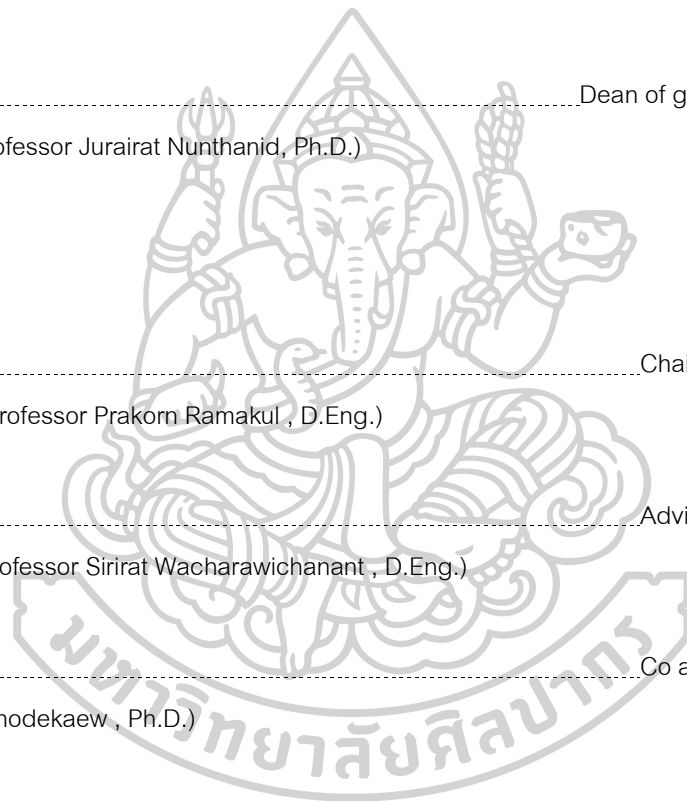
.....Chair person  
(Associate Professor Prakorn Ramakul , D.Eng.)

.....Advisor  
(Assistant Professor Sirirat Wacharawichanant , D.Eng.)

.....Co advisor  
( Siriporn Tanodekaew , Ph.D.)

.....Committee  
(Assistant Professor Okorn Mekasuwandumrong , D.Eng.)

.....External Examiner  
(Associate Professor Anongnat Somwangthanaroj , Ph.D.)



59404201 : Major (CHEMICAL ENGINEERING)

Keyword : polyvinyl alcohol and titanium dioxide composite films, surfactant, thermal treatment, photocatalytic activity, antimicrobial

MISS SIRINAN RATCHAWONG : DEVELOPMENT OF SURFACTANT ADDED POLYVINYL ALCOHOL AND TITANIUM DIOXIDE COMPOSITE FILMS THESIS ADVISOR : ASSISTANT PROFESSOR SIRIRAT WACHARAWICHANANT, D.Eng.

This work aims to study the effect of surfactant, thermal treatment and titanium dioxide ( $\text{TiO}_2$ ) particle sizes on properties of polyvinyl alcohol (PVA) and  $\text{TiO}_2$  composite films. The films were prepared via solution casting with the addition of surfactant, sodium dodecylbenzene sulfonate (SDBS) or sodium dodecyl sulfate (SDS), for improving dispersion of  $\text{TiO}_2$  in PVA matrix, and further thermally treated at  $180^\circ\text{C}$  for 2 h. The ability of films in photocatalytic removal of organic substance and antimicrobial activity were studied. The dispersion of  $\text{TiO}_2$  particles observed by scanning electron microscopy (SEM) showed the improved dispersion of  $\text{TiO}_2$  both micro and nanoparticles in the PVA matrix with the addition of surfactant. Fourier-transform infrared spectroscopy (FTIR) was used to study functional groups of the molecule on the film surface, indicated interaction between PVA chains and  $\text{TiO}_2$  both micro and nanoparticles. The crystallinity of PVA studied by X-ray diffraction (XRD) increased with thermal treatment, whereas XRD pattern of  $\text{TiO}_2$  remained at the main peak of  $2\theta=25.3^\circ$ . The mechanical properties of PVA/ $\text{TiO}_2$  composite films with  $\text{TiO}_2$  microparticles improved with the addition of SDBS and PVA/ $\text{TiO}_2$  composite films with  $\text{TiO}_2$  nanoparticles improved with thermal treatment. The thermal decomposition of PVA/ $\text{TiO}_2$  composites films with surfactant addition was slightly delayed after thermal treatment. The thermal treatment increased PVA crystalline in the films and also changed film color to brownish resulting in increasing absorption in the visible wavelength region. The  $\text{TiO}_2$  absorption in ultraviolet (UV) wavelength region increased according to  $\text{TiO}_2$  content as measured by ultraviolet-visible spectroscopy (UV-Vis). The photocatalysis application of PVA/ $\text{TiO}_2$  composite films were examined from removal efficiency of methylene blue (MB) under UV light. The results showed the greater MB removal efficiency of the PVA/ $\text{TiO}_2$  composite films with SDBS addition. Moreover, the thermal treatment improved MB removal efficiency of PVA/ $\text{TiO}_2$  composite films by adsorption and absorption mechanisms. The antimicrobial activity showed the same trend as photocatalytic activity as these improved with SDBS addition.

## ACKNOWLEDGEMENTS

The author wished to express her gratitude and appreciation to their advisor, Assistant Professor Dr. Sirirat Wacharawichanant and Dr. Siriporn Tanodekaew for their support, stimulating, useful discussions throughout this research and devotion to revise this thesis otherwise it cannot be completed in short time.

In addition, the author would like to gratefully acknowledge Associate Professor Dr. Prakorn Ramakul, as the chairman of the committee, Assistant Professor Dr. Okorn Mekasuwandumrong, and Associate Professor Dr. Anongnate Somwangthanaroj as the members of thesis committee for their kind evaluation of work and valuable suggestions that could be beneficially used to improve working behavior.

In particular, special thanks for the kind suggestions and useful help to members of Polymer Innovation Laboratory and members of the research zone for their assistance.

The author would like to thanks the center of excellence on Catalysis and Catalytic reaction Engineering, Department of Chemical Engineering, Faculty of Engineering, Chulalongkorn University for differential scanning calorimeter (DSC), thermogravimetric analysis (TGA), ultraviolet-visible spectroscopy (UV-Vis), Fourier transform infrared spectroscopy (FTIR), and X-Ray Diffractometer (XRD). Many thanks for UV-Vis to Assistant Professor Dr. Tarawipa Puangpetch.

Most importantly, the author would like to express the highest gratitude to my family and my best friend, who always supported pay attention to though these years for their encouragement, love, care, and other their wills.

Sirinan RATCHAWONG

## TABLE OF CONTENTS

|  | Page |
|--|------|
| ABSTRACT.....                                      | D    |
| ACKNOWLEDGEMENTS.....                              | E    |
| TABLE OF CONTENTS.....                             | F    |
| LIST OF TABLES.....                                | J    |
| LIST OF FIGURES.....                               | L    |
| CHAPTER 1 INTRODUCTION.....                        | 1    |
| CHAPTER 2 THEORY.....                              | 4    |
| 2.1 Polyvinyl alcohol (PVA).....                   | 4    |
| 2.2 Titanium dioxide (TiO <sub>2</sub> ).....      | 5    |
| 2.3 Surfactant.....                                | 6    |
| 2.3.1 Sodium dodecyl benzene sulfonate (SDBS)..... | 6    |
| 2.3.2 Sodium dodecyl sulfate (SDS).....            | 7    |
| 2.4 Polymer nanocomposites.....                    | 8    |
| 2.5 Polymer solution casting.....                  | 8    |
| 2.6 Universal tensile testing.....                 | 9    |
| 2.7 Differential scanning calorimeter (DSC).....   | 10   |
| 2.8 Thermogravimetric analysis (TGA).....          | 11   |
| 2.9 Scanning electron microscopy (SEM).....        | 11   |
| 2.10 Transmission electron microscopy (TEM).....   | 13   |
| 2.11 Ultraviolet–visible spectroscopy.....         | 14   |

|   |    |
|---|----|
| 2.12 X-Ray diffraction (XRD) .....  | 15 |
| 2.13 Fourier transform infrared spectroscopy (FTIR).....                          | 15 |
| 2.14 Photocatalytic activity.....   | 16 |
| 2.15 Antimicrobial activity assay .....   | 17 |
| CHAPTER 3 LITERATURE REVIEWS.....   | 18 |
| 3.1 TiO <sub>2</sub> particles.....   | 18 |
| 3.2 TiO <sub>2</sub> immobilization.....  | 18 |
| 3.3 PVA/TiO <sub>2</sub> composite films .....                                    | 18 |
| 3.4 Surfactant .....  | 19 |
| 3.5 Thermal treatment.....  | 19 |
| CHAPTER 4 EXPERIMENTAL PROCEDURE.....   | 21 |
| 4.1 Material .....  | 21 |
| 4.1.1 Polyvinyl alcohol (PVA) .....   | 21 |
| 4.1.2 Titanium dioxide (TiO <sub>2</sub> ) .....                                  | 21 |
| 4.1.3 Sodium dodecyl benzene sulfonate (SDBS).....                                | 21 |
| 4.1.4 Sodium dodecyl sulfate (SDS).....   | 21 |
| 4.1.5 Methylene blue (MB).....  | 21 |
| 4.1.6 Deionized (DI) water .....  | 21 |
| 4.2 Sample preparation .....  | 21 |
| 4.2.1 Part I: Study properties of PVA/TiO <sub>2</sub> composite films .....      | 21 |
| 4.2.2 Part II: Study properties of PVA/TiO <sub>2</sub> nanocomposite films ..... | 22 |
| 4.3 Sample characterization .....   | 23 |
| 4.3.1 Transmission electron microscope (TEM) .....                                | 23 |



|  |    |
|--|----|
| 4.3.2 Scanning electron microscopy (SEM).....                              | 23 |
| 4.3.3 Universal tensile testing.....                                       | 23 |
| 4.3.4 Differential scanning calorimeter (DSC) .....                        | 23 |
| 4.3.5 Thermogravimetric analysis (TGA) .....                               | 24 |
| 4.3.6 Ultraviolet-visible spectroscopy (UV-vis).....                       | 24 |
| 4.3.7 Fourier-transform infrared spectroscopy (FTIR) .....                 | 24 |
| 4.3.8 X-ray diffraction (XRD).....   | 24 |
| 4.3.9 Photocatalytic activity test.....                                    | 24 |
| 4.3.10 Antimicrobial activity assay .....                                  | 24 |
| CHAPTER 5 RESULTS AND DISCUSSION .....                                     | 27 |
| 5.1 Characterization TiO <sub>2</sub> particles .....                      | 27 |
| 5.2 PVATiO <sub>2</sub> composite films .....                              | 29 |
| 5.2.1 The dispersion of TiO <sub>2</sub> particles in PVA matrix .....     | 29 |
| 5.2.2 FTIR analysis .....  | 29 |
| 5.2.3 XRD analysis .....   | 30 |
| 5.2.4 Mechanical properties.....   | 37 |
| 5.2.5 TGA analysis .....   | 40 |
| 5.2.6 DSC analysis .....   | 44 |
| 5.2.7 UV absorption .....  | 45 |
| 5.2.8 Photocatalytic activity .....  | 48 |
| 5.3 PVATiO <sub>2</sub> nanocomposite films .....                          | 50 |
| 5.3.1 The dispersion of TiO <sub>2</sub> nanoparticles in PVA matrix. .... | 50 |
| 5.3.2 FTIR analysis .....  | 50 |

5.3.3 XRD analysis .....50

5.3.4 Mechanical properties .....61

5.3.5 TGA analysis.....65

5.3.6 DSC analysis .....69

5.3.7 UV absorption .....71

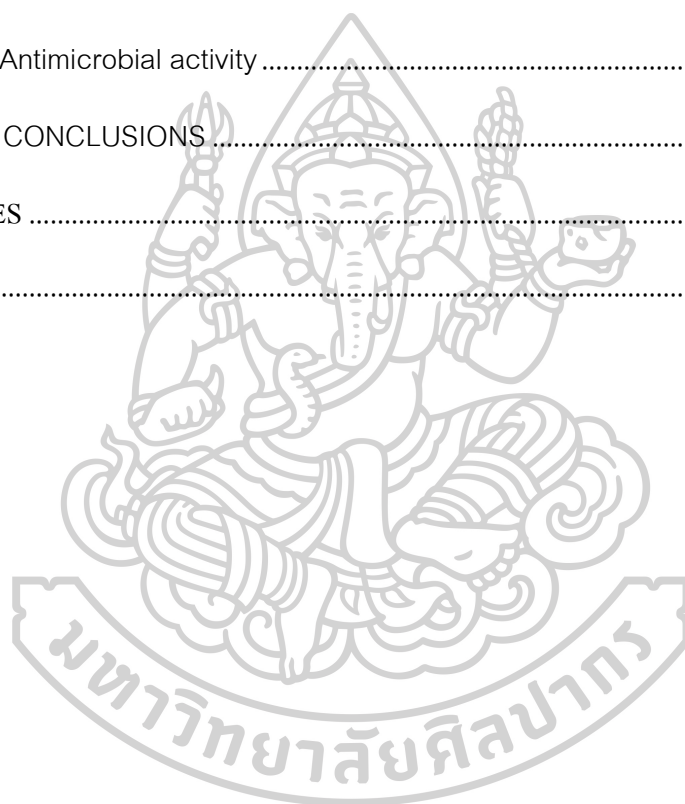
5.3.8 Photocatalytic activity .....74

5.3.9 Antimicrobial activity .....76

CHAPTER 6 CONCLUSIONS .....77

REFERENCES .....78

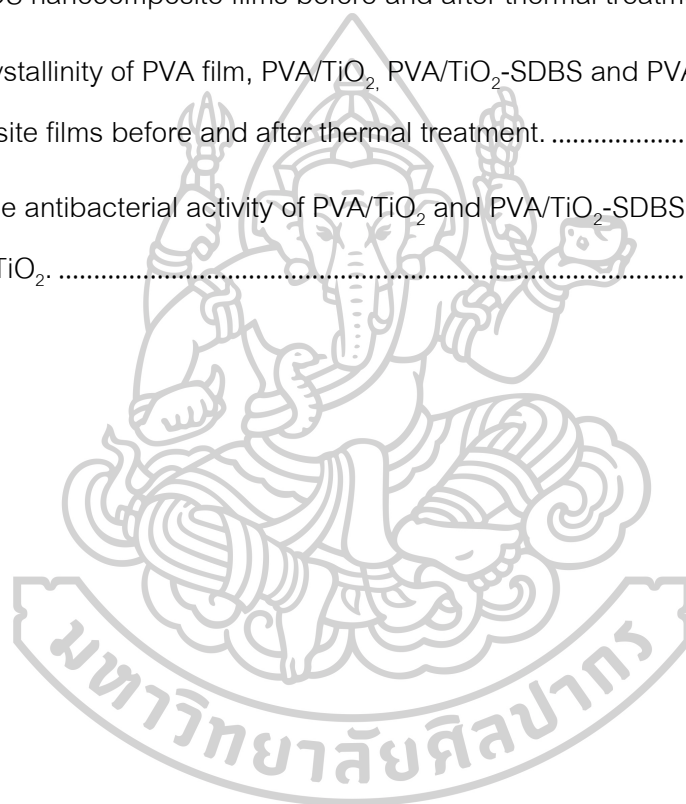
VITA .....85



## LIST OF TABLES

|  | Page |
|--|------|
| Table 1 Physical properties of SDBS and SDS [19]. .....  | 7    |
| Table 2 Tensile strength of PVA film, PVA/TiO <sub>2</sub> composite films and PVA/TiO <sub>2</sub> -SDBS composite films before and after thermal treatment. ....   | 38   |
| Table 3 Strain at break at break of PVA film, PVA/TiO <sub>2</sub> composite films and PVA/TiO <sub>2</sub> -SDBS composite films before and after thermal treatment. ....   | 38   |
| Table 4 Young's modulus of PVA film, PVA/TiO <sub>2</sub> composite films and PVA/TiO <sub>2</sub> -SDBS composite films before and after thermal treatment. ....  | 40   |
| Table 5 The decomposition temperature of 50 %weight loss (T <sub>d50</sub> ) of SDBS particles, PVA film, PVA/TiO <sub>2</sub> composite films and PVA/TiO <sub>2</sub> -SDBS composite films before and after thermal treatment. .... | 43   |
| Table 6 The char yield of SDBS particles, PVA film, PVA/TiO <sub>2</sub> composite films and PVA/TiO <sub>2</sub> -SDBS composite films before and after thermal treatment. ....   | 43   |
| Table 7 Melting point temperature (T <sub>m</sub> ) of PVA film, PVA/TiO <sub>2</sub> and PVA/TiO <sub>2</sub> -SDBS composite films before and after thermal treatment. ....  | 44   |
| Table 8 Crystallinity of PVA film, PVA/TiO <sub>2</sub> and PVA/TiO <sub>2</sub> -SDBS composite films before and after thermal treatment. ....  | 45   |
| Table 9 The tensile Strength of PVA film, PVA/TiO <sub>2</sub> , PVA/TiO <sub>2</sub> -SDBS and PVA/TiO <sub>2</sub> -SDS nanocomposite films before and after thermal treatment. ....   | 62   |
| Table 10 The strain at break of PVA film, PVA/TiO <sub>2</sub> , PVA/TiO <sub>2</sub> -SDBS and PVA/TiO <sub>2</sub> -SDS nanocomposite films before and after thermal treatment. ....   | 63   |
| Table 11 Young's modulus of PVA film, PVA/TiO <sub>2</sub> , PVA/TiO <sub>2</sub> -SDBS and PVA/TiO <sub>2</sub> -SDS nanocomposite films before and after thermal treatment. ....   | 64   |

|  |    |
|--|----|
| Table 12 Decomposition temperature of SDBS, SDS particles, PVA film, PVA/TiO <sub>2</sub> , PVA/TiO <sub>2</sub> -SDBS and PVA/TiO <sub>2</sub> -SDS nanocomposite films before and after thermal treatment..... | 68 |
| Table 13 The char yield of SDBS, SDS particles, PVA film, PVA/TiO <sub>2</sub> , PVA/TiO <sub>2</sub> -SDBS and PVA/TiO <sub>2</sub> -SDS nanocomposite films before and after thermal treatment. ....           | 69 |
| Table 14 Melting point temperature (T <sub>m</sub> ) of PVA film, PVA/TiO <sub>2</sub> , PVA/TiO <sub>2</sub> -SDBS and PVA/TiO <sub>2</sub> -SDS nanocomposite films before and after thermal treatment. ....   | 70 |
| Table 15 Crystallinity of PVA film, PVA/TiO <sub>2</sub> , PVA/TiO <sub>2</sub> -SDBS and PVA/TiO <sub>2</sub> -SDS nanocomposite films before and after thermal treatment. ....                                 | 71 |
| Table 16 The antibacterial activity of PVA/TiO <sub>2</sub> and PVA/TiO <sub>2</sub> -SDBS nanocomposite films at 5 wt% of TiO <sub>2</sub> . ....   | 76 |



## LIST OF FIGURES

|  | Page |
|--|------|
| Figure 1 Preparation of PVA by radical polymerization of vinyl acetate [8].  | 4    |
| Figure 2 The structure of vinyl alcohol (a) and PVA (b) synthesized by the hydrolysis of polyvinyl acetate [9].              | 4    |
| Figure 3 Crystalline structures of titanium dioxide anatase (a), rutile (b), brookite (c) [15].                              | 5    |
| Figure 4 Surfactant classification according to the composition of their head: nonionic, anionic, cationic, amphoteric [18]. | 6    |
| Figure 5 Production of SDS [20].   | 8    |
| Figure 6 The preparation of polymer composites by solution casting method [23].  | 9    |
| Figure 7 Load-elongation curve from a tensile test (a) and corresponding engineering stress-strain curve (b) [25].           | 9    |
| Figure 8 Types of differential scanning calorimeters (DSC): (a) Heat Flux, (b) Power Compensation [27].                      | 10   |
| Figure 9 A full DSC curve of quenched (amorphous) poly (ethylene terephthalate). Endotherm is down. [28].                    | 10   |
| Figure 10 The TGA and DTG curves of calcium oxalate monohydrate decomposition [29].  | 11   |
| Figure 11 Schematic illustration of the components of scanning electron microscope. [30].                                    | 12   |
| Figure 12 Schematic illustration of the components of transmission electron microscopes. [30].                               | 13   |
| Figure 13 Schematic of a conventional spectrophotometer.[33].  | 14   |

|   |    |
|---|----|
| Figure 14 Illustration of the geometry used for the simplified derivation of Bragg's law [34].  | 15 |
| Figure 15 The optical diagram of FTIR spectrometer [35].  | 16 |
| Figure 16 Elementary steps taking place in a photocatalytic cycle [36].   | 16 |
| Figure 17 Ultrasonic bath.  | 22 |
| Figure 18 Petri dish glass.   | 22 |
| Figure 19 Oven.   | 23 |
| Figure 20 Universal tensile testing (EZ-LX model, Shimadzu, Japan).   | 25 |
| Figure 21 TA Instruments (SDT Q600, TA Instruments, UK).  | 25 |
| Figure 22 UV-vis spectrophotometer (Cary 5000, Varian, USA).  | 25 |
| Figure 23 UV-vis spectrophotometer (T92+, PG Instruments, UK).  | 26 |
| Figure 24 Fourier-transform infrared spectroscopy (Nicolet 6700, Thermo Scientific, USA).   | 26 |
| Figure 25 XRD pattern of TiO <sub>2</sub> (a) microparticles and (b) nanoparticles.   | 28 |
| Figure 26 TEM image of TiO <sub>2</sub> (a) microparticles and (b) nanoparticles.   | 28 |
| Figure 27 SEM image of TiO <sub>2</sub> (a) microparticles and (b) nanoparticles.   | 28 |
| Figure 28 SEM images with BSE of PVA/TiO <sub>2</sub> composite films without and with surfactant at magnitude 500X.                      | 31 |
| Figure 29 SEM images with BSE of PVA/TiO <sub>2</sub> composite films without and with surfactant at magnitude 5000X.                     | 32 |
| Figure 30 Infrared spectra of TiO <sub>2</sub> microparticles, PVA film and PVA/TiO <sub>2</sub> composite films.                         | 33 |
| Figure 31 Infrared spectra of TiO <sub>2</sub> microparticles, PVA film and PVA/TiO <sub>2</sub> composite films after thermal treatment. | 33 |

|   |           |
|---|-----------|
| Figure 32 Infrared spectra of TiO <sub>2</sub> microparticles, SDBS, PVA film and PVA/TiO <sub>2</sub> -SDBS composite films.....   | 34        |
| Figure 33 Infrared spectra of TiO <sub>2</sub> microparticles, SDBS, PVA film and PVA/TiO <sub>2</sub> -SDBS composite films after thermal treatment. ....  | 34        |
| Figure 34 Infrared spectra of PVA film, PVA/TiO <sub>2</sub> and PVA/TiO <sub>2</sub> -SDBS composite films before and after thermal treatment.....   | 35        |
| <b>Figure 35 XRD pattern of pure PVA before and after thermal treatment .....</b>   | <b>35</b> |
| Figure 36 XRD pattern of TiO <sub>2</sub> microparticles and SDBS particles.....  | 35        |
| Figure 37 XRD pattern of PVA/TiO <sub>2</sub> composite films. ....   | 36        |
| Figure 38 XRD pattern of PVA/TiO <sub>2</sub> composite films after thermal treatment. ....   | 36        |
| Figure 39 XRD pattern of PVA/TiO <sub>2</sub> -SDBS composite films.....  | 36        |
| Figure 40 XRD pattern of PVA/TiO <sub>2</sub> -SDBS composite films after thermal treatment. ....   | 37        |
| Figure 41 XRD pattern of PVA/TiO <sub>2</sub> and PVA/TiO <sub>2</sub> -SDBS composite films.....   | 37        |
| Figure 42 XRD pattern of PVA/TiO <sub>2</sub> and PVA/TiO <sub>2</sub> -SDBS composite films after thermal treatment.....   | 37        |
| Figure 43 Tensile strength of PVA film and PVA/TiO <sub>2</sub> composite films at 5 wt% of TiO <sub>2</sub> without and with TiO <sub>2</sub> :SDBS ratios of 1:1 and 1:2 before and after thermal treatment.....          | 38        |
| Figure 44 Strain at break at break of PVA film and PVA/TiO <sub>2</sub> composite films at 5 wt% of TiO <sub>2</sub> without and with TiO <sub>2</sub> :SDBS ratios of 1:1 and 1:2 before and after thermal treatment ..... | 39        |
| Figure 45 Young's modulus of PVA film and PVA/TiO <sub>2</sub> composite films at 5 wt% of TiO <sub>2</sub> without and with TiO <sub>2</sub> :SDBS ratios of 1:1 and 1:2 before and after thermal treatment.....           | 40        |
| Figure 46 TGA analyses of PVA film and PVA/TiO <sub>2</sub> composite films. ....   | 41        |
| Figure 47 TGA analyses of PVA film and PVA/TiO <sub>2</sub> composite films after thermal treatment.....  | 41        |

|   |    |
|---|----|
| Figure 48 TGA analyses of SDBS particles, PVA film and PVA/TiO <sub>2</sub> -SDBS composite films. ....   | 42 |
| Figure 49 TGA analyses of SDBS particles, PVA film and PVA/TiO <sub>2</sub> -SDBS composite films after thermal treatment. ....   | 42 |
| Figure 50 TGA analyses of PVA film and PVA/TiO <sub>2</sub> composite films 5 wt% of TiO <sub>2</sub> without and with TiO <sub>2</sub> :SDBS ratio 1:1 and 1:2 are compared before and after thermal treatment. ....                   | 42 |
| Figure 51 PVA film before (a) and after (b) thermal treatment. ....   | 45 |
| Figure 52 UV-visible absorption spectra for PVA film and PVA/TiO <sub>2</sub> composite films. ....   | 46 |
| Figure 53 UV-visible absorption spectra for PVA film and PVA/TiO <sub>2</sub> composite films with thermal treatment. ....  | 46 |
| Figure 54 UV-visible absorption spectra for PVA film and PVA/TiO <sub>2</sub> -SDBS composite films. ....   | 47 |
| Figure 55 UV-visible absorption spectra for PVA film and PVA/TiO <sub>2</sub> -SDBS composite films with thermal treatment. ....  | 47 |
| Figure 56 UV-visible absorption spectra for PVA film and PVA/TiO <sub>2</sub> composite films 5 wt% of TiO <sub>2</sub> without and with TiO <sub>2</sub> :SDBS ratio 1:1 and 1:2 are compared without and with thermal treatment. .... | 47 |
| Figure 57 Extent of MB removal of PVA film before and after thermal treatment without UV irradiation. ....  | 48 |
| Figure 58 Extent of MB removal of PVA film, PVA/TiO <sub>2</sub> and PVA/TiO <sub>2</sub> -SDBS composite films ....  | 49 |
| Figure 59 Extent of MB removal of PVA film, PVA/TiO <sub>2</sub> and PVA/TiO <sub>2</sub> -SDBS composite films after thermal treatment. ....   | 49 |
| Figure 60 Extent of MB removal of PVA film, PVA/TiO <sub>2</sub> and PVA/TiO <sub>2</sub> -SDBS composite films 5 wt% of TiO <sub>2</sub> before and after thermal treatment. ....  | 49 |



|  |    |
|--|----|
| Figure 61 SEM images with BSE of PVA/TiO <sub>2</sub> nanocomposite films without and with surfactant at magnitude 500X. ....  | 51 |
| Figure 62 SEM images with BSE of PVA/TiO <sub>2</sub> nanocomposite films without and with surfactant at magnitude 5000X. ....   | 52 |
| Figure 63 Infrared spectra of TiO <sub>2</sub> nanoparticles, PVA film and PVA/TiO <sub>2</sub> nanocomposite films. ....  | 53 |
| Figure 64 Infrared spectra of TiO <sub>2</sub> nanoparticles, PVA film and PVA/TiO <sub>2</sub> nanocomposite films after thermal treatment. ....                                    | 53 |
| Figure 65 Infrared spectra of TiO <sub>2</sub> nanoparticles, SDBS, PVA film and PVA/TiO <sub>2</sub> -SDBS nanocomposite films. ....  | 54 |
| Figure 66 Infrared spectra of TiO <sub>2</sub> nanoparticles, SDBS, PVA film and PVA/TiO <sub>2</sub> -SDBS nanocomposite films after thermal treatment. ....                        | 55 |
| Figure 67 Infrared spectra of TiO <sub>2</sub> nanoparticles, SDS, PVA film and PVA/TiO <sub>2</sub> -SDS nanocomposite films. ....  | 56 |
| Figure 68 Infrared spectra of TiO <sub>2</sub> nanoparticles, SDS, PVA film and PVA/TiO <sub>2</sub> -SDS nanocomposite films after thermal treatment. ....                          | 57 |
| Figure 69 Infrared spectra of PVA film, PVA/TiO <sub>2</sub> nanocomposite films at 5 wt% of TiO <sub>2</sub> without and with surfactants, before and after thermal treatment. .... | 58 |
| Figure 70 XRD patterns of TiO <sub>2</sub> nanoparticles, SDBS and SDS. ....   | 58 |
| Figure 71 XRD pattern of PVA/TiO <sub>2</sub> nanocomposite films. ....  | 59 |
| Figure 72 XRD pattern of PVA/TiO <sub>2</sub> nanocomposite films after thermal treatment. ....  | 59 |
| Figure 73 XRD pattern of PVA/TiO <sub>2</sub> -SDBS nanocomposite films. ....  | 59 |
| Figure 74 XRD pattern of PVA/TiO <sub>2</sub> -SDBS nanocomposite films after thermal treatment. ....  | 60 |
| Figure 75 XRD pattern of PVA/TiO <sub>2</sub> -SDS nanocomposite films. ....   | 60 |

|   |    |
|---|----|
| Figure 76 XRD pattern of PVA/TiO <sub>2</sub> -SDS nanocomposite films after thermal treatment. .60   | 60 |
| Figure 77 XRD pattern of PVA/TiO <sub>2</sub> nanocomposite films at 5wt% of TiO <sub>2</sub> without and with surfactants, before and after thermal treatment.....61                       | 61 |
| Figure 78 Tensile strength of PVA film and PVA/TiO <sub>2</sub> nanocomposite films at 5wt% of TiO <sub>2</sub> without and with surfactants, before and after thermal treatment.....62     | 62 |
| Figure 79 The strain at break of PVA film and PVA/TiO <sub>2</sub> nanocomposite films at 5 wt% of TiO <sub>2</sub> without and with surfactants, before and after thermal treatment.....63 | 63 |
| Figure 80 Young's modulus of PVA film and PVA/TiO <sub>2</sub> nanocomposite films 5 wt% of TiO <sub>2</sub> without and with surfactants, before and after thermal treatment.....64        | 64 |
| Figure 81 TGA analyses of PVA film and PVA/TiO <sub>2</sub> nanocomposite films.....65  | 65 |
| Figure 82 TGA analyses of PVA film and PVA/TiO <sub>2</sub> nanocomposite films after thermal treatment.....65  | 65 |
| Figure 83 TGA analyses of SDBS particles, PVA film and PVA/TiO <sub>2</sub> -SDBS nanocomposite films.....66  | 66 |
| Figure 84 TGA analyses of SDBS particles, PVA film and PVA/TiO <sub>2</sub> -SDBS nanocomposite films after thermal treatment.....66  | 66 |
| Figure 85 TGA analyses of SDS particles, PVA film and PVA/TiO <sub>2</sub> -SDS nanocomposite films. ....66   | 66 |
| Figure 86 TGA analyses of SDS particles, PVA film and PVA/TiO <sub>2</sub> -SDS nanocomposite films after thermal treatment. ....67   | 67 |
| Figure 87 TGA analyses of PVA film and PVA/TiO <sub>2</sub> nanocomposite films at 5wt% of TiO <sub>2</sub> without and with surfactants, before and after thermal treatment. ....67        | 67 |
| Figure 88 UV-visible absorption spectra for PVA film and PVA/TiO <sub>2</sub> nanocomposite films. ....72   | 72 |

|   |    |
|---|----|
| Figure 89 UV-visible absorption spectra for PVA film and PVA/TiO <sub>2</sub> nanocomposite films after thermal treatment. ....   | 72 |
| Figure 90 UV-visible absorption spectra for PVA film and PVA/TiO <sub>2</sub> -SDBS nanocomposite films. ....   | 72 |
| Figure 91 UV-visible absorption spectra for PVA film and PVA/TiO <sub>2</sub> -SDBS nanocomposite films after thermal treatment. ....   | 73 |
| Figure 92 UV-visible absorption spectra for PVA film and PVA/TiO <sub>2</sub> -SDS nanocomposite films. ....  | 73 |
| Figure 93 UV-visible absorption spectra for PVA film and PVA/TiO <sub>2</sub> -SDS nanocomposite films after thermal treatment. ....  | 73 |
| Figure 94 UV-visible absorption spectra for PVA film and PVA/TiO <sub>2</sub> nanocomposite films at 5 wt% of TiO <sub>2</sub> without and with surfactants, before and after thermal treatment. .... | 74 |
| Figure 95 Extent of MB removal of PVA film, PVA/TiO <sub>2</sub> , PVA/TiO <sub>2</sub> -SDBS and PVA/TiO <sub>2</sub> -SDS nanocomposite films. ....   | 75 |
| Figure 96 Extent of MB removal of PVA film, PVA/TiO <sub>2</sub> , PVA/TiO <sub>2</sub> -SDBS and PVA/TiO <sub>2</sub> -SDS nanocomposite films after thermal treatment. ....                         | 75 |
| Figure 97 Extent of MB removal of PVA film and PVA/TiO <sub>2</sub> nanocomposite films 5wt% of TiO <sub>2</sub> without and with surfactants, before and after thermal treatment. ....               | 76 |

## CHAPTER 1

### INTRODUCTION

The nanocatalysts; for example, nanosized semiconductor materials ( $\text{TiO}_2$ ,  $\text{ZnO}$ ,  $\text{CdS}$  and  $\text{WO}_3$ ), nanosized zero-valence metal ( $\text{Fe}^0$ ,  $\text{Cu}^0$  and  $\text{Zn}^0$ ) and nanosized bimetallic materials ( $\text{Fe/Pd}$ ,  $\text{Fe/Ni}$ ,  $\text{Fe/Al}$  and  $\text{Zn/Pd}$ ) have attracted considerable interest due to their large surface area. Those nano-catalysts have been applied in abatement of environmental contaminants in water or industrial effluents, air and soil. Khan et al. [1] presented parameters affecting the photocatalytic degradation of dyes using  $\text{TiO}_2$ . The effect of photocatalyst concentration on the decomposition of the dye was reported. The rate of decomposition was found to increase with an increase in catalyst concentration to a limit and then decrease to a constant value due to the increased solution opacity as increasing the catalyst loading. Moreover, a loss in surface area by agglomeration (particle-particle interactions) at high catalyst concentration was also observed. The nanoparticle size, however, brings limitation regarding difficulties in separation and reuse. The running costs are high in order to prevent the release of nanoparticles into the environment that may be harmful to ecosystems and human health [2, 3]. Immobilization of nanoparticles on polymeric supports has been an alternative method to solve the problem. The choice of the polymeric supports is usually guided by their mechanical and thermal behaviors and other properties such as hydrophobic/hydrophilic balance, chemical stability, bio-compatibility, optical and/or electronic properties and chemical functionalities (i.e. solvation, wettability, templating effect, etc.) [3]. The particle aggregation or poor particle distribution on polymeric supports usually decreases catalytic efficiency [4].

Polymer materials are inexpensive, readily available and mechanically stable with high durability. Many of them have high UV-resistance, do not undergo oxidation readily as well as being thermoplastic. The thermal softening properties of thermoplastic polymer ease the coating of catalyst particles by simple thermal treatment methods [4]. In recent studies, various polymeric supports such as polyethylene sheets, thin polyethylene films, polystyrene (PS) beads, expanded polystyrene (EPS) beads, cellulose microspheres, fluoropolymer resins, polyethylene terephthalate (PET) bottles, polypropylene (PP) granules, cellulose fibers, polypropylene fabric (PPF), polyvinyl chloride (PVC), polyvinyl alcohol (PVA), polyaniline (PANI), polycarbonate (PC), poly(methyl methacrylate) (PMMA), polyvinyl acetate (PVAc), poly(styrene)-co-poly(4-vinylpyridine) (PSP4VP), rubber latex (an elastic hydrocarbon polymer) and poly-chloro-para xylene have been attempted for anchoring photocatalyst particles [2].

In this work, PVA is selected as a polymeric support. PVA is a well-known hydrophilic polymer with good film-forming ability, transparency, chemical resistance, water solubility, biodegradability, flexibility and cost-effectiveness. Nanoparticle selected for this work is  $\text{TiO}_2$ , a semiconductor photocatalysis. When  $\text{TiO}_2$  is stimulated by ultraviolet light, it can destroy or break down organic compounds including some bacteria without releasing toxins.  $\text{TiO}_2$  has benefits as one of the most efficient photocatalyst because it is highly stable, economical, non-toxic (to environment or humans), high turnover applicable on various substrates. It possesses high catalytic activity, strong oxidizing power and stable against photo corrosion and chemical resistance [5]. Hee Dong Jang et al. [6] studied effects of particle size and phase composition of titanium dioxide nanoparticles on the photocatalytic properties through methylene blue degradation as well as inactivation of *Escherichia coli* and *Pseudomonas aeruginosa*. The results showed the effect of anatase on increased methylene blue degradation as well as decomposition of bacteria. There were many studies on the effects of anatase and rutile crystalline phase in  $\text{TiO}_2$  upon photocatalyzed organic degradation [1, 4, 5]. Recently, several researchers have investigated PVA immobilized  $\text{TiO}_2$ . Wenwen Yan et al. [5] studied multicycle photocatalytic reduction of Cr(VI) over transparent PVA/ $\text{TiO}_2$  nanocomposite films under visible light. Moreover, Ping Lei et al. [4] studied a simple way to prepare a crosslinked between PVA and  $\text{TiO}_2$  by thermal treatment. The covalent bonding between PVA and  $\text{TiO}_2$  nanoparticles prevented the loss of  $\text{TiO}_2$  nanoparticles during multi-cycle use. However, the nanoparticles in PVA support may form agglomeration or particles aggregate [2, 3]. Yan Geng et al. [7] studied the effects of surfactant treatment on mechanical and electrical properties of carbon nanotubes (CNT)/epoxy nanocomposites. The results showed the enhanced interfacial interactions by surfactant treatment gave rise to improve dispersion and wetting of CNTs in polymer matrix, and hence enhancing the mechanical and fracture properties of the nanocomposite. Therefore, surfactant is used to improve the dispersion of nanoparticles in this work coupled with a conventional mechanical method using ultrasonication. Thermal treatment is also applied to improve the immobilization of  $\text{TiO}_2$  nanoparticles on PVA film.

The aim of this work is to develop the PVA/ $\text{TiO}_2$  composite film for photocatalytic degradation and antibacterial applications. PVA/ $\text{TiO}_2$  nanocomposite films are prepared by solution casting which is a simple method. Two types of surfactant; sodium dodecylbenzene sulfonate (SDBS) and sodium dodecyl sulfate (SDS) were used in the film preparation in combined with thermal treatment process. The effects of  $\text{TiO}_2$  particle size as well as surfactant and thermal treated

PVA/TiO<sub>2</sub> nanocomposite films on the film properties are investigated. The photocatalytic activity of PVA/TiO<sub>2</sub> composite film for the degradation of methylene blue, as well as the efficiency in inhibition of bacterial growth is evaluated.



## CHAPTER 2

### THEORY

#### 2.1 Polyvinyl alcohol (PVA)

Polyvinyl alcohol (PVA) was first prepared by Hermann and Haehnel in 1924 through hydrolysis of polyvinyl acetate in ethanol using potassium hydroxide. Nowadays, PVA in industrial applications is generally obtained from hydrolysis of homopolymer of vinyl acetate (VAc) (Figure 1) [8].

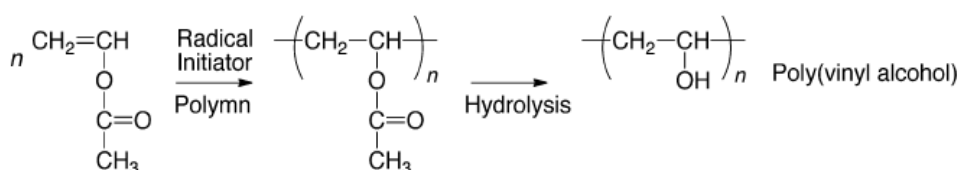


Figure 1 Preparation of PVA by radical polymerization of vinyl acetate [8].

PVA is a linear synthetic polymer produced via partial or full hydrolysis of polyvinyl acetate to remove the acetate groups (Figure 2) [9]. The molecular weights of PVA products are in the ranges of 20,000–400,000 g/mol. Their solubility, flexibility, tensile strength and adhesiveness depend on the length of the initial vinyl acetate polymer and the degree of hydrolysis under alkaline or acidic conditions [10].

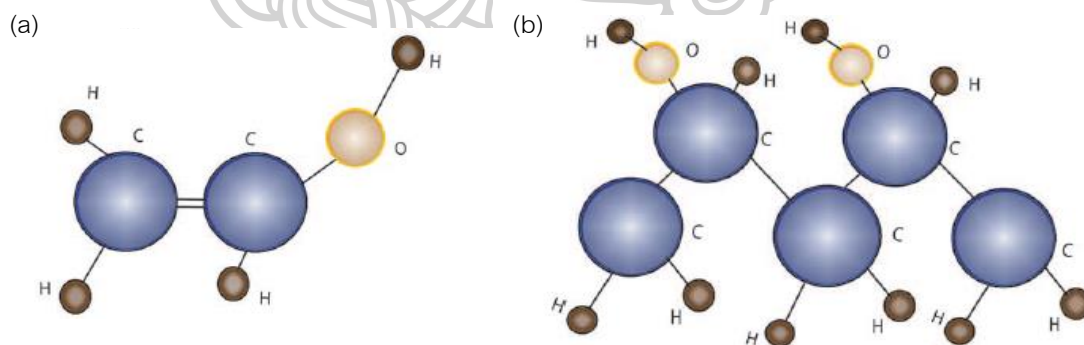


Figure 2 The structure of vinyl alcohol (a) and PVA (b) synthesized by the hydrolysis of polyvinyl acetate [9].

PVA is partially crystalline and a hydrophilic polymer. PVA has several advantages such as chemical resistance, water solubility, biodegradability, substantial tensile strength and superior flexibility and hardness. PVA is a water-soluble polymer. The water solubility and physical properties of PVA, including its film forming, are highly affected by the degree of hydrolysis, molecular weight, and its crystallinity [11]. It has been applied in the industrial, commercial, medical, and food sectors



and has been used to produce many end products, such as lacquers, resins, surgical threads, and food packaging materials [10].

## 2.2 Titanium dioxide (TiO<sub>2</sub>)

Titanium dioxide (TiO<sub>2</sub>) was discovered in 1821 and commercialized in the early 20<sup>th</sup> century. It can be found mainly as a pigment in powder form, providing whiteness to products such as paints, paper, coating plastics, food packaging materials, ink, cosmetics and so on. It is widely used due to its low toxicity, chemical stability and affordability. In 1972, Fujishima and Honda discovered the phenomenon of photocatalytic splitting of water on a TiO<sub>2</sub> electrode under ultraviolet (UV) light. This well-known chemical phenomenon involves electrolysis of water, which is related to photocatalysis [12]. TiO<sub>2</sub> is considered very close to an ideal semiconductor for photocatalysis. It is generally applied for removing industrial waste because of its high stability, low cost and safety toward both humans and environment [2].

TiO<sub>2</sub> belongs to the family of transition metal oxides. There are at least 8 different crystalline structures of titanium dioxide, four naturally polymorphs (rutile, anatase, brookite, Ti (B)) and four high pressure synthesized polymorphs (TiO<sub>2</sub> (II), TiO<sub>2</sub> (H), baddelleyite and cotinnite) [13]. Among them, anatase, rutile and brookite are the most common crystalline forms and most worldwide manufacturing. These three crystalline forms are TiO<sub>6</sub> octahedral structures but different by the distortion of each octahedral structure and by the assembly patterns of the octahedral chains [14]. Anatase is made up from octahedral structure that is connected by their corner (vertice), whereas octahedral structure of rutile is connected by their edges. For brookite, both octahedral corner and edges are connected (Figure 3) [15]. Most photocatalytic studies have been focused on anatase and rutile, which their energy band gap are 3.2 and 3.0 eV, respectively [16].

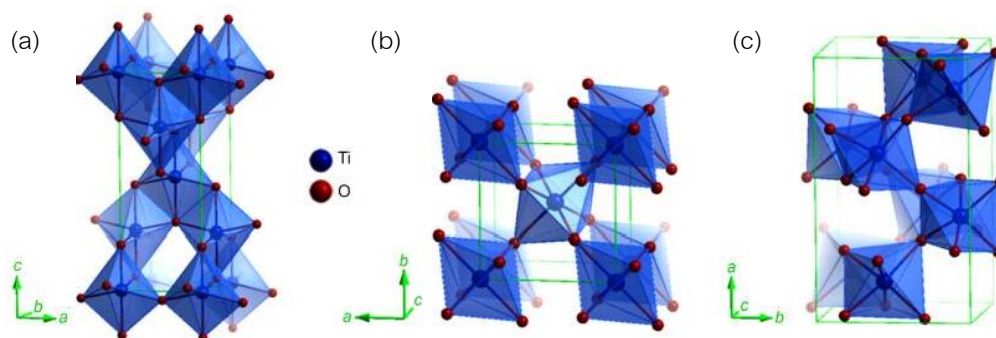


Figure 3 Crystalline structures of titanium dioxide anatase (a), rutile (b), brookite (c) [15].



## 2.3 Surfactant

Surface-active agents, or surfactants, are usually organic compounds that are amphiphilic by having two different groups, one polar and the other nonpolar, at opposite ends of a single molecule. The polar group is referred to as hydrophilic or lipophobic head, and the nonpolar as hydrophobic or lipophilic tail. The nonpolar end is generally a long-chain hydrocarbon, which can be linear, branched, or aromatic. Most commonly, surfactants are broadly categorized according to polar head group as anionic, cationic, nonionic, or amphoteric (zwitterionic) [17]. A non-ionic surfactant has no charged groups in its head. The head of an ionic surfactant carries a net positive or negative charge. If the charge is negative, the surfactant is more specifically called anionic; if the charge is positive, it is called cationic. If a surfactant contains a head with two oppositely charged groups, it is termed amphoteric (Figure 4) [18].

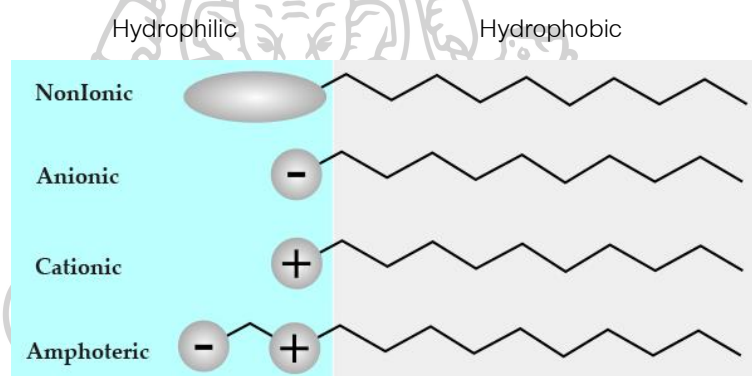
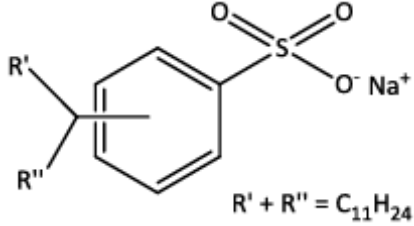
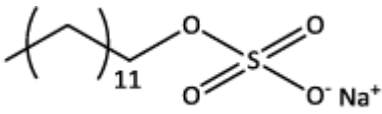


Figure 4 Surfactant classification according to the composition of their head: nonionic, anionic, cationic, amphoteric [18].

### 2.3.1 Sodium dodecyl benzene sulfonate (SDBS)

Sodium Dodecyl benzenesulfonate is one of a group of salts of alkylbenzene sulfonates with the formula  $\text{CH}_3(\text{CH}_2)_{11}\text{C}_6\text{H}_4\text{SO}_3\text{Na}$ . SDBS is an anionic surfactant, consisting of a hydrophilic sulfonate head-group and a hydrophobic alkylbenzene tail-group which used in cosmetics as surfactant cleansing agents. Some basic physical properties of SDBD are shown in Table 1. Sodium Dodecyl benzenesulfonate is soluble in water and partially soluble in alcohol, with dermal absorption dependent on pH. Dodecyl benzenesulfonate salts are not toxic in single-dose oral and dermal animal tests, and no systemic toxicities were observed in repeat-dose dermal animal studies[19].

Table 1 Physical properties of SDBS and SDS [19].

| Property                       | SDBS   | SDS  |
|--------------------------------|--|--|
| Chemical structure             | <br>$R' + R'' = C_{11}H_{24}$ |  |
| Molecular weight               | 348.48 g/mol   | 288.38 g/mol   |
| Melting point                  | 300 °C   | 204-207 °C   |
| Form                           | Off-white to light yellow powder or flakes   | Cream-colored flakes, crystals or powder   |
| Solubility                     | 200 g/ L water (at 293K)   | 150 g/ L water (at 293K)   |
| pH (aqueous)                   | 7 - 8  | 7.3-8.5  |
| Density (liquid)               | 1.0  | 0.938  |
| Critical micelle concentration | 2.73 mM (at 298K)  | 8.2 mM (at 298K)   |

### 2.3.2 Sodium dodecyl sulfate (SDS)

Sodium dodecyl sulfate, synonymously sodium lauryl sulfate (SDS or SLS, respectively), is a synthetic organic compound with the formula  $CH_3(CH_2)_{10}CH_2SO_4Na$  i.e. 12-carbon tail attached to a sulfate group. SDS is an anionic surfactant which synthetic process was first described in Germany between the two world wars [19]. SDS can be prepared by reacting dodecyl alcohol (dodecanol) with sulfuric acid. The resulting dodecyl sulfate is converted to the sodium salt by a reaction with sodium hydroxide (Figure 5). Some basic physical properties of SDS are shown in Table 1. SDS is a cheap, highly effective cleansing and foaming agent, so it is used in industrial products including car wash soap, engine degreasers and floor cleaners. It is also an ingredient in a wide range of personal care products such as soaps, shampoos and toothpastes [20].

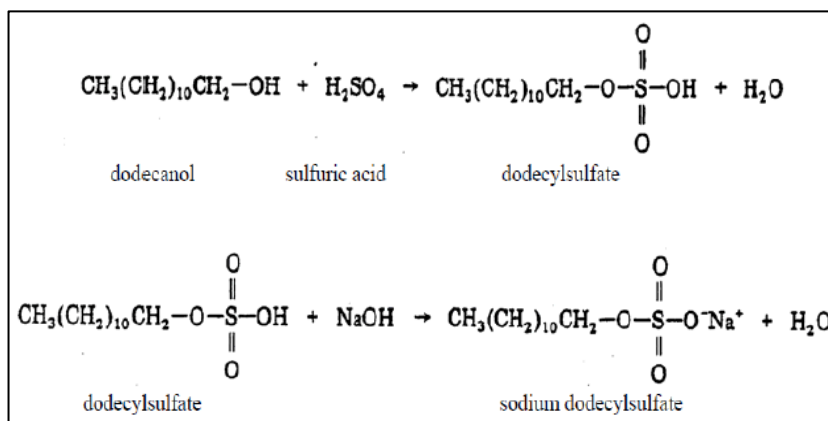


Figure 5 Production of SDS [20].

## 2.4 Polymer nanocomposites

Composite is a multiphase material made by combining two or more constituent materials often ones that have very different properties, when combined, produce a material with completely different characteristics from the individual components. First polymer composites were developed during the 1940s for military and aerospace applications [21]. In the current century, polymer matrix based nanocomposites have generated a significant amount of attention. The polymer matrix, called the continuous phase, is mixed with the reinforcing agent which is nanoparticle. Various nanoparticles such as nanoclay, carbon nanotubes and metal nanoparticles have been incorporated with different polymers in order to develop materials with better barrier, electrical, optical, thermal or mechanical properties. The reason for the production of polymer nanocomposites is the restriction of the use of polymers in engineering [22]. Also, numerous polymer nanocomposites have been applied in environmental applications for deduction of contaminants from various environmental media with the main mechanisms responsible is catalytic degradation and adsorption [3].

## 2.5 Polymer solution casting

In solution casting, polymer or polymer composite is dissolved or dispersed in solution, coated onto a carrier substrate, and then the water or solvent is removed by drying to create a solid layer on the carrier. The resulting cast layer can be stripped from the carrier substrate to produce a stand-alone film. The preparation of polymer composites by solution casting method is shown in Figure 6 [23].

Solution casting process offers many advantages including more uniform film thickness distribution, higher film dimensional stability and optical purity. Also, multi-layer coating processes enable the addition of functional coatings during the film casting process, eliminating the cost of secondary coating steps [24].

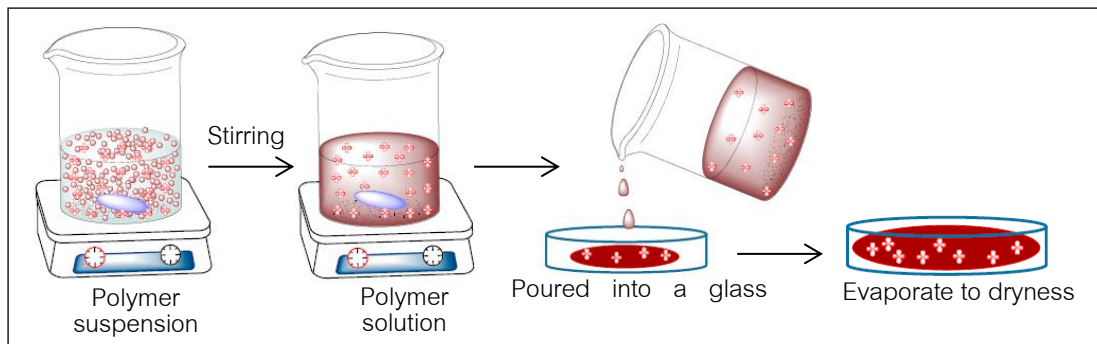


Figure 6 The preparation of polymer composites by solution casting method [23].

## 2.6 Universal tensile testing

One of the most fundamental mechanical tests that can be performed on a material is the tensile test which a sample is subjected to a controlled tension until failure. The tensile force is directly recorded as a function of the increase in gage length as shown in Figure 7(a). These data are converted to engineering stress and strain (Figure 7(b)), a stress-strain curve that is identical in shape to the force-elongation curve. The advantage of dealing with stress versus strain rather than load versus elongation is that the stress-strain curve is virtually independent of specimen dimensions.

Engineering stress, or nominal stress,  $s$ , is defined as  $s = F/A_0$  where  $F$  is the tensile force and  $A_0$  is the initial cross-sectional area of the gage section. Engineering strain, or nominal strain,  $e$ , is defined as  $e = \Delta L/L_0$  where  $L_0$  is the initial gage length and  $\Delta L$  is the change in gage length ( $L - L_0$ ). Properties that are directly measured via a tensile test are ultimate tensile strength, breaking strength, maximum elongation and reduction in area. From these measurements the following properties can also be determined; Young's modulus, poisson's ratio, yield strength, and strain-hardening characteristics [25].

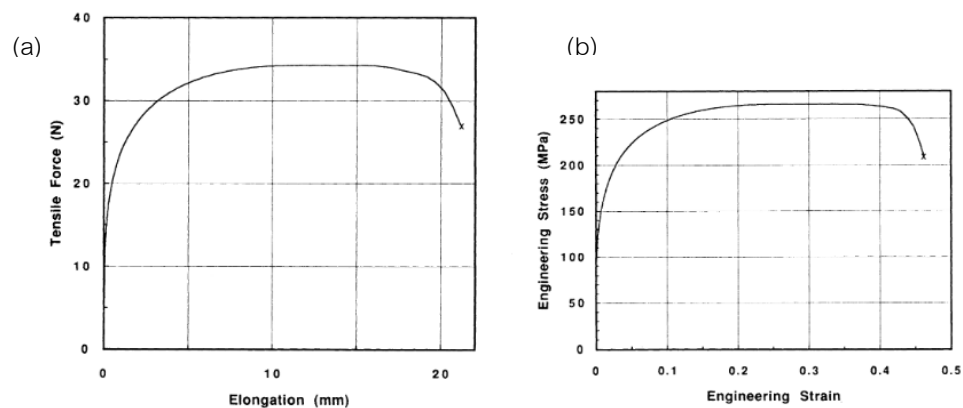


Figure 7 Load-elongation curve from a tensile test (a) and corresponding engineering stress-strain curve (b) [25].

## 2.7 Differential scanning calorimeter (DSC)

Differential Scanning Calorimetry (DSC) is a thermal analysis technique in which the change in material's heat capacity ( $C_p$ ) with temperature is measured. A sample of known mass is heated or cooled and the changes in its heat capacity are tracked as changes in the heat flow. This allows the detection of material transitions such as melts, glass transitions, phase changes, and curing.

DSC is a commercially available instrument which has two types; heat flux and power compensation type as shown in Figure 8. Heat flux DSC is a technique in which the temperature difference between the sample and the reference material is measured as a function of temperature. The power compensation type is a technique in which the difference of thermal energy that is applied to the sample and the reference material per unit of time is measured as a function of temperature to equalize their temperature.

The example of heating curve of quenched poly(ethylene terephthalate) (PET) is shown in Figure 9. The measurement recorded at a heating rate of  $10\text{ }^\circ\text{C}/\text{min}$  showed the glass transition (at  $\sim 80\text{ }^\circ\text{C}$ ), followed by cold crystallization and melting of crystals formed in non-isothermal cold crystallization. The baseline during the transition was drawn to show that the crystallization process lasts to the beginning of melting [26].

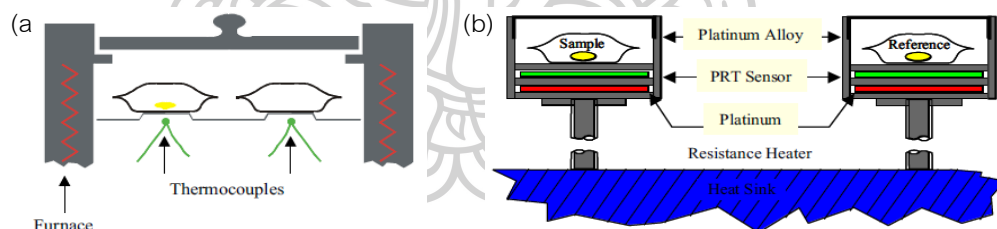


Figure 8 Types of differential scanning calorimeters (DSC): (a) Heat Flux, (b) Power Compensation [27].

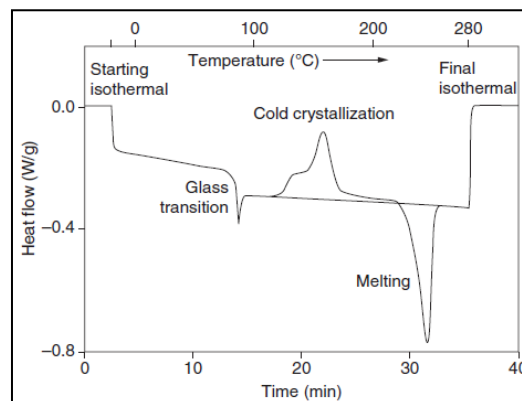


Figure 9 A full DSC curve of quenched (amorphous) poly(ethylene terephthalate). Endotherm is down. [28].

## 2.8 Thermogravimetric analysis (TGA)

Thermogravimetric Analysis is a technique in which the mass of a substance is monitored as a function of temperature or time as the sample specimen is subjected to a controlled temperature program in a controlled atmosphere. The results of a TGA measurement are usually displayed as a TGA curve in which mass or percent mass is plotted against temperature and/or time. An alternative and complementary presentation is to use the first derivative of the TGA curve with respect to temperature or time. This shows the rate at which the mass changes and is known as the differential thermogravimetric or DTG curve.

Mass changes occur when the sample loses material in one of several different ways or reacts with the surrounding atmosphere. Different effects can cause a sample to lose, or even gain, mass and so produce steps in the TGA curve or peaks in the DTG curve. The instrument can quantify loss of water, loss of solvent, loss of plasticizer, decarboxylation, pyrolysis, oxidation, decomposition, weight % filler, metallic catalytic residue, and weight % ash. The example of stepwise decomposition of calcium oxalate monohydrate measured at heating rate 30 K/min under nitrogen atmosphere is shown in Figure 10. The TGA curve is normalized (divided by the sample weight) and therefore begins at 100%. The temperature range of the three mass losses is particularly clear in the normalized first derivative or DTG curve [29].

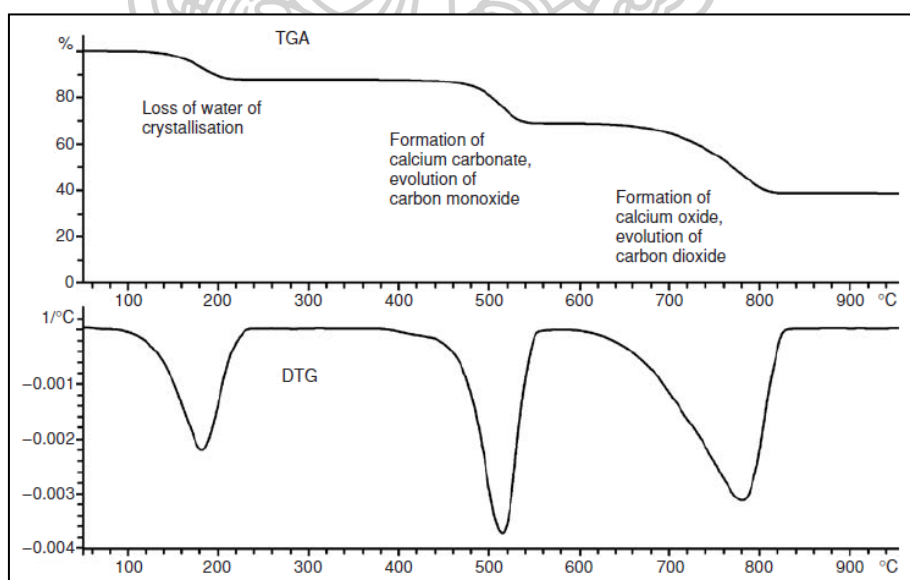


Figure 10 The TGA and DTG curves of calcium oxalate monohydrate decomposition [29].

## 2.9 Scanning electron microscopy (SEM)

Scanning electron microscope (SEM) is a powerful magnification tool that utilizes focused beams of electrons to obtain information. The high-resolution, three-dimensional images produced by



SEM provide topographical, morphological and compositional information makes them invaluable in a variety of science and industry applications. SEM components are shown in Figure 11.

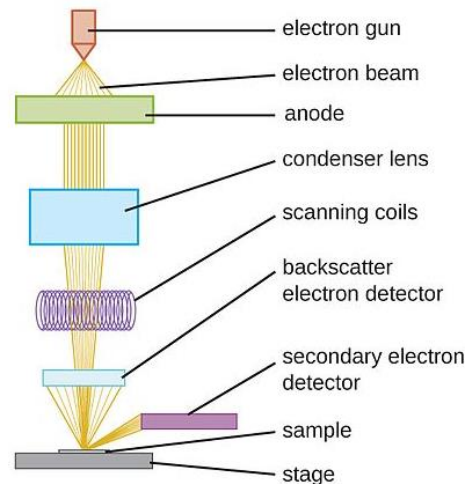


Figure 11 Schematic illustration of the components of scanning electron microscope. [30]

SEM provides details of surface information by tracing a sample in a raster pattern with an electron beam. The process begins with electrons are generated at the top of the column by the electron gun. Most samples require some preparation before being placed in the vacuum chamber. Of the variety of different preparation processes, the two most commonly used prior to SEM analysis are sputter coating for non-conductive samples and dehydration of most biological specimens. In addition, all samples need to be able to handle the vacuum chamber in which the vacuum protects the electron source from being contaminated, it also allows the user to acquire a high-resolution image. The scatter patterns made by the interaction yield information on size, shape, texture and composition of the sample and the interaction of electrons with a sample can result in the generation of two types of electrons used for imaging are the backscattered (BSE) and the secondary electrons (SE). BSE as well as x-rays which are incidental electrons reflected backwards which images provide composition data related to element and compound detection. Diffracted backscatter electrons determine crystalline structures as well as the orientation of minerals and micro-fabrics. SEM produces black and white, three-dimensional images with a magnification up to 10 nm resolution. Although SEM is not as powerful as its TEM counterpart, the intense interactions that take place on the surface of the specimen provide a greater depth of view, higher-resolution and, ultimately, a more detailed surface picture [31, 32].

## 2.10 Transmission electron microscopy (TEM)

Transmission electron microscope (TEM) utilizes energetic electrons to provide morphological, compositional and crystallographic information of samples. At a maximum potential magnification of 1 nm, TEMs are the most powerful microscopes allowing for a wide range of educational, science and industry applications. TEM components are shown in Figure 12.

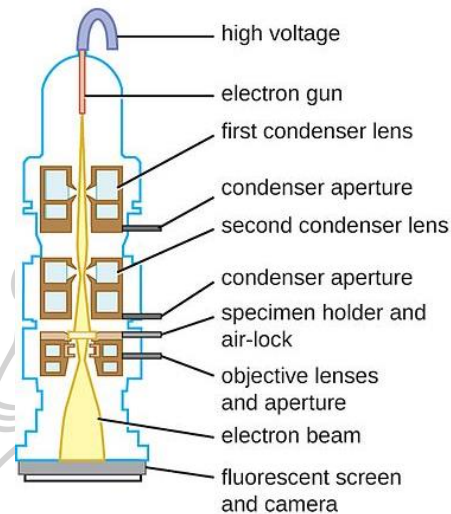


Figure 12 Schematic illustration of the components of transmission electron microscopes. [30]

TEM produces high-resolution, two-dimensional images, and black-white image from the interaction that takes place between prepared samples and energetic electrons in the vacuum chamber. TEM has three essential parts obtain first is an electron gun, which produces the electron beam, and the condenser system, which focuses the beam onto the object, second is the image-producing system, consisting of the objective lens, movable specimen stage, and intermediate and projector lenses, which focus the electrons passing through the specimen to form a real, highly magnified image, and the image-recording system, which converts the electron image. The speed of electrons directly correlates to electron wavelength which the faster electrons move, the shorter wavelength and the greater the quality and detail of the image. The lighter areas of the image represent the places where a greater number of electrons were able to pass through the sample and the darker areas reflect the dense areas of the object. These differences provide information on the structure, texture, shape and size of the sample. To obtain a TEM analysis, samples need to be sliced thin enough for electrons to pass through, a property known as electron transparency. Samples need to be able to withstand the vacuum chamber and often require special preparation before viewing [32].



## 2.11 Ultraviolet-visible spectroscopy

Ultraviolet and visible spectrometers have been in general use for the last 35 years. In many applications, other techniques could be employed but none rival UV-visible spectrometry for its simplicity, versatility, speed, accuracy and cost-effectiveness. In general, there are two major measurement techniques which are quantitative and qualitative analyses.

The spectrophotometer provides a beam of monochromatic radiation to illuminate a sample and so measures the ratio  $I / I_0$  where  $I_0$  is the intensity of the incident radiation and  $I$  is the intensity of the transmitted radiation. The ratio  $I / I_0$  is called transmittance (T).

Follow the Beer-Bouguer-Lambert law:

$$T = I / I_0 = e^{-kbc} \quad (\text{eq.1})$$

Mathematically, absorbance (A) is related to transmittance (T) by the expression:

$$A = -\log T = -\log(I / I_0) = \log(I_0 / I) = \epsilon bc \quad (\text{eq.2})$$

where  $e$  is the base of natural logarithms,  $k$  is a constant,  $b$  is the path length (usually in centimeters),  $c$  is the concentration of the absorbing species (usually expressed in grams per liter or milligrams per liter) and  $\epsilon$  is the molar absorption or extinction coefficient.

The conventional single-beam spectrophotometer consists of the component parts shown in Figure 13. There are many combinations of sources, monochromators, measuring systems etc. which can be assembled to form integrated spectrophotometers with varying degrees of accuracy and suitability for applications [33].

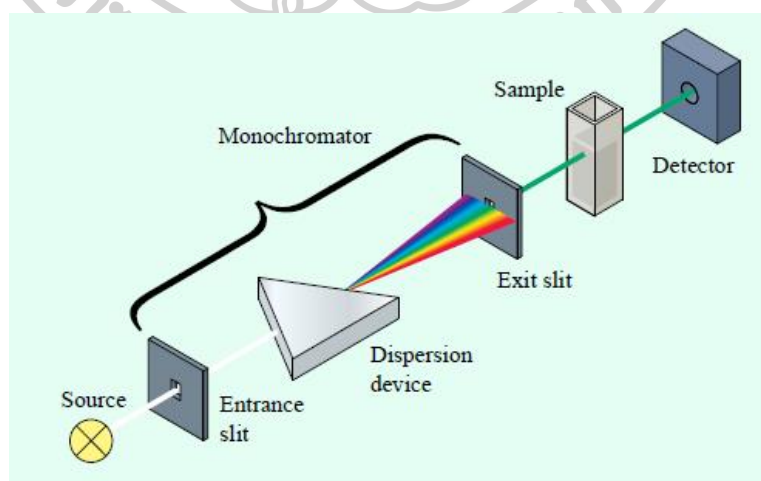


Figure 13 Schematic of a conventional spectrophotometer.[33].

## 2.12 X-Ray diffraction (XRD)

The atomic planes of a crystal cause an incident beam of X-rays to interfere with one another as they leave the crystal. The phenomenon is called X-ray diffraction. XRD is a non-destructive technique to identify crystalline phases and orientation, determine structural properties and atomic arrangement, and measure thickness of thin films and multi-layers. X-ray scattering equipment typically have the following components: an X-ray source, collimation, sample positioning system, detector and data-analysis software [32, 34].

The diffracted intensities are recorded as a function of the scattering vector (or momentum transfer)  $q$ , which is related to the scattering angle  $2\theta$  by the relation:

$$q = (4\pi \sin \theta) / \lambda \quad (\text{eq.3})$$

When coherently scattered X-rays from atoms in neighboring planes interfere with each other, then Bragg's law holds:

$$n\lambda = 2d \sin \theta \text{ or } d = 2\pi / q \quad (\text{eq.4})$$

where  $d$  is the distance between the atomic planes (d-spacing),  $\lambda$  is the wavelength,  $n$  is an integer.

Value of  $n=1$  corresponds to the reflection of the first order for a given set of atomic planes. The second and higher orders of reflections occur at larger values of  $2\theta$ . Illustration of the geometry used for the simplified derivation of Bragg's law is shown in Figure 14.

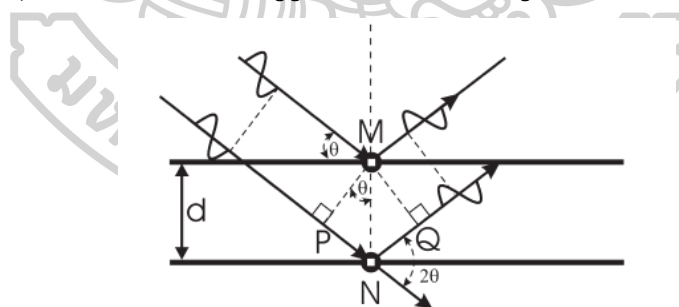


Figure 14 Illustration of the geometry used for the simplified derivation of Bragg's law [34].

## 2.13 Fourier transform infrared spectroscopy (FTIR)

Fourier Transform Infrared Spectrometer (FTIR) is widely used to identify organic (and in some cases inorganic) materials which the infrared absorption bands identify molecular components and structures and can be hyphenated to chromatography, the mechanism of chemical reactions and the detection of unstable substances can be investigated with such instruments.

A common FTIR spectrometer consists of an IR source, interferometer, sample compartment, detector, amplifier, A/D convertor, and a computer. The source generates radiation

passes the sample through the interferometer and reaches the detector. The signal is amplified and transformed to a digital signal by the amplifier and analog-to-digital converter, respectively. Eventually, the Fourier Transform converts the detector output to an interpretable spectrum which that analysts can use to identify or quantify the material. Figure 15 is a diagram of the FTIR spectrometer.

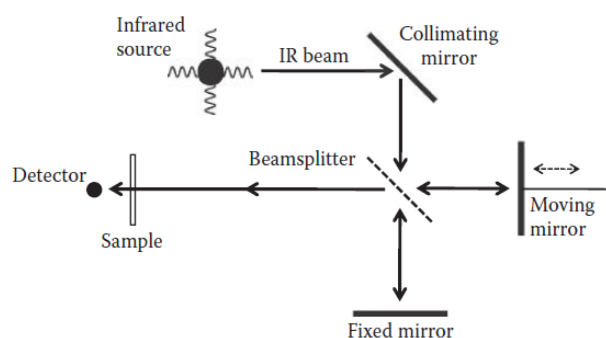


Figure 15 The optical diagram of FTIR spectrometer [35].

Since different molecules with different combination of atoms produce their unique spectra, infrared spectroscopy can be used to qualitatively identify substances. In addition, the intensity of the peaks in the spectrum is proportional to the amount of substance present, enabling its application for quantitative analysis.

#### 2.14 Photocatalytic activity

Photocatalysis is a reaction which uses light to activate the catalyst which increases the rate of a reaction by reducing the activation energy. The photocatalytic properties are derived from the formation of photogenerated charge carriers (hole and electron) which basic steps taking place in a photocatalytic cycle: light absorption (i), electron excitation (ii), electron and hole migration (iii), oxidation and reduction reactions (iv), or geminate electron recombination (v) [36] as shown in Figure 16.

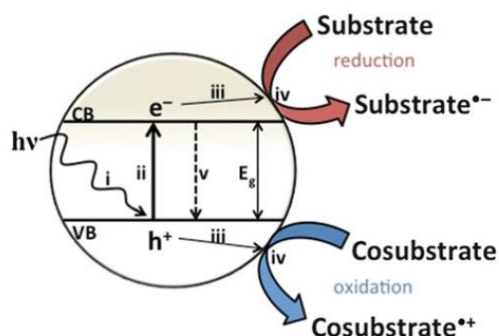
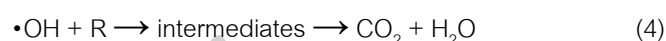
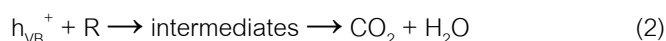


Figure 16 Elementary steps taking place in a photocatalytic cycle [36].

One of the most common photocatalytic process using UV/TiO<sub>2</sub> which is based on adsorption of photons with energy higher than 3.2 eV or wavelengths lower than ~390 nm. The mechanism for photocatalytic reactions consists of several intermediate steps which are shown below:



where R represents the organic compound.

Equation (1) shows excitation step, resulting in an electron in the conductive band ( $e_{\text{CB}}^-$ ) and formation of a positive hole in the valence band ( $h_{\text{VB}}^+$ ). The  $h_{\text{VB}}^+$  reacts with organic compounds resulting in their oxidation end products; CO<sub>2</sub> and H<sub>2</sub>O as shown in equation (2). After that the  $h_{\text{VB}}^+$  reacts with water to generate hydroxyl radical ( $\cdot\text{OH}$ ) in equation (3). Eventually, hydroxyl radical ( $\cdot\text{OH}$ ), an electrophilic nature, is converted to CO<sub>2</sub> and water as shown in equation (4). The conductive band can react with O<sub>2</sub> forming an anion radical superoxide as shown in equation (5) [37].

### 2.15 Antimicrobial activity assay

Antimicrobial or antibacterial refers to the inhibition of bacterial growth and reproduction. The photocatalytic process of TiO<sub>2</sub> has been known for its ability to kill both Gram-positive and Gram-negative bacteria which exhibit bactericidal properties through reactive oxygen species (ROS) generation from the mechanism for photocatalytic reactions. The aggressive superoxide ions ( $\text{O}_2^{\cdot-}$ ) are generated by the CB electron reduces, and the holes accelerate hydroxyl radical ( $\cdot\text{OH}$ ) formation on the material surface. These active radicals subsequently inhibit the growth of germs and bacteria that are known to be antimicrobial active through the direct oxidation of intracellular coenzyme, reducing the respiratory activity and thereby causing cell death [38].

## CHAPTER 3

### LITERATURE REVIEWS

#### 3.1 TiO<sub>2</sub> particles

Titania is considered the best choice for general photocatalytic needs as it fits other desirable criteria. TiO<sub>2</sub> is cheap, nontoxic, photolytically and chemically stable, and reusable with a high turnover rate [2]. TiO<sub>2</sub> is a large band semiconductor, anatase and rutile which energy band gap are 3.2 and 3.0 eV, respectively have been focused on photocatalytic studies [16]. Anatase TiO<sub>2</sub> possesses the higher photocatalytic activity of the degradation of organic compounds than rutile TiO<sub>2</sub> due to its structure that has a deeper region and more potential compared with the rutile phase [39]. Various reports have established that TiO<sub>2</sub> is much more effective as a photocatalyst in the form of nanoparticles than in bulk powder [40], related to the band gap of nanoparticles that smaller than that of bulk powder [41]. Hee Dong Jang et al. [6] reported a higher degree of decomposition of methylene blue by the TiO<sub>2</sub> nanoparticles under the illumination of the black light as the particle size decreased and anatase mass fraction increased. In addition, TiO<sub>2</sub> possesses strong bactericidal activity both gram-positive and gram-negative bacteria [42].

#### 3.2 TiO<sub>2</sub> immobilization

Various polymer materials have been used as support for TiO<sub>2</sub> such as PVA [43], polyvinyl chloride (PVC) [44], polyaniline (PANI) [45], poly 1-naphthylamine (PNA) [46], and poly-3-hydroxybutyrate (P(3HB)) [47] to reduce both cost and time consuming in post-treatment separation for TiO<sub>2</sub> recovery. TiO<sub>2</sub> catalyst requires long settling time and efficient solid-liquid (phase) separation, thus it is usually lost in the separation process [48, 49]. Nanthini Sridewi et al. [47] reported that P(3HB)-TiO<sub>2</sub> nanocomposite photocatalytic films showed good decolorization performance due to evenly distributed TiO<sub>2</sub> particles on the surface of P(3HB) films, which yielded almost 100% color removal. The photocatalytic films were able to completely decolorize real industrial batik dye wastewater in 3 h.

#### 3.3 PVA/TiO<sub>2</sub> composite films

PVA has several advantages such as chemical resistance, water solubility, biodegradability, substantial tensile strength and superior flexibility and hardness. PVA is a water-soluble polymer. The water solubility and physical properties of PVA, including its film forming, are highly affected by the degree of hydrolysis, molecular weight, and its crystallinity [11]. Recently, several researchers prepared TiO<sub>2</sub> immobilized PVA film, which concentration of TiO<sub>2</sub> was less than 20 wt% [4, 5, 50-54].

A.M.Shehap et al. [39] reported that there were hydrogen bonding between OH groups of PVA and titanium ions resulting in charge transfer complex formation. For photocatalytic application, Ping Lei et al. [4] reported that the photocatalytic activity of the PVA/TiO<sub>2</sub> composite films evaluated from the degradation rate of methyl orange (MO) in an aqueous solution exhibited a remarkable ultraviolet (UV) photocatalytic activity approximately close to the TiO<sub>2</sub> slurry system. In addition, the good swelling ability of PVA matrix provided the MO molecules with more opportunities to fully contact with TiO<sub>2</sub>, thus benefited the photocatalysis. For antibacterial application, Shivani Singh Surah et al. [42] reported that PVA/TiO<sub>2</sub> nanocomposite films possessed antimicrobial activity against *E.coli* and *pseudomonas* bacteria which depicted their use in food packaging and preserving surfaces.

### 3.4 Surfactant

Several methods have been used to modify the surface of TiO<sub>2</sub> particles to improve dispersion of particles [55-57], and to enhance their ability in removal of contamination from aqueous solutions [58, 59]. One of commonly methods is the adsorption of surfactant on the particles. Tahereh Fereidooni Moghadam et al. [55] reported that sodium dodecyl sulfate as anionic surfactant improved dispersion of ZnO nanoparticles in aqueous SDS solution by using an ultrasonic. Yeari Song et al. [57] reported that SDBS surfactant plays the roles of exfoliator and stabilizer by binding to the graphene surface, resulting in good dispersion stability of graphene in both water and organic solvents. Ping Zhang et al. [59] found that SDS surface-modified mesoporous ZnFe<sub>2</sub>O<sub>4</sub> nanoparticles had a remarkably high maximum adsorptive capacity for aqueous MB removal, whereas unmodified ZnFe<sub>2</sub>O<sub>4</sub> nanoparticles suffered from particle agglomeration, which reduced surface area.

### 3.5 Thermal treatment

Thermal treatment of PVA at high temperature causes dehydration and hydrogen bond formation between OH groups in PVA, resulting in increased its crystallinity. Mohammad Saied Enayati et al. [60] found that thermal treatment at 180 °C appeared to be an effective way for the large increase of crystallinity and cross-linking of PVA. Several works studied the thermal treatment of PVA/TiO<sub>2</sub> composite films and found the crystallite development with thermal treatment as same as that of pure PVA [52-54]. In addition, Ti-O-C chemical bond formation via dehydration reaction between TiO<sub>2</sub> and PVA appeared during the thermal treatment process [4, 51]. Emanuela Filippo et al. [51] studied the preparation of TiO<sub>2</sub>/PVA hybrid nanoparticles with thermal treatment at 180°C for 2 h. They found the crystalline form of TiO<sub>2</sub> nanoparticles remained unchanged during the thermal treatment and the active –OH groups on the surface of TiO<sub>2</sub> begin to react with the –OH groups in

PVA molecular chains through dehydration reaction. Therefore, the conjugated PVA chains could be linked firmly onto the  $\text{TiO}_2$  surfaces through C–O–Ti bonds.





## CHAPTER 4

### EXPERIMENTAL PROCEDURE

This chapter describes methodology of the research including the chemicals used in the experiment, sample preparation and sample characterization of PVA/TiO<sub>2</sub> composite films.

#### 4.1 Material

##### 4.1.1 Polyvinyl alcohol (PVA)

PVA (a molecular weight range of 77,000-82,000) in a clear colored flake form was produced by Ajax Finechem, Australia.

##### 4.1.2 Titanium dioxide (TiO<sub>2</sub>)

TiO<sub>2</sub> micro size particles (anatase phase) with a mean diameter of 80 nm and TiO<sub>2</sub> nano size particles (anatase phase) with a mean diameter of 20 nm, both in the form of white powder, were produced by Sigma-Aldrich Company.

##### 4.1.3 Sodium dodecyl benzene sulfonate (SDBS)

SDBS, off-white to light yellow powder or a flake was produced by Sigma-Aldrich Company.

##### 4.1.4 Sodium dodecyl sulfate (SDS)

SDS in the form of cream-colored flakes, crystals or powder was produced by Carlo Erba Reagents Company.

##### 4.1.5 Methylene blue (MB)

MB in the form of dark blue powder was produced by Ajax Finechem, Australia.

##### 4.1.6 Deionized (DI) water

DI water was solvent. Ion-free water was obtained by filtering through DI water purifier (MEDICA EDI 15/30, Elga, England).

#### 4.2 Sample preparation

##### 4.2.1 Part I: Study properties of PVA/TiO<sub>2</sub> composite films

The PVA/TiO<sub>2</sub> composite films with 0.5, 1, 5, and 10 wt% of TiO<sub>2</sub> microparticles without and with surfactant were prepared. TiO<sub>2</sub> microparticles were dispersed in either 50 mL DI water or aqueous SDBS using the weight ratios of TiO<sub>2</sub>:SDBS at 1:1 and 1:2 in 50 mL DI water. The mixture was heated to 80°C, added with 2 g of PVA, and then continuously stirred at 80°C for 3 h. After that, the mixture was sonicated with ultrasonic bath (Figure 17) for 1 h before casting onto a petri dish glass (Figure 18). The solvent was evaporated in an oven (Figure 19) at 60°C for 12 h. Finally, the dried composite films were collected with the thickness of ~80 μm and characterized. Some



PVA/TiO<sub>2</sub> composite films were further subjected to thermal treatment at 180°C for 2 h in the oven before characterization.

#### 4.2.2 Part II: Study properties of PVA/TiO<sub>2</sub> nanocomposite films

The PVA/TiO<sub>2</sub> nanocomposite films with 0.5, 1, 2, 4, and 5 wt% of TiO<sub>2</sub> nanoparticles without and with surfactant were prepared. TiO<sub>2</sub> nanoparticles were dispersed in either 50 mL DI water or aqueous surfactant solution (SDBS or SDS) using the weight ratios of TiO<sub>2</sub>:surfactant at 1:1 in 50 mL DI water. The mixture was heated to 80°C, added with 2 g of PVA, and then continuously stirred at 80°C for 3 h. After that, the mixture was sonicated with ultrasonic bath (Figure 17) for 1 h before casting onto a petri dish glass (Figure 18). The solvent was evaporated in an oven (Figure 19) at 60°C for 12 h. Finally, the dried nanocomposite films were collected with the thickness of ~80 μm and characterized. Some PVA/TiO<sub>2</sub> nanocomposite films were further subjected to thermal treatment at 180°C for 2 h in the oven before characterization.



Figure 17 Ultrasonic bath.



Figure 18 Petri dish glass.



Figure 19 Oven.

### 4.3 Sample characterization

#### 4.3.1 Transmission electron microscope (TEM)

TEM (JEM-1230, JEOL, USA) was used to observe the average size of  $\text{TiO}_2$  particles. The  $\text{TiO}_2$  particles were prepared in a colloidal suspension form and were dropped onto a TEM grid and simply allowed to dry then detected with an accelerating voltage of 80 kV.

#### 4.3.2 Scanning electron microscopy (SEM)

SEM (MIRA3, TESCAN, Czech) was used to observe the morphology and dispersion of  $\text{TiO}_2$  particles in PVA matrix of the composite films. All samples were coated with gold and detected by backscattered electrons (BSE) with an accelerating voltage of 10 kV.

#### 4.3.3 Universal tensile testing

Universal tensile testing (EZ-LX model, Shimadzu, Japan), as shown in Figure 20, was used to examine mechanical properties of the composite films following ASTM D882. The specimen size was 120 x 15 mm and gage length 100 mm. The tensile test was performed at a crosshead speed of 50 mm/min. The results obtained represented the average of the results of five samples.

#### 4.3.4 Differential scanning calorimeter (DSC)

DSC (SDT Q600, TA Instruments, UK), as shown in Figure 21, was used to characterize thermal behavior of the composite films. The composite films obtained from solution casting method were cut into small pieces of a mass range between 5-10 mg and were placed in aluminum pans. The measurement was carried out in a nitrogen atmosphere at temperature range of 180-250°C at heating rate of 10°C/min.

#### 4.3.5 Thermogravimetric analysis (TGA)

TGA (SDT Q600, TA Instruments, UK), as shown in Figure 22, was used to characterize thermal stability and thermal degradation process of the composite films. The composite films obtained from solution casting method were cut into small pieces of a mass range between 10-15 mg. The measurement was carried out in a nitrogen atmosphere at temperature range of 50-600°C at heating rate of 10°C/min.

#### 4.3.6 Ultraviolet-visible spectroscopy (UV-vis)

UV-vis spectrophotometer (Cary 5000, Varian, USA), as shown in Figure 23, was used to evaluate UV absorption of the composite films in the wavelength range of 200-800 nm. UV-vis spectrophotometer (T92+, PG Instruments, UK), as shown in Figure 31, was used to measure UV absorption of MB aqueous solution in the wavelength range of 200-800 nm to determine the photocatalytic activity of the composite films.

#### 4.3.7 Fourier-transform infrared spectroscopy (FTIR)

FTIR (Nicolet 6700, Thermo Scientific, USA), as shown in Figure 24 was used to measure the surface functional groups of samples in the wavenumber range from 400 to 4000  $\text{cm}^{-1}$ .

#### 4.3.8 X-ray diffraction (XRD)

XRD (D8 advance, Bruker, USA) operated at 40 kV and 30 mA with wavelength about 0.154 nm was used to examine diffraction pattern of samples. Samples were scanned in the  $2\theta$  range from 20 to 80° with a step size of 0.02°.

#### 4.3.9 Photocatalytic activity test

PVA/TiO<sub>2</sub> composite film with a size of 50 x 100 mm was dipped into 300 mL MB aqueous solution (10 mg/L) and irradiated with 4 UV lamps (UVC at 253.7 nm peak wavelength). During the photocatalytic reaction, 5 mL of MB solution was taken out at fixed intervals to determine MB concentration using UV-vis spectrophotometer.

#### 4.3.10 Antimicrobial activity assay

The film sample (1 g) with size dimension 50 x 50 mm was swelled 24 h in DI water before test according to the ASTM E2149-13a protocol. *Escherichia coli* and *Staphylococcus aureus* were cultured in flask at 35°C for 48 h. Then, 10 mL of *Escherichia coli* and *Staphylococcus aureus* suspension with concentration  $3.5 \times 10^5$  and  $1.5 \times 10^5$  cells/ml was added into a test tube contained the film sample, and agitated in an orbital mixer at 250 rpm for 24 h at 35°C. After serial dilution, the

numbers of viable cells of bacteria (CFU) were determined by plate counting on agar and used to calculate the following percentage reduction and log reduction;

$$\% \text{ Reduction} = \frac{C-A}{C} \times 100$$

$$\text{Log}_{10} \text{ bacterial reduction} = \text{Log}_{10} C - \text{Log}_{10} A$$

Where, A and C are CFU per milliliter after the specified contact time for flask containing the treated substrate and untreated substrate, respectively.



Figure 20 Universal tensile testing (EZ-LX model, Shimadzu, Japan).



Figure 21 TA Instruments (SDT Q600, TA Instruments, UK).



Figure 22 UV-vis spectrophotometer (Cary 5000, Varian, USA).



Figure 23 UV-vis spectrophotometer (T92+, PG Instruments, UK).



Figure 24 Fourier-transform infrared spectroscopy (Nicolet 6700, Thermo Scientific, USA).



## CHAPTER 5

### RESULTS AND DISCUSSION

This research studied the effects of surfactant, thermal treatment and TiO<sub>2</sub> particles size on the properties of the PVA/TiO<sub>2</sub> composite film. The photocatalytic activity of PVA/TiO<sub>2</sub> nanocomposite film for the degradation of methylene blue, as well as the efficiency in inhibition of bacterial growth was evaluated. The chapter was divided into three sections. The first section was characterization of TiO<sub>2</sub> particles. The second section studied the effects of surfactant and thermal treatment on the properties of PVA/TiO<sub>2</sub> composite films in which TiO<sub>2</sub> is micro size particles (anatase phase). The ratio of TiO<sub>2</sub>: surfactant (SDBS) was varied. Their photocatalytic efficiency by removal MB was also studied. The last section compared the effect of surfactants (SDBS and SDS) on the properties of PVA/TiO<sub>2</sub> composite films in which TiO<sub>2</sub> is nano size particles (anatase phase). Their photocatalytic efficiency by removal MB including their antimicrobial activity were studied.

#### 5.1 Characterization TiO<sub>2</sub> particles

Figure 25 shows the XRD spectra of TiO<sub>2</sub> particles which their patterns were similar to those found in literature [61]. XRD spectrum of TiO<sub>2</sub> anatase structure occurs mainly about 2 $\theta$  = 25.3°. The average crystalline size of microparticles and nanoparticles was 56.72 and 13.72 nm, respectively, as calculated from Scherrer formula:

$$D_p = \frac{(0.94 \times \lambda)}{(\beta \times \cos\theta)}$$

where, D<sub>p</sub> = average crystallite size,  $\beta$  = line broadening in radians,  $\theta$  = Bragg angle and  $\lambda$  = X-ray wavelength which default value of wavelength of laser is 0.15418 (Cu K-alpha).

Figure 26 shows TEM images of TiO<sub>2</sub> particles. The diameter of TiO<sub>2</sub> microparticle was varied from 40 to 120 nm, whereas the diameter of TiO<sub>2</sub> nanoparticle was around 20 nm.

Figure 27 shows SEM images of TiO<sub>2</sub> particles. The microparticles showed loose agglomerate, whereas the nanoparticles showed poorer dispersion and agglomeration than the microparticles.



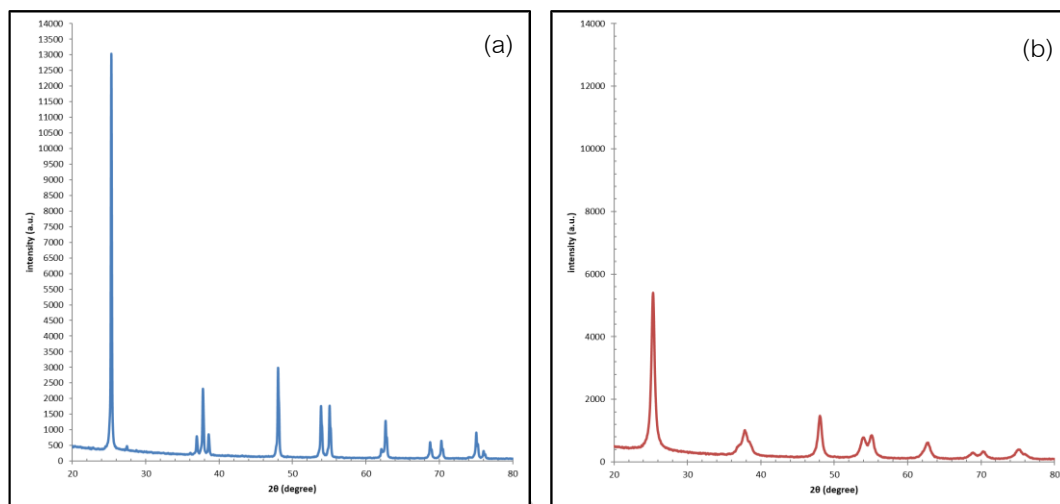


Figure 25 XRD pattern of  $\text{TiO}_2$  (a) microparticles and (b) nanoparticles.

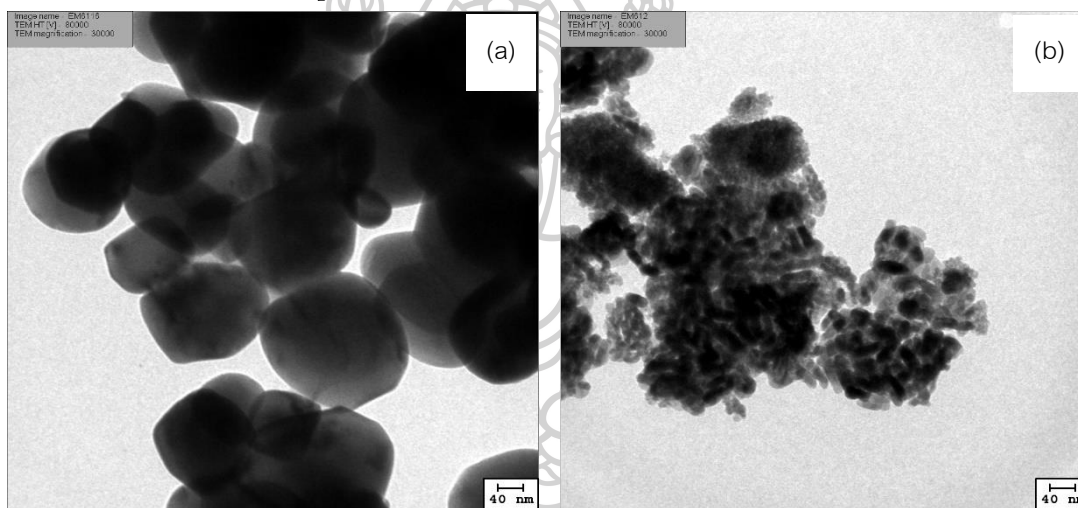


Figure 26 TEM image of  $\text{TiO}_2$  (a) microparticles and (b) nanoparticles.

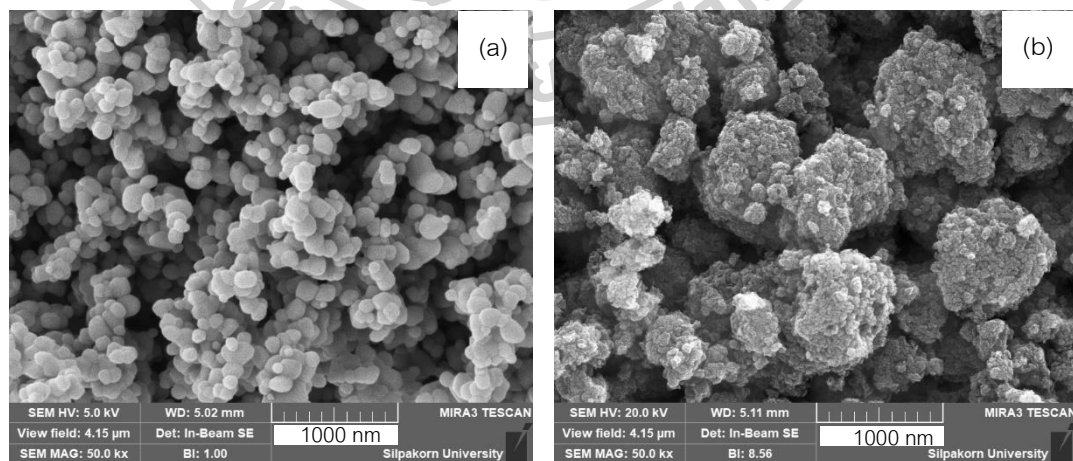


Figure 27 SEM image of  $\text{TiO}_2$  (a) microparticles and (b) nanoparticles.

## 5.2 PVA/TiO<sub>2</sub> composite films

### 5.2.1 The dispersion of TiO<sub>2</sub> particles in PVA matrix.

Figures 28 and 29 show SEM images at the bottom surface of PVA/TiO<sub>2</sub> composite films with varied SDBS and TiO<sub>2</sub> amounts. The agglomeration of TiO<sub>2</sub> particles increased with increased TiO<sub>2</sub> content. The poor dispersion of TiO<sub>2</sub> in the PVA matrix was clearly observed when the TiO<sub>2</sub> amount was greater than 5 wt%. The PVA/TiO<sub>2</sub> composite films with TiO<sub>2</sub>:SDBS (1:1) showed better TiO<sub>2</sub> dispersion than PVA/TiO<sub>2</sub> composite films without SDBS at the same amount of TiO<sub>2</sub>. However, the dispersion of TiO<sub>2</sub> became poorer with increasing SDBS to the TiO<sub>2</sub>: SDBS ratio of 1:2 as seen agglomeration of TiO<sub>2</sub> particles due to the higher micelle concentration of SDBS than critical micelle concentration [62].

### 5.2.2 FTIR analysis

The FTIR was used to obtain information on the surface chemistry of PVA and PVA/TiO<sub>2</sub> composite films before and after thermal treatment according to the changes in the vibration modes and the band position between 400-4000 cm<sup>-1</sup>. The FTIR spectra of TiO<sub>2</sub> microparticles, PVA film and PVA/TiO<sub>2</sub> composite films before and after thermal treatment as shown in Figures 30 and 31, respectively, appeared no difference in the absorption band of PVA and TiO<sub>2</sub> when compared with that previously reported [43]. The broad of O-H absorption band was observed around 3000-3600 cm<sup>-1</sup> for PVA and new peaks at 1580 cm<sup>-1</sup> and 1730 cm<sup>-1</sup> clearly appeared after thermal treatment which indicated C=C formation by dehydration and C=O formation of condensates of aldehydes by thermo oxidative decomposition of PVA, respectively [53, 63]. The absorption band of TiO<sub>2</sub> particles observed in the region of 500-900 cm<sup>-1</sup> corresponding to the vibration of Ti-O-Ti group increased with increasing TiO<sub>2</sub> content. The thermal treatment improved the interaction between TiO<sub>2</sub> and PVA chains as observed decreased intensity of the O-H group of PVA and increased intensity of Ti-O groups after thermal treatment [64]. Moreover, a peak at 1095 cm<sup>-1</sup> involving C-O stretching of PVA also decreased as increased TiO<sub>2</sub> content.

The FTIR spectra of PVA film and PVA/TiO<sub>2</sub>-SDBS composite films with TiO<sub>2</sub>:SDBS (1:1) before and after thermal treatment are shown in Figures 32 and 33, respectively. The FTIR spectra of PVA/TiO<sub>2</sub>-SDBS composite films with TiO<sub>2</sub>:SDBS (1:1) were the same as those of PVA/TiO<sub>2</sub> composite films both before and after thermal treatment. In addition, PVA/TiO<sub>2</sub>-SDBS composite films with TiO<sub>2</sub>:SDBS (1:1) appeared a peak at 2910 cm<sup>-1</sup> of C-H stretching vibration of SDBS. This peak increased with increasing SDBS and was clearly observed in the spectrum of PVA/TiO<sub>2</sub>-SDBS



composite films with TiO<sub>2</sub>:SDBS (1:1) at 5 wt% of TiO<sub>2</sub>. Figure 34 shows FTIR spectra of PVA/TiO<sub>2</sub> and PVA/TiO<sub>2</sub>-SDBS composite films with TiO<sub>2</sub>:SDBS (1:1) and (1:2) before and after thermal treatment. The PVA/TiO<sub>2</sub>-SDBS composite films with TiO<sub>2</sub>:SDBS (1:2) after thermal treatment showed a lower absorption peak of C=C formation than TiO<sub>2</sub>:SDBS (1:1) indicating less dehydration of PVA in thermal treatment by the addition of SDBS.

### 5.2.3 XRD analysis

XRD spectra of TiO<sub>2</sub>, SDBS particles, PVA film, and composite films before and after thermal treatment were scanned in the 2 $\theta$  range from 20 to 80° as shown in Figures 35-42. PVA polymer exhibits a semi-crystalline structure with a main peak at 2 $\theta$  = 19.6° [60] and a new peak at 2 $\theta$  = 22.5° appeared after thermal treatment as shown in Figure 35. This new peak indicated crystallinity development after thermal treatment by water elimination in agreement with the FTIR results. Figure 36 presents XRD spectrum of TiO<sub>2</sub> particles which anatase structure occurs mainly about 2 $\theta$  = 25.3°.

Figures 36 and 37 show the XRD spectra of PVA/TiO<sub>2</sub> composite films before and after thermal treatment, respectively. The peak of TiO<sub>2</sub> crystalline observed in PVA/TiO<sub>2</sub> composites films increased as increasing TiO<sub>2</sub> content. Figures 38 and 39 show XRD spectra of PVA/TiO<sub>2</sub>-SDBS composite films with TiO<sub>2</sub>:SDBS (1:1) before and after thermal treatment, respectively. The spectra were in the same pattern as those of the PVA/TiO<sub>2</sub> composite films before and after thermal treatment. Figure 40 and 41 show the comparison of XRD pattern between PVA/TiO<sub>2</sub> and PVA/TiO<sub>2</sub>-SDBS composite films with TiO<sub>2</sub>:SDBS (1:1) and (1:2) at 5 wt% TiO<sub>2</sub> before and after thermal treatment, respectively. The addition of SDBS affected TiO<sub>2</sub> anatase structure as observed a decrease in TiO<sub>2</sub> crystalline peak in TiO<sub>2</sub>:SDBS (1:1) and (1:2). The effects was more pronounce after thermal treatment, in agreement with the previous study [65, 66] that found crystalline structure change upon SDBS addition and thermal treatment.

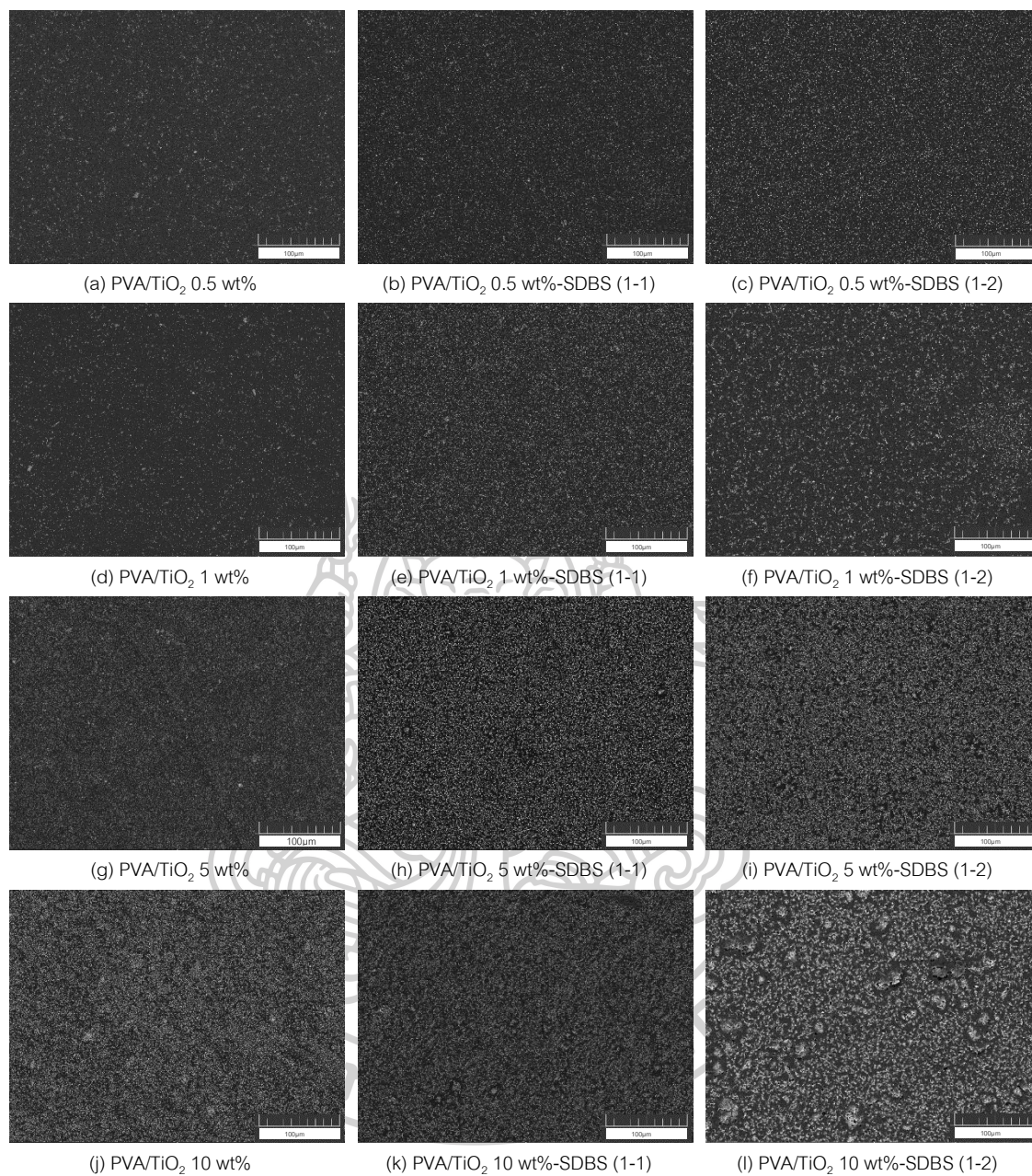


Figure 28 SEM images with BSE of PVA/TiO<sub>2</sub> composite films without and with surfactant at magnitude 500X.



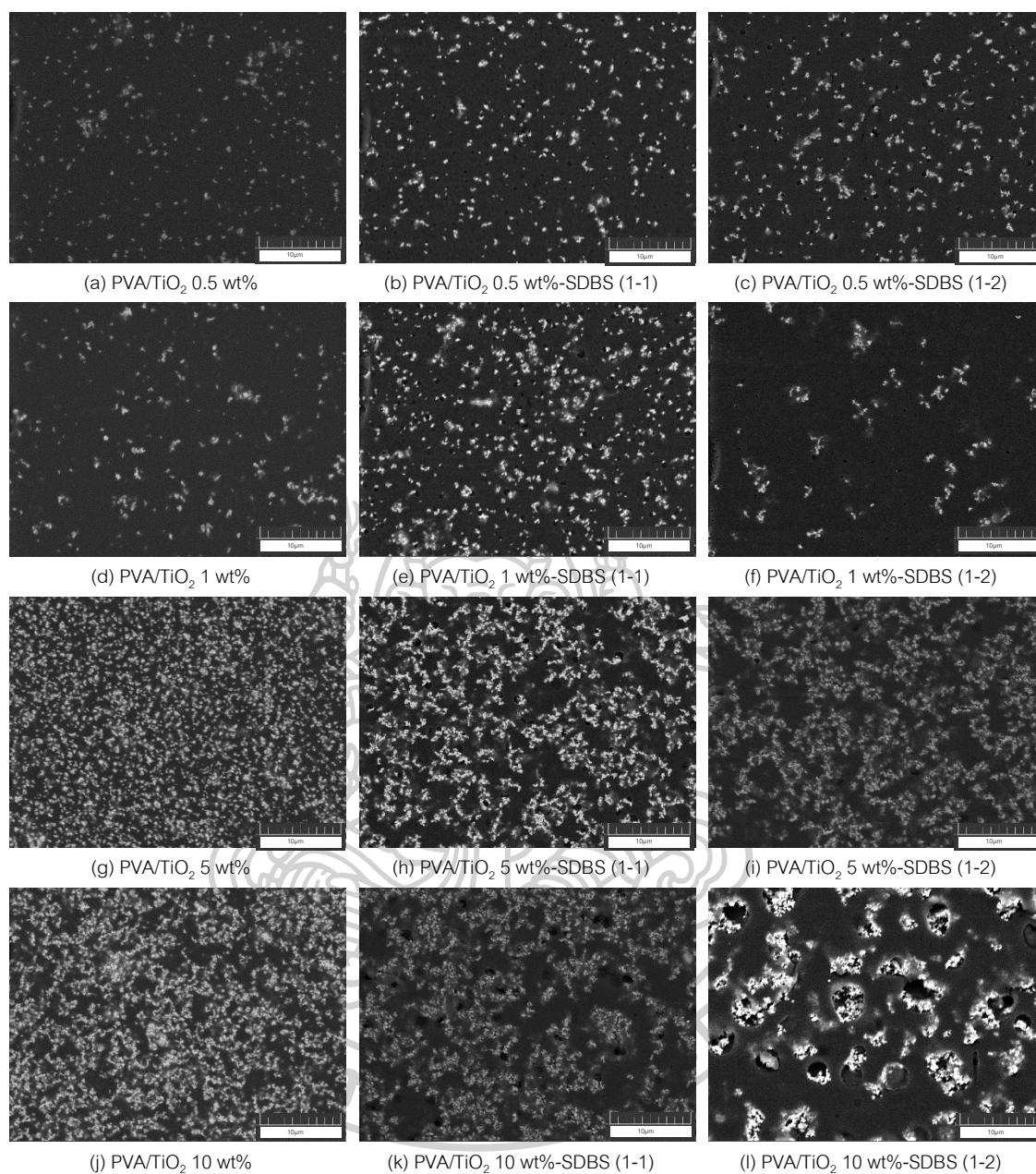


Figure 29 SEM images with BSE of PVA/TiO<sub>2</sub> composite films without and with surfactant at magnitude 5000X.

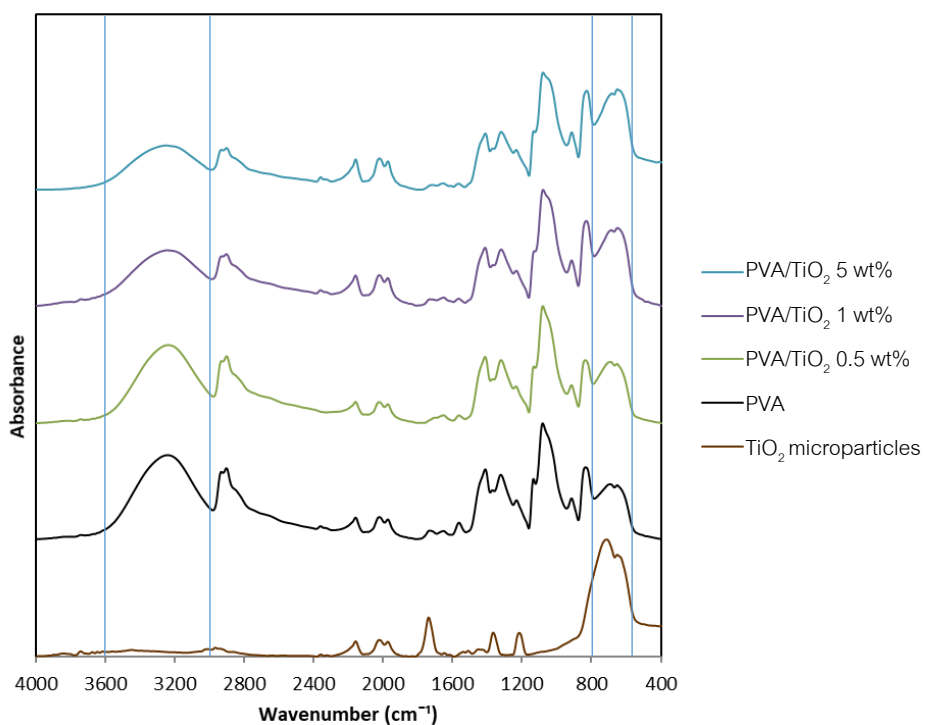


Figure 30 Infrared spectra of TiO<sub>2</sub> microparticles, PVA film and PVA/TiO<sub>2</sub> composite films.

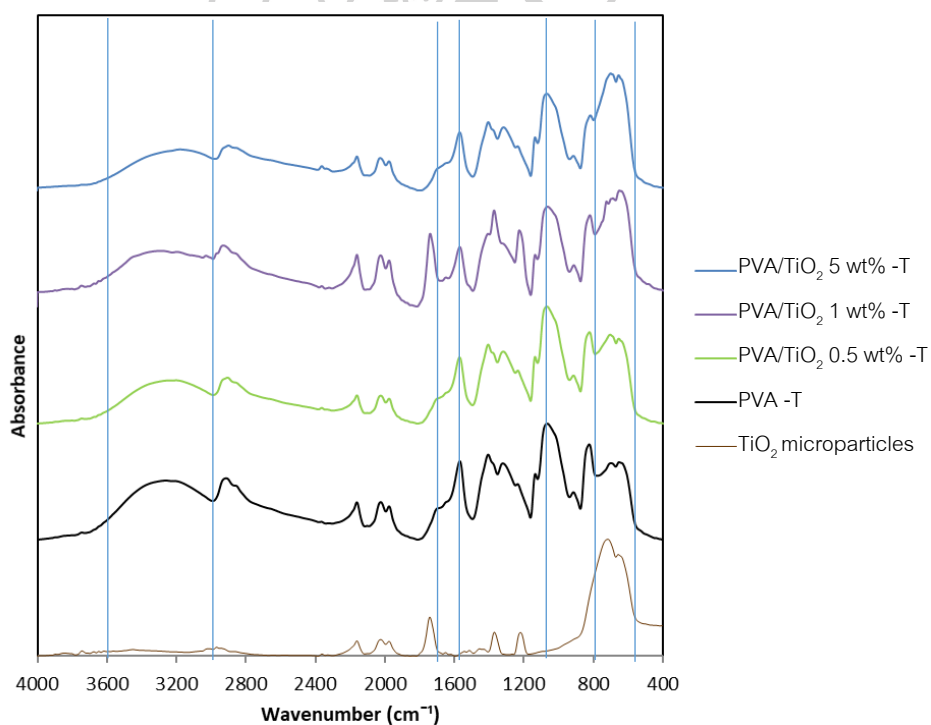


Figure 31 Infrared spectra of TiO<sub>2</sub> microparticles, PVA film and PVA/TiO<sub>2</sub> composite films after thermal treatment.

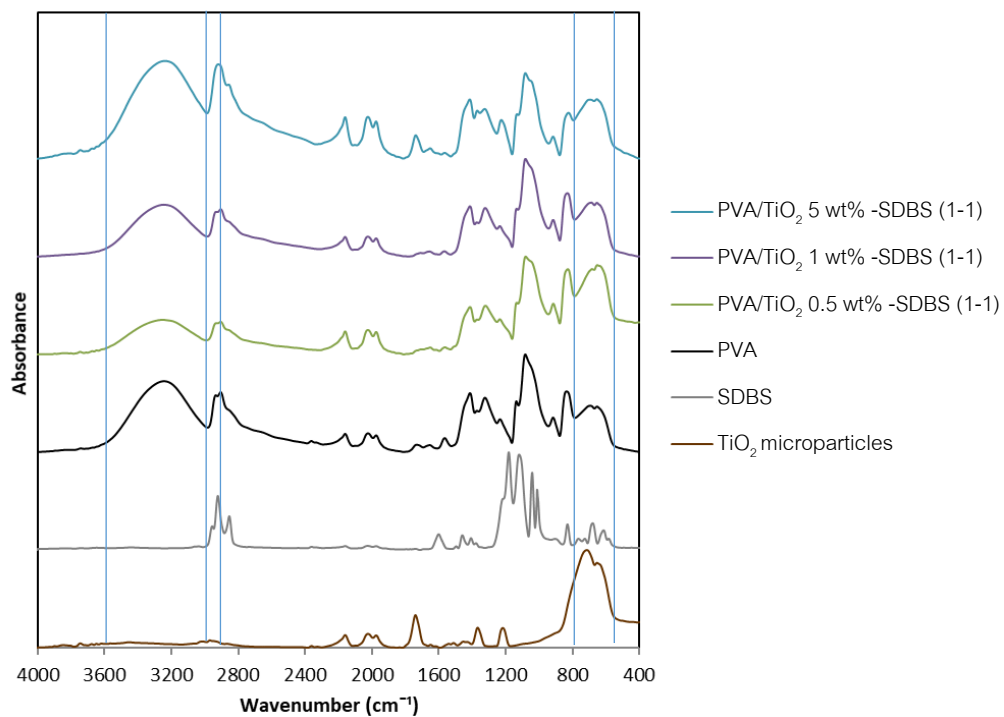


Figure 32 Infrared spectra of TiO<sub>2</sub> microparticles, SDBS, PVA film and PVA/TiO<sub>2</sub>-SDBS composite films.

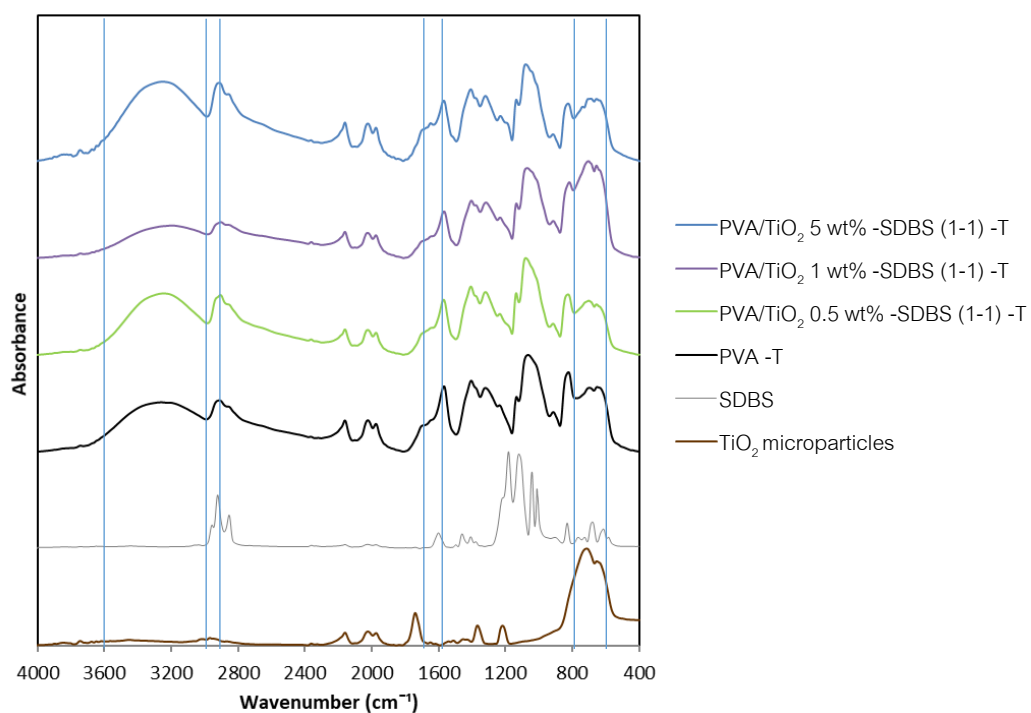


Figure 33 Infrared spectra of TiO<sub>2</sub> microparticles, SDBS, PVA film and PVA/TiO<sub>2</sub>-SDBS composite films after thermal treatment.

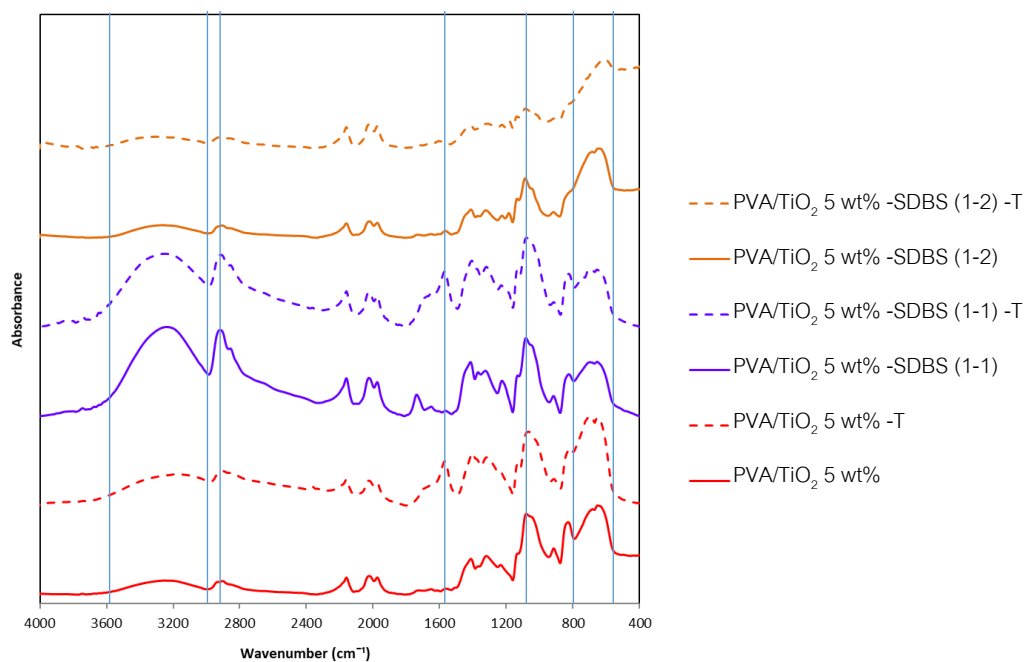


Figure 34 Infrared spectra of PVA film, PVA/TiO<sub>2</sub> and PVA/TiO<sub>2</sub>-SDBS composite films before and after thermal treatment.

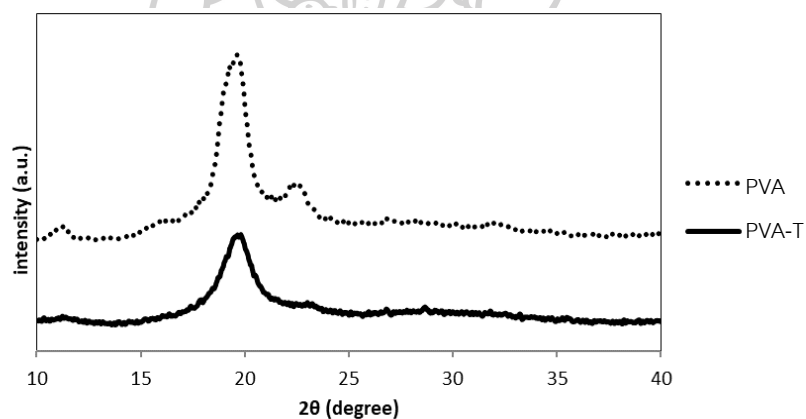


Figure 35 XRD pattern of pure PVA before and after thermal treatment

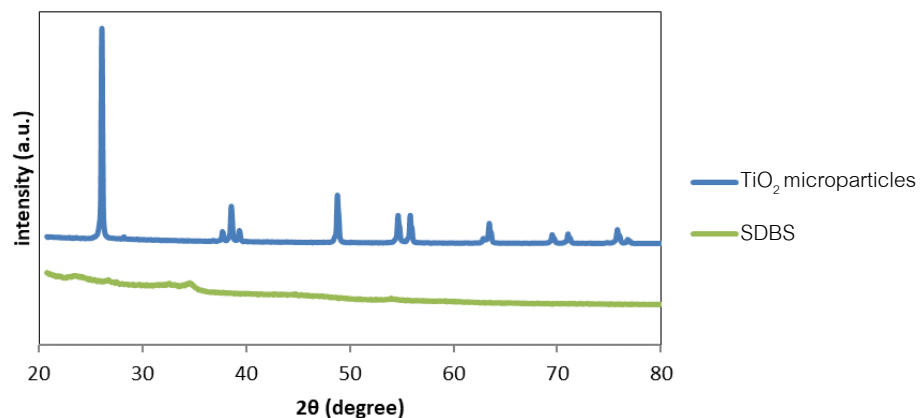
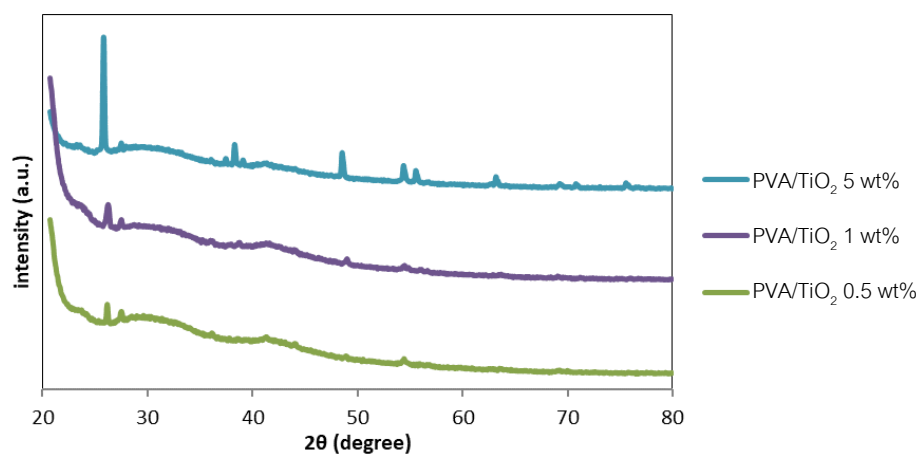
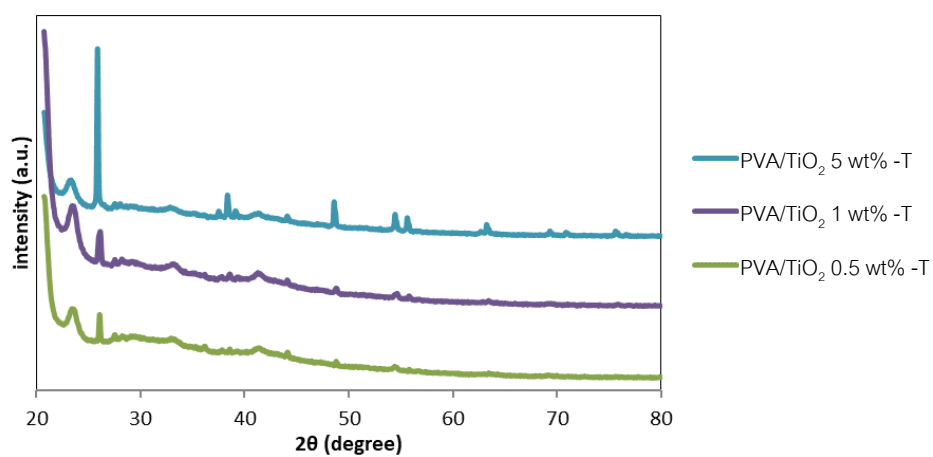
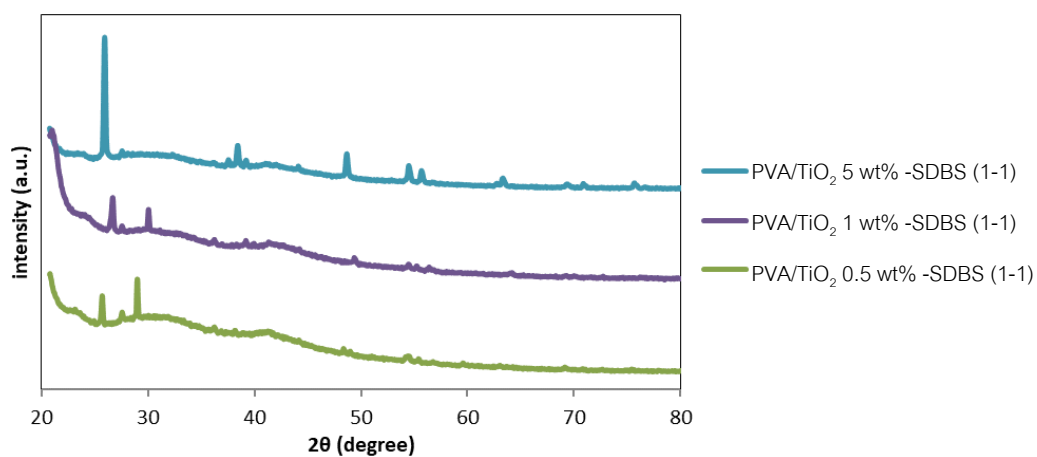


Figure 36 XRD pattern of TiO<sub>2</sub> microparticles and SDBS particles.

Figure 37 XRD pattern of PVA/TiO<sub>2</sub> composite films.Figure 38 XRD pattern of PVA/TiO<sub>2</sub> composite films after thermal treatment.Figure 39 XRD pattern of PVA/TiO<sub>2</sub>-SDBS composite films.



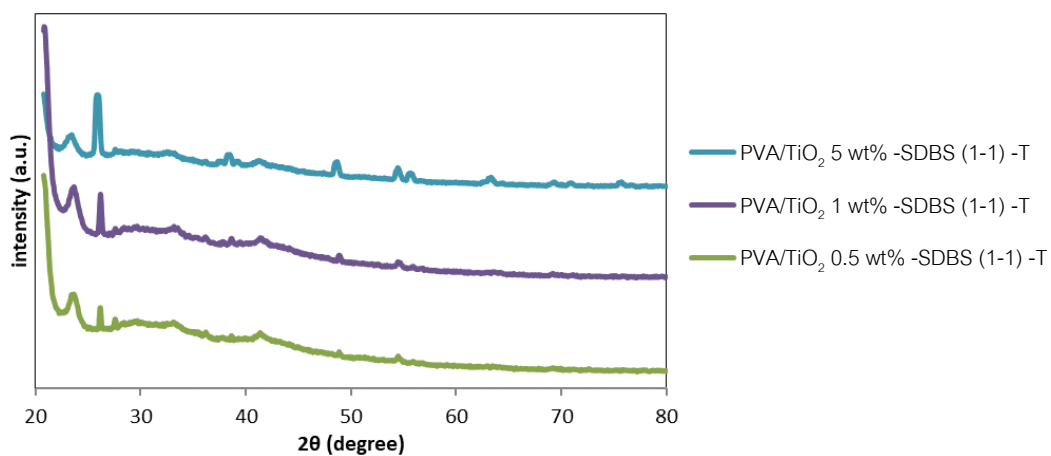


Figure 40 XRD pattern of PVA/TiO<sub>2</sub>-SDBS composite films after thermal treatment.

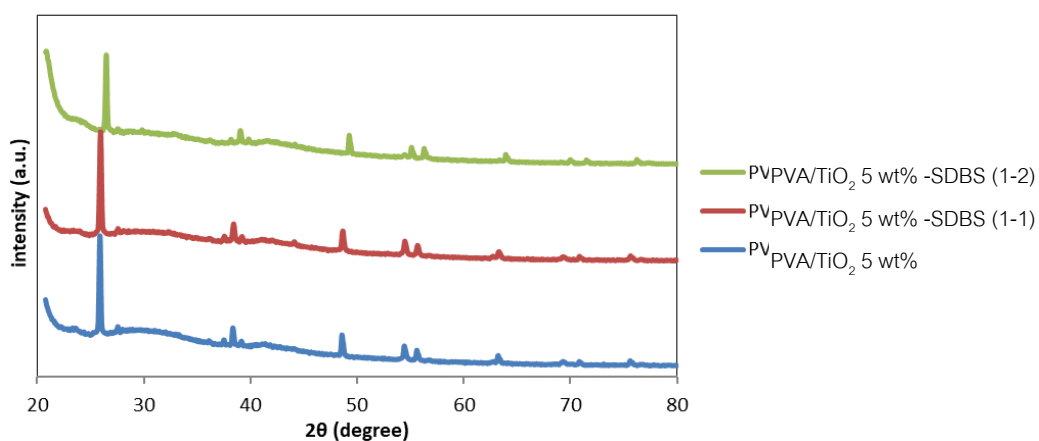


Figure 41 XRD pattern of PVA/TiO<sub>2</sub> and PVA/TiO<sub>2</sub>-SDBS composite films.

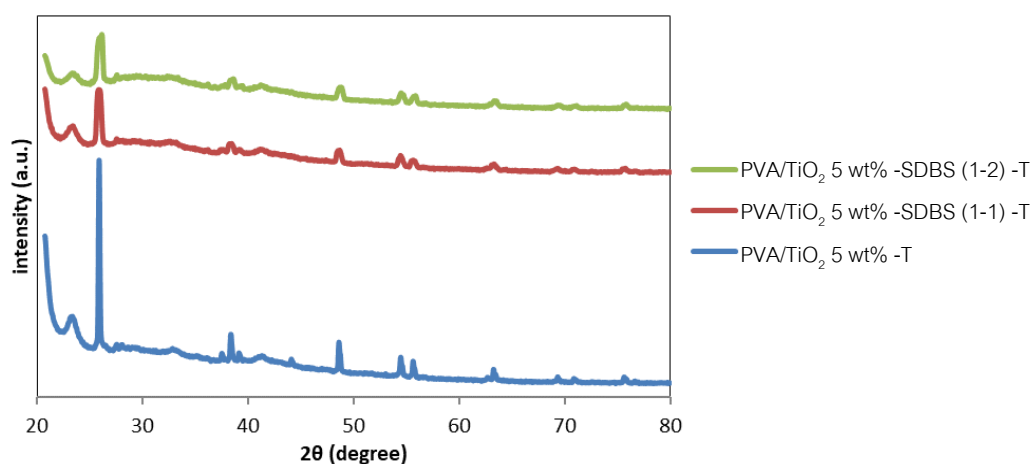


Figure 42 XRD pattern of PVA/TiO<sub>2</sub> and PVA/TiO<sub>2</sub>-SDBS composite films after thermal treatment.

#### 5.2.4 Mechanical properties

The mechanical behavior of composite films containing various TiO<sub>2</sub> contents without and with SDBS both before and after thermal treatment were tested with the tensile test. Table 2 and

Figure 43 show the tensile strength, Table 3 and Figure 44 show the strain at break and Table 4 and Figure 45 show the Young's modulus of PVA film, PVA/TiO<sub>2</sub> and PVA/TiO<sub>2</sub>-SDBS composite films before and after thermal treatment. All the mechanical properties showed the same trend, in which the addition of TiO<sub>2</sub> or SDBS did not improved the mechanical properties of PVA/TiO<sub>2</sub> composite films. The composite film with TiO<sub>2</sub>:SDBS ratio of 1:2 exhibited the poorest properties. Moreover, the mechanical properties of all films decreased after thermal treatment.

Table 2 Tensile strength of PVA film, PVA/TiO<sub>2</sub> composite films and PVA/TiO<sub>2</sub>-SDBS composite films before and after thermal treatment.

| Sample                                   | Tensile Strength (MPa)   |                         |
|--|--------------------------|-------------------------|
|  | Before thermal treatment | After thermal treatment |
| PVA                                      | 130.3 ± 10.2             | 121.3 ± 18.5            |
| PVA/TiO <sub>2</sub> 0.5 wt%             | 122.6 ± 7.8              | 151.1 ± 10.1            |
| PVA/TiO <sub>2</sub> 1 wt%               | 125.7 ± 14.3             | 140.4 ± 5.1             |
| PVA/TiO <sub>2</sub> 5 wt%               | 128.8 ± 6.7              | 127.1 ± 10.6            |
| PVA/TiO <sub>2</sub> 0.5 wt% -SDBS (1-1) | 142.6 ± 8.3              | 128.6 ± 6.7             |
| PVA/TiO <sub>2</sub> 1 wt% -SDBS (1-1)   | 141.7 ± 10.4             | 129.7 ± 13.9            |
| PVA/TiO <sub>2</sub> 5 wt% -SDBS (1-1)   | 131.4 ± 6.0              | 100.3 ± 6.9             |
| PVA/TiO <sub>2</sub> 5 wt% -SDBS (1-2)   | 107.0 ± 9.6              | 72.5 ± 12.5             |

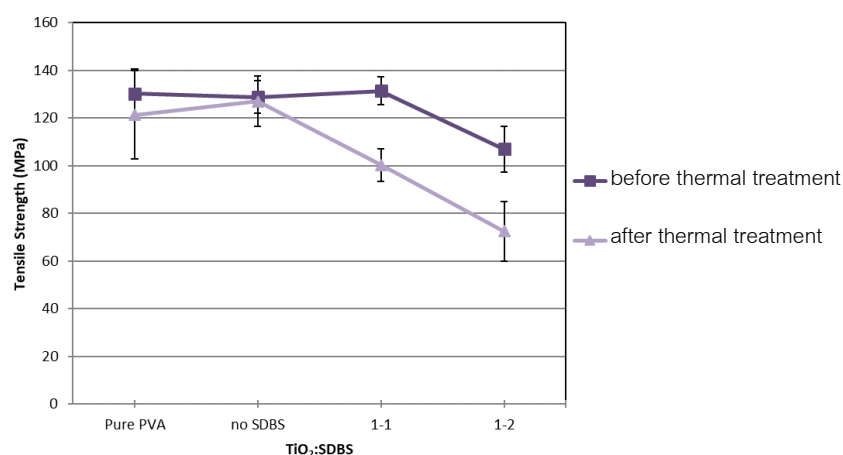


Figure 43 Tensile strength of PVA film and PVA/TiO<sub>2</sub> composite films at 5 wt% of TiO<sub>2</sub> without and with TiO<sub>2</sub>:SDBS ratios of 1:1 and 1:2 before and after thermal treatment.

Table 3 Strain at break at break of PVA film, PVA/TiO<sub>2</sub> composite films and PVA/TiO<sub>2</sub>-SDBS composite films before and after thermal treatment.

| Sample                                   | Strain at Break (%)      |                         |
|--|--------------------------|-------------------------|
|  | Before thermal treatment | After thermal treatment |
| PVA                                      | 3.22 ± 0.21              | 2.30 ± 0.50             |
| PVA/TiO <sub>2</sub> 0.5 wt%             | 3.15 ± 0.23              | 3.37 ± 0.46             |
| PVA/TiO <sub>2</sub> 1 wt%               | 2.36 ± 0.39              | 3.07 ± 0.73             |
| PVA/TiO <sub>2</sub> 5 wt%               | 2.71 ± 0.37              | 2.07 ± 0.21             |
| PVA/TiO <sub>2</sub> 0.5 wt% -SDBS (1-1) | 2.68 ± 0.23              | 2.96 ± 0.23             |
| PVA/TiO <sub>2</sub> 1 wt% -SDBS (1-1)   | 2.53 ± 0.23              | 2.66 ± 0.68             |
| PVA/TiO <sub>2</sub> 5 wt% -SDBS (1-1)   | 2.72 ± 0.14              | 2.15 ± 0.33             |
| PVA/TiO <sub>2</sub> 5 wt% -SDBS (1-2)   | 2.12 ± 0.30              | 1.71 ± 0.21             |

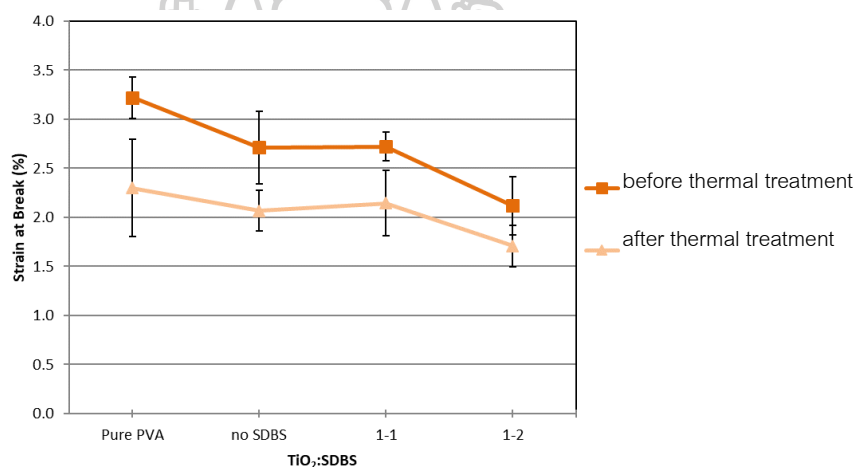


Figure 44 Strain at break at break of PVA film and PVA/TiO<sub>2</sub> composite films at 5 wt% of TiO<sub>2</sub> without and with TiO<sub>2</sub>:SDBS ratios of 1:1 and 1:2 before and after thermal treatment

Table 4 Young's modulus of PVA film, PVA/TiO<sub>2</sub> composite films and PVA/TiO<sub>2</sub>-SDBS composite films before and after thermal treatment.

| Sample                                   | Young's Modulus (MPa)    |                         |
|--|--------------------------|-------------------------|
|  | Before thermal treatment | After thermal treatment |
| PVA                                      | 7245.0 ± 354.1           | 7975.8 ± 461.3          |
| PVA/TiO <sub>2</sub> 0.5 wt%             | 7364.7 ± 535.2           | 9337.0 ± 505.8          |
| PVA/TiO <sub>2</sub> 1 wt%               | 7423.6 ± 747.8           | 7959.2 ± 509.8          |
| PVA/TiO <sub>2</sub> 5 wt%               | 7984.5 ± 185.8           | 8775.1 ± 392.4          |
| PVA/TiO <sub>2</sub> 0.5 wt% -SDBS (1-1) | 8704.0 ± 273.6           | 7311.5 ± 144.5          |
| PVA/TiO <sub>2</sub> 1 wt% -SDBS (1-1)   | 8920.8 ± 59.1            | 7630.7 ± 749.6          |
| PVA/TiO <sub>2</sub> 5 wt% -SDBS (1-1)   | 8587.1 ± 201.4           | 7062.5 ± 98.9           |
| PVA/TiO <sub>2</sub> 5 wt% -SDBS (1-2)   | 8084.5 ± 540.6           | 6491.9 ± 441.6          |

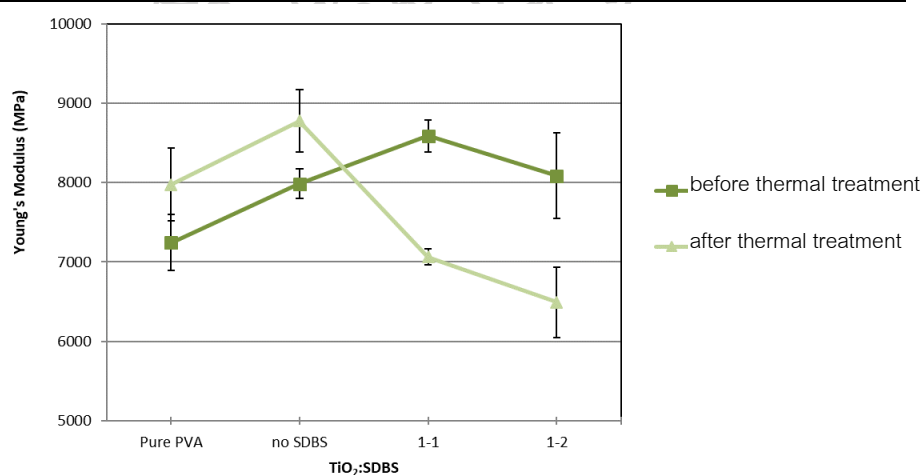


Figure 45 Young's modulus of PVA film and PVA/TiO<sub>2</sub> composite films at 5 wt% of TiO<sub>2</sub> without and with TiO<sub>2</sub>:SDBS ratios of 1:1 and 1:2 before and after thermal treatment

### 5.2.5 TGA analysis

The thermal degradation of PVA/TiO<sub>2</sub> composite films before and after thermal treatment and PVA/TiO<sub>2</sub>-SDBS composite films before and after thermal treatment are shown in Figures 46-50, respectively. The thermal degradation of the composite films before and after thermal treatment was like that of the PVA film, which proceeded by three degradation steps. The first step at temperature range 80-140°C was due to the evaporation of water. The second step around 210-370°C was a major weight loss due to the chain scission for degradation of PVA, and followed by a further breakage polymeric chain in the third step around 410-460°C [67]. It was clearly seen that the TiO<sub>2</sub>

and SDBS addition in composite film likely delayed the thermal degradation process of films by decreasing the rate of degradation in the second step which was the predominant decomposition process. The results were confirmed by determination the decomposition temperature at 50% weight loss ( $T_{d50}$ ) as presented in Table 5. As expected,  $T_{d50}$  increased with increasing  $\text{TiO}_2$  and SDBS contents, and also increased after thermal treatment. The remaining weight at temperature  $600^\circ\text{C}$  of PVA film and PVA/ $\text{TiO}_2$  composite films without and with SDBS before and after thermal treatment are shown in Table 6. The remaining weight enhanced according to  $\text{TiO}_2$  content in the film, and also increased after thermal treatment.

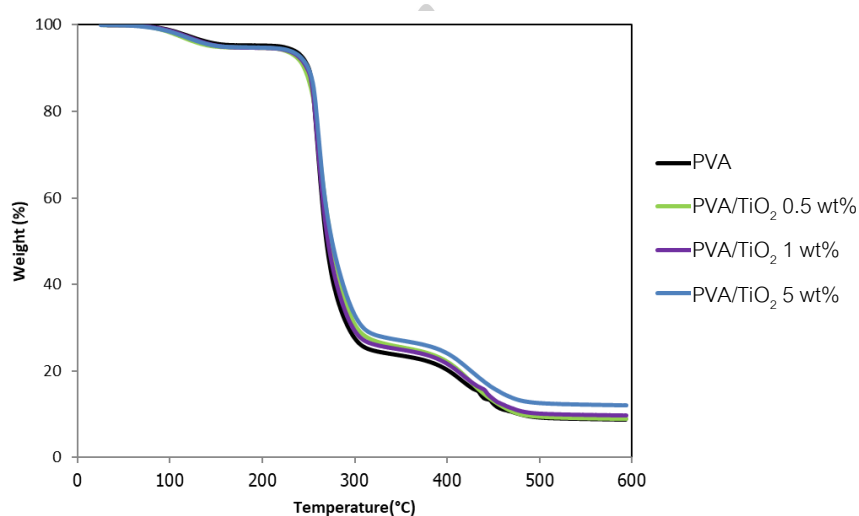


Figure 46 TGA analyses of PVA film and PVA/ $\text{TiO}_2$  composite films.

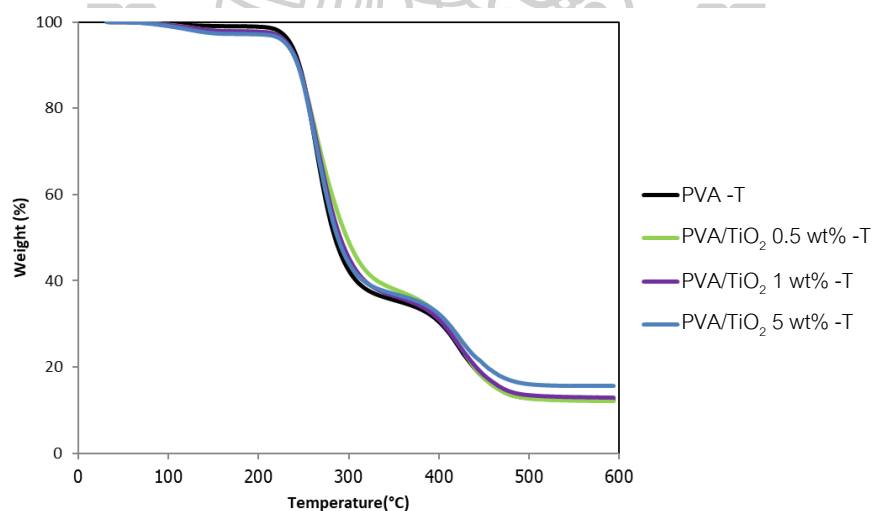


Figure 47 TGA analyses of PVA film and PVA/ $\text{TiO}_2$  composite films after thermal treatment.

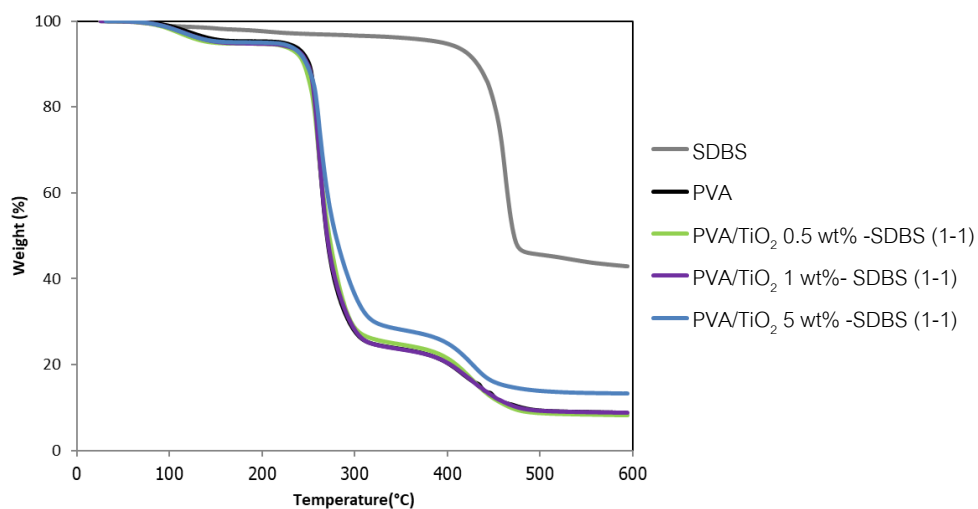


Figure 48 TGA analyses of SDBS particles, PVA film and PVA/TiO<sub>2</sub>-SDBS composite films.

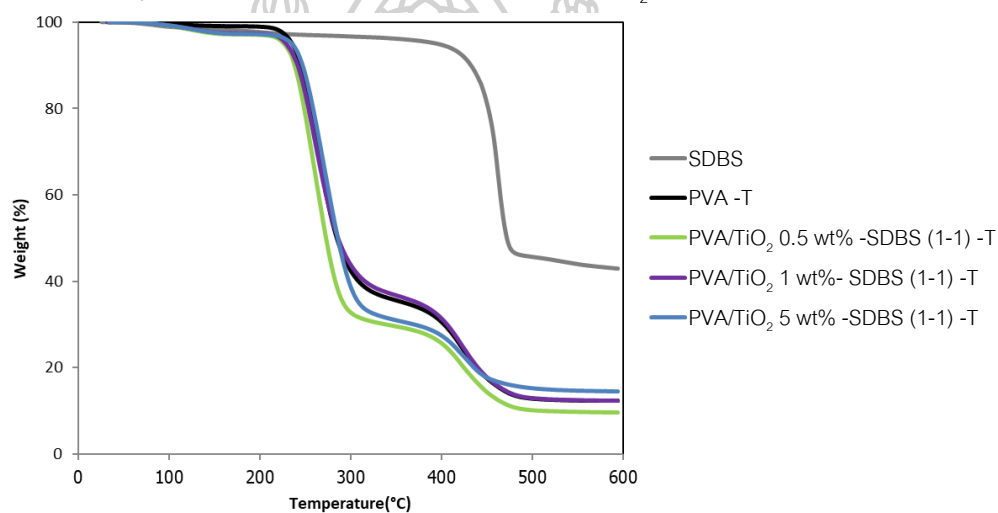


Figure 49 TGA analyses of SDBS particles, PVA film and PVA/TiO<sub>2</sub>-SDBS composite films after thermal treatment.

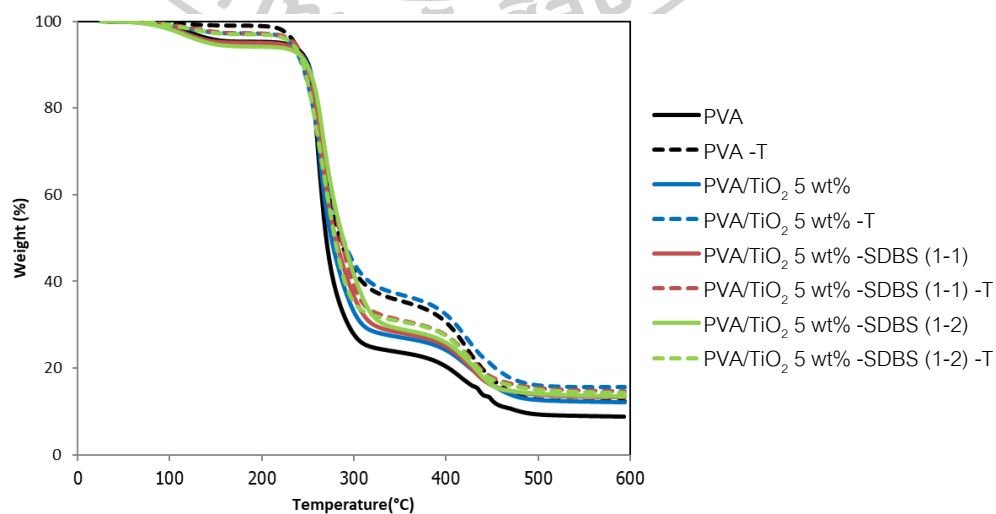


Figure 50 TGA analyses of PVA film and PVA/TiO<sub>2</sub> composite films 5 wt% of TiO<sub>2</sub> without and with TiO<sub>2</sub>:SDBS ratio 1:1 and 1:2 are compared before and after thermal treatment.

Table 5 The decomposition temperature of 50 %weight loss ( $T_{d50}$ ) of SDBS particles, PVA film, PVA/TiO<sub>2</sub> composite films and PVA/TiO<sub>2</sub>-SDBS composite films before and after thermal treatment.

| Sample                                   | $T_{d50}$ (°C)           |                         |
|--|--------------------------|-------------------------|
|  | Before thermal treatment | After thermal treatment |
| SDBS                                     | 472                      | -                       |
| PVA                                      | 270                      | 285                     |
| PVA/TiO <sub>2</sub> 0.5 wt%             | 275                      | 298                     |
| PVA/TiO <sub>2</sub> 1 wt%               | 271                      | 291                     |
| PVA/TiO <sub>2</sub> 5 wt%               | 275                      | 288                     |
| PVA/TiO <sub>2</sub> 0.5 wt% -SDBS (1-1) | 273                      | 273                     |
| PVA/TiO <sub>2</sub> 1 wt% -SDBS (1-1)   | 270                      | 286                     |
| PVA/TiO <sub>2</sub> 5 wt% -SDBS (1-1)   | 280                      | 286                     |
| PVA/TiO <sub>2</sub> 5 wt% -SDBS (1-2)   | 288                      | 279                     |

Table 6 The char yield of SDBS particles, PVA film, PVA/TiO<sub>2</sub> composite films and PVA/TiO<sub>2</sub>-SDBS composite films before and after thermal treatment.

| Sample                                   | Char yield (%)           |                         |
|--|--------------------------|-------------------------|
|  | Before thermal treatment | After thermal treatment |
| SDBS                                     | 42.9                     | -                       |
| PVA                                      | 8.7                      | 12.3                    |
| PVA/TiO <sub>2</sub> 0.5 wt%             | 8.9                      | 12.2                    |
| PVA/TiO <sub>2</sub> 1 wt%               | 9.6                      | 12.9                    |
| PVA/TiO <sub>2</sub> 5 wt%               | 12.1                     | 15.7                    |
| PVA/TiO <sub>2</sub> 0.5 wt% -SDBS (1-1) | 8.1                      | 9.6                     |
| PVA/TiO <sub>2</sub> 1 wt% -SDBS (1-1)   | 8.8                      | 12.4                    |
| PVA/TiO <sub>2</sub> 5 wt% -SDBS (1-1)   | 13.4                     | 14.6                    |
| PVA/TiO <sub>2</sub> 5 wt% -SDBS (1-2)   | 13.5                     | 14.2                    |



### 5.2.6 DSC analysis

The melting point temperature ( $T_m$ ) of PVA film, PVA/TiO<sub>2</sub> and PVA/TiO<sub>2</sub>-SDBS composite films before and after thermal treatment are shown in Table 7. The results showed no significant change between the melting point temperature of PVA/TiO<sub>2</sub> composite films without and with SDBS before and after thermal treatment. Table 8 show the percent crystallinity of PVA film, PVA/TiO<sub>2</sub> and PVA/TiO<sub>2</sub>-SDBS composite films before and after thermal treatment. The crystallinity of PVA reduced after adding TiO<sub>2</sub> and SDBS, and even more reduced after thermal treatment.

Table 7 Melting point temperature ( $T_m$ ) of PVA film, PVA/TiO<sub>2</sub> and PVA/TiO<sub>2</sub>-SDBS composite films before and after thermal treatment.

| Sample                                  | $T_m$ (°C)               |                         |
|---|--------------------------|-------------------------|
|   | Before thermal treatment | After thermal treatment |
| PVA                                     | 224.5                    | 223.1                   |
| PVA/TiO <sub>2</sub> 0.5 wt%            | 223.5                    | 222.8                   |
| PVA/TiO <sub>2</sub> 1 wt%              | 223.9                    | 223.3                   |
| PVA/TiO <sub>2</sub> 5 wt%              | 224.2                    | 222.6                   |
| PVA/TiO <sub>2</sub> 0.5 wt%-SDBS (1-1) | 223.8                    | 222.8                   |
| PVA/TiO <sub>2</sub> 1 wt%-SDBS (1-1)   | 224.2                    | 222.8                   |
| PVA/TiO <sub>2</sub> 5 wt%-SDBS (1-1)   | 223.4                    | 222.6                   |
| PVA/TiO <sub>2</sub> 5 wt%-SDBS (1-2)   | 223.7                    | 222.0                   |

Table 8 Crystallinity of PVA film, PVA/TiO<sub>2</sub> and PVA/TiO<sub>2</sub>-SDBS composite films before and after thermal treatment.

| Sample                                  | Crystallinity (%)        |                         |
|---|--------------------------|-------------------------|
|   | Before thermal treatment | After thermal treatment |
| PVA                                     | 30.4                     | 22.3                    |
| PVA/TiO <sub>2</sub> 0.5 wt%            | 26.9                     | 22.2                    |
| PVA/TiO <sub>2</sub> 1 wt%              | 28.9                     | 21.7                    |
| PVA/TiO <sub>2</sub> 5 wt%              | 26.0                     | 26.9                    |
| PVA/TiO <sub>2</sub> 0.5 wt%-SDBS (1-1) | 24.3                     | 19.6                    |
| PVA/TiO <sub>2</sub> 1 wt%-SDBS (1-1)   | 27.2                     | 22.2                    |
| PVA/TiO <sub>2</sub> 5 wt%-SDBS (1-1)   | 23.3                     | 19.4                    |
| PVA/TiO <sub>2</sub> 5 wt%-SDBS (1-2)   | 24.0                     | 22.3                    |

### 5.2.7 UV absorption

The UV absorption of the TiO<sub>2</sub> microparticles, PVA film, and PVA/TiO<sub>2</sub> composite films without and with SDBS both before and after thermal treatment was evaluated using a UV-Vis spectrophotometer in the wavelength range of 200-800 nm. PVA films before and after thermal treatment are shown in Figure 51. PVA film discolored after thermal treatment from colorless to brown color due to condensates of aldehydes formed by thermo oxidative decomposition [63, 68].

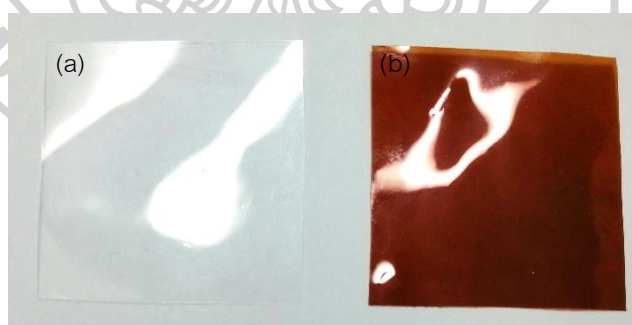


Figure 51 PVA film before (a) and after (b) thermal treatment.

Figures 52-56 show the UV absorption spectra of TiO<sub>2</sub> microparticles, PVA film, and PVA/TiO<sub>2</sub> composite films without and with SDBS before and after thermal treatment. A huge absorption band at wavelength below 350 nm belonging to TiO<sub>2</sub> absorption was observed in the composite films, which its intensity depended upon the TiO<sub>2</sub> content in the PVA/TiO<sub>2</sub> composite film. It was clearly seen that the transparency of the PVA/TiO<sub>2</sub> composite films before thermal treatment presented in the visible region (400–800 nm) decreased according to increasing TiO<sub>2</sub> content. The absorption spectra

of the films after thermal treatment showed strong absorption band in the visible region due to discoloration of the films which ascribed to the conjugated C=C bond of the polyene [54, 69], as previously observed in FTIR spectra. The comparison between absorption spectra of PVA/TiO<sub>2</sub> and PVA/TiO<sub>2</sub>-SDBS composite films with TiO<sub>2</sub>:SDBS ratios of 1:1 and 1:2 before and after thermal treatment are shown in Figure 56. The intensity of TiO<sub>2</sub> absorption band of the PVA/TiO<sub>2</sub> composite film was the highest following by PVA/TiO<sub>2</sub>-SDBS composite films with TiO<sub>2</sub>:SDBS (1:1) and (1:2), respectively. This result indicated SDBS decreased TiO<sub>2</sub> absorption.

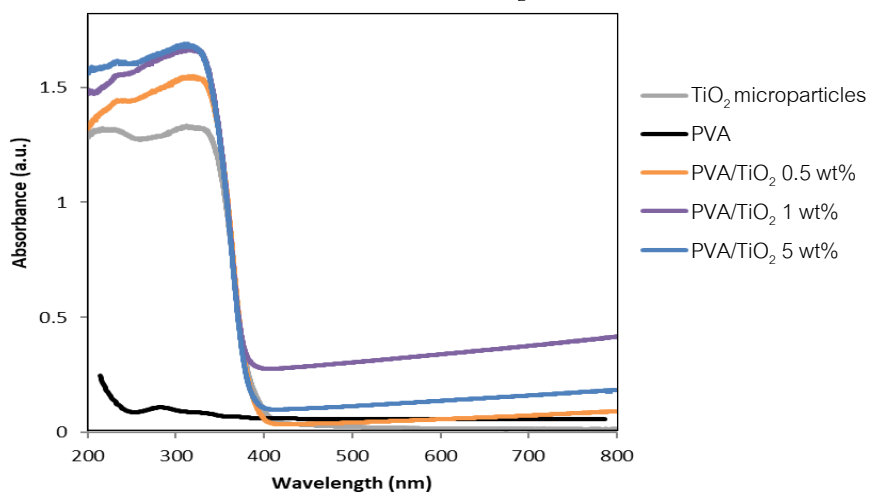


Figure 52 UV-visible absorption spectra for PVA film and PVA/TiO<sub>2</sub> composite films.

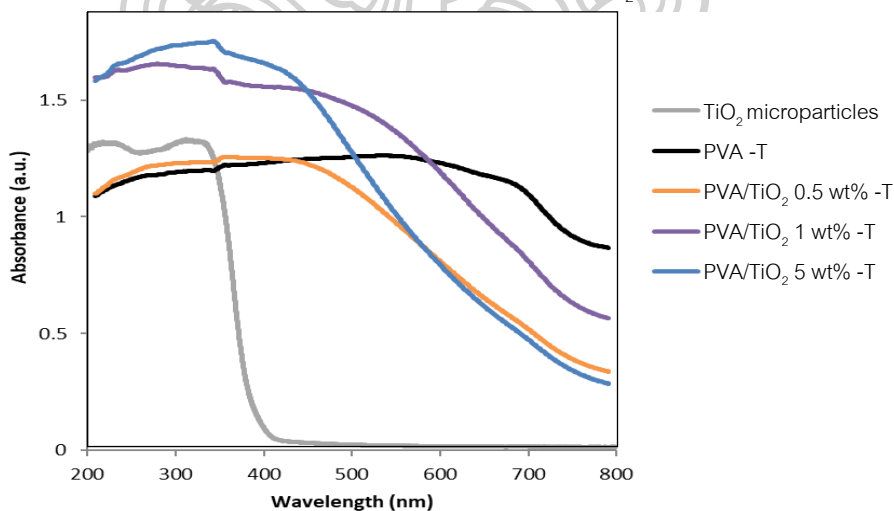


Figure 53 UV-visible absorption spectra for PVA film and PVA/TiO<sub>2</sub> composite films with thermal treatment.

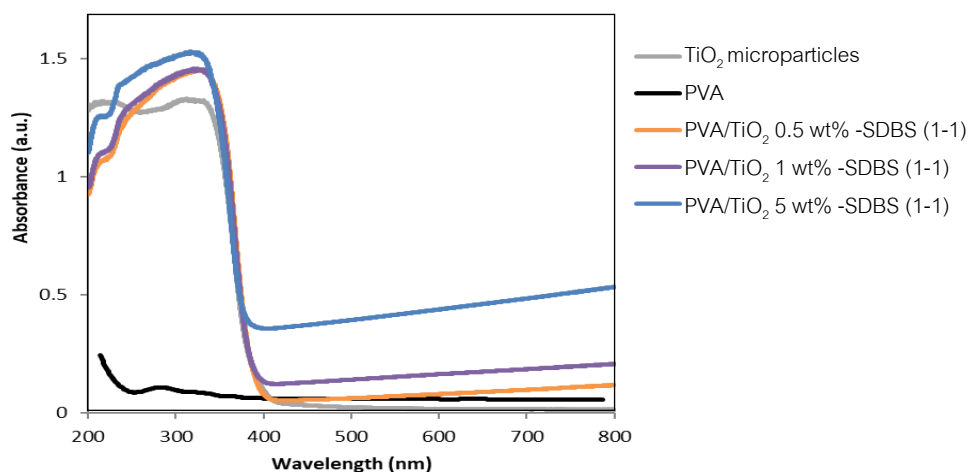


Figure 54 UV-visible absorption spectra for PVA film and PVA/TiO<sub>2</sub>-SDBS composite films.

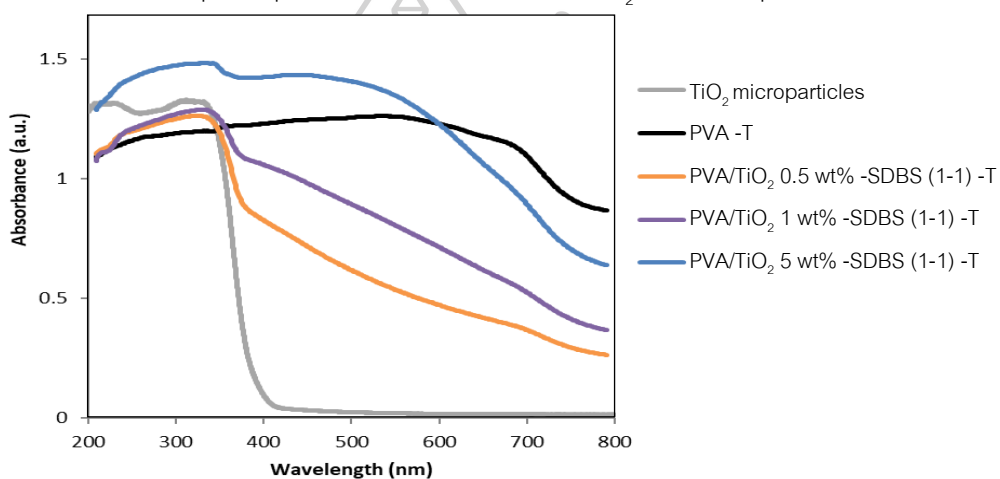


Figure 55 UV-visible absorption spectra for PVA film and PVA/TiO<sub>2</sub>-SDBS composite films with thermal treatment.

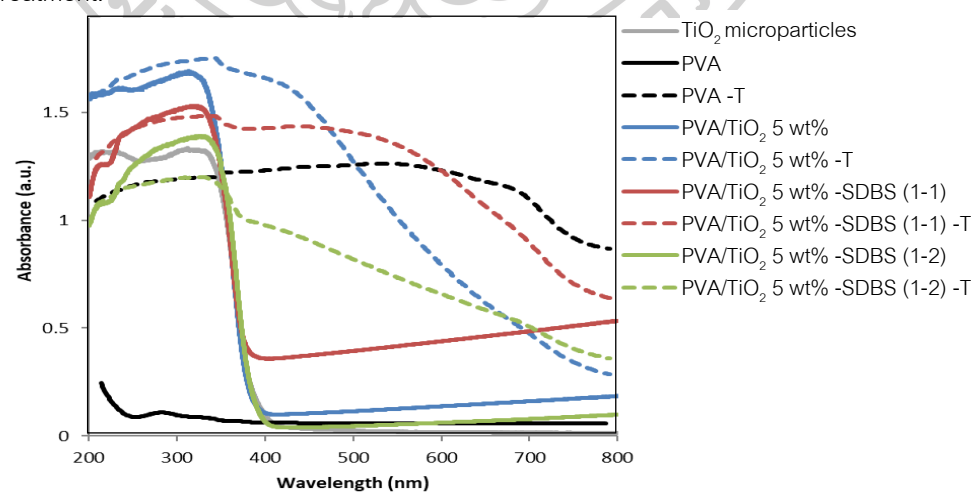


Figure 56 UV-visible absorption spectra for PVA film and PVA/TiO<sub>2</sub> composite films 5 wt% of TiO<sub>2</sub> without and with TiO<sub>2</sub>:SDBS ratio 1:1 and 1:2 are compared without and with thermal treatment.

### 5.2.8 Photocatalytic activity

The MB removal by film absorption was determined by investigation of the PVA films, before and after thermal treatment, in MB aqueous solution without UV irradiation as shown in Figure 57. The PVA film before thermal treatment showed less MB absorption than after thermal treatment. It reached full absorption after 30 min with 15% MB removal, whereas the film after thermal treatment reached full absorption after 180 min with 89% MB removal.

The Photocatalytic activity was determined from the efficiency of the films on the MB removal under UV light irradiation. The extent of MB removal ( $C/C_0$ ) was plotted as a function of irradiation time as shown in Figure 58-60. The PVA film without  $TiO_2$  could remove MB by adsorption [70]. The MB removal efficiency of  $TiO_2$  microparticles, which was a result of photocatalysis increased as increasing irradiation time and  $TiO_2$  content. Immobilization of  $TiO_2$  in the PVA matrix decreased MB removal efficiency due to some  $TiO_2$  particles immersed in PVA matrix [2], as observed a lower MB removal of the films than  $TiO_2$  particles. The addition of SDBS significantly improved MB removal efficiency of PVA/ $TiO_2$  composite films since its anionic structure also affected the MB removal with strong electrostatic interactions between the negatively charged surfactants modified  $TiO_2$  adsorbent and the cationic MB molecules [59]. After thermal treatment, the PVA film could absorb MB with free volume occurring from the new arrangement of the PVA chain crystalline [60, 66]. Therefore, the PVA film and PVA/ $TiO_2$  composite films without and with SDBS after thermal treatment improved MB removal by adsorption and absorption mechanism [4]. The comparison between the MB removal of PVA film, PVA/ $TiO_2$  and PVA/ $TiO_2$ -SDBS composite films at 5 wt% of  $TiO_2$  before and after thermal treatment is shown in Figure 58. The trend of MB removal slightly increased according to irradiation time after thermal treatment which was a result of adsorption and absorption mechanism when compared with MB removal absent UV irradiation.

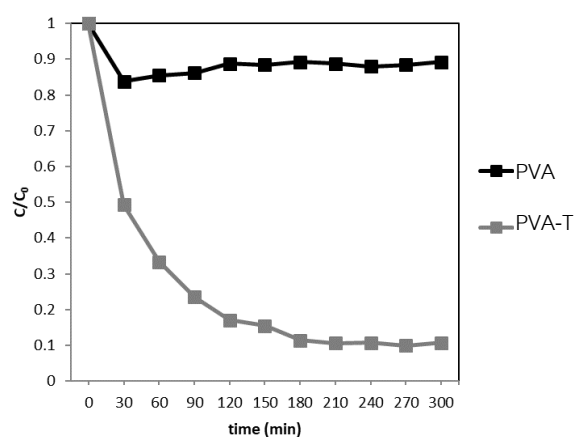


Figure 57 Extent of MB removal of PVA film before and after thermal treatment without UV irradiation.

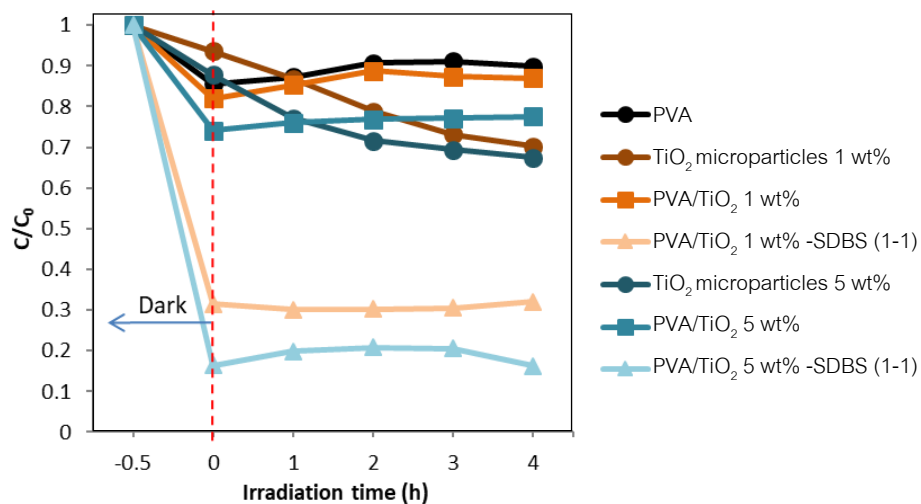


Figure 58 Extent of MB removal of PVA film, PVA/TiO<sub>2</sub> and PVA/TiO<sub>2</sub>-SDBS composite films

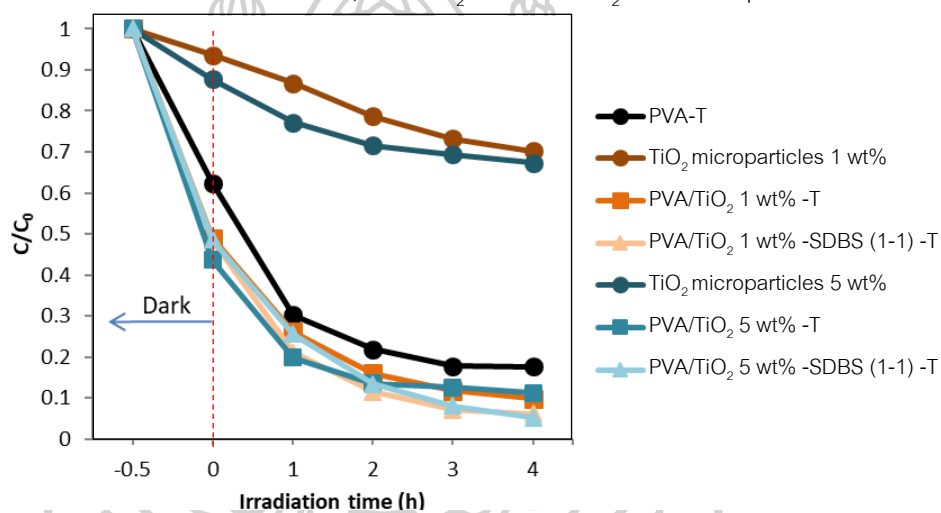


Figure 59 Extent of MB removal of PVA film, PVA/TiO<sub>2</sub> and PVA/TiO<sub>2</sub>-SDBS composite films after thermal treatment.

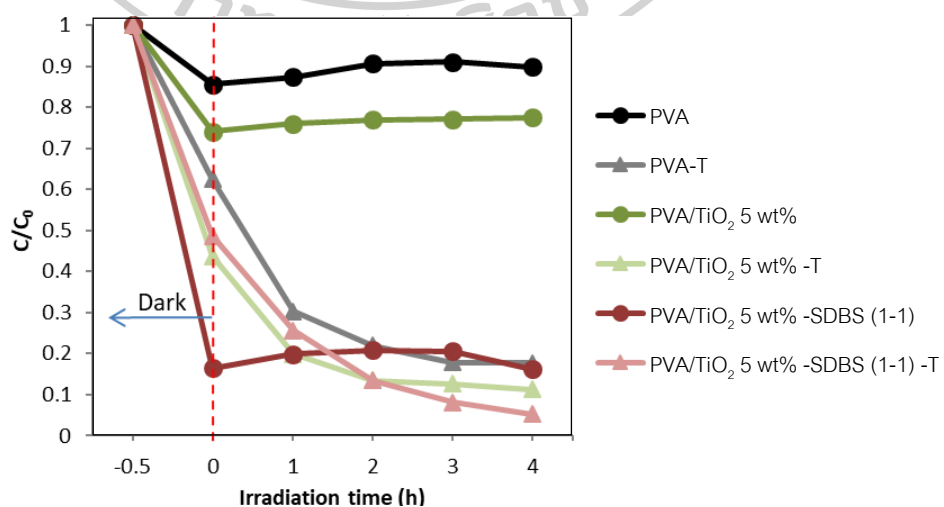


Figure 60 Extent of MB removal of PVA film, PVA/TiO<sub>2</sub> and PVA/TiO<sub>2</sub>-SDBS composite films 5 wt% of TiO<sub>2</sub> before and after thermal treatment.

From all results, it was shown that  $\text{TiO}_2$  and SDBS contents affected properties of the PVA/ $\text{TiO}_2$  composite film. The addition of SDBS resulted in the uniform  $\text{TiO}_2$  particle-dispersion in the PVA matrix, if the  $\text{TiO}_2$  content was not greater than 5 wt%. However, the increased SDBS amount to the  $\text{TiO}_2$ : SDBS ratio of 1:2 led to the poor dispersion of  $\text{TiO}_2$  particles, and hence the poor mechanical properties of the film. Therefore, the  $\text{TiO}_2$  content below 5 wt% with the  $\text{TiO}_2$ : SDBS ratio 1:1 was selected as the optimized condition for preparing the PVA/ $\text{TiO}_2$  nanocomposite films in the next section.

### 5.3 PVA/ $\text{TiO}_2$ nanocomposite films

In this section, the PVA/ $\text{TiO}_2$  composite films were prepared using nanosized  $\text{TiO}_2$  particles. The effects of surfactant types, SDBS and SDS, on the film properties were studied and compared.

#### 5.3.1 The dispersion of $\text{TiO}_2$ nanoparticles in PVA matrix.

Figures 61 and 62 show SEM images at the bottom surface of PVA/ $\text{TiO}_2$  nanocomposite films with varied SDBS, SDS and  $\text{TiO}_2$  amounts. It was observed that the addition of surfactants both SDBS and SDS could improve the dispersion ability of  $\text{TiO}_2$  nanoparticles in the PVA matrix as same as those found for PVA/ $\text{TiO}_2$  composite films.

#### 5.3.2 FTIR analysis

The FTIR spectra of  $\text{TiO}_2$  nanoparticles, PVA film and PVA/ $\text{TiO}_2$  nanocomposite films varying surfactant types and  $\text{TiO}_2$  amounts, before and after thermal treatment are shown in Figures 63-68. The spectra showed increasing  $\text{TiO}_2$  absorption band in the region of  $500\text{-}900\text{ cm}^{-1}$  with increasing  $\text{TiO}_2$  content, as previously observed for PVA/ $\text{TiO}_2$  composite films. The effect of surfactants is shown in Figure 69, in which the dehydration of PVA after thermal treatment was reduced by the addition of SDBS or SDS.

#### 5.3.3 XRD analysis

The XRD spectra of  $\text{TiO}_2$ , SDBS, SDS particles, and nanocomposite films before and after thermal treatment were scanned in the  $2\theta$  range from  $20$  to  $80^\circ$  as shown in Figures 70-77. Figure 70 shows the XRD spectrum of  $\text{TiO}_2$  nanoparticles anatase structure which main peak occurs about  $2\theta = 25.3^\circ$  and the XRD spectrum of SDS patterns similarly to those found in the literature [61]. The spectra showed an increase of  $\text{TiO}_2$  crystalline peak as increasing  $\text{TiO}_2$  content for the PVA/ $\text{TiO}_2$  nanocomposite films. The XRD patterns compared between PVA/ $\text{TiO}_2$ , PVA/ $\text{TiO}_2$ -SDBS and PVA/ $\text{TiO}_2$ -SDS nanocomposite films before and after thermal treatment are shown in Figure 77.



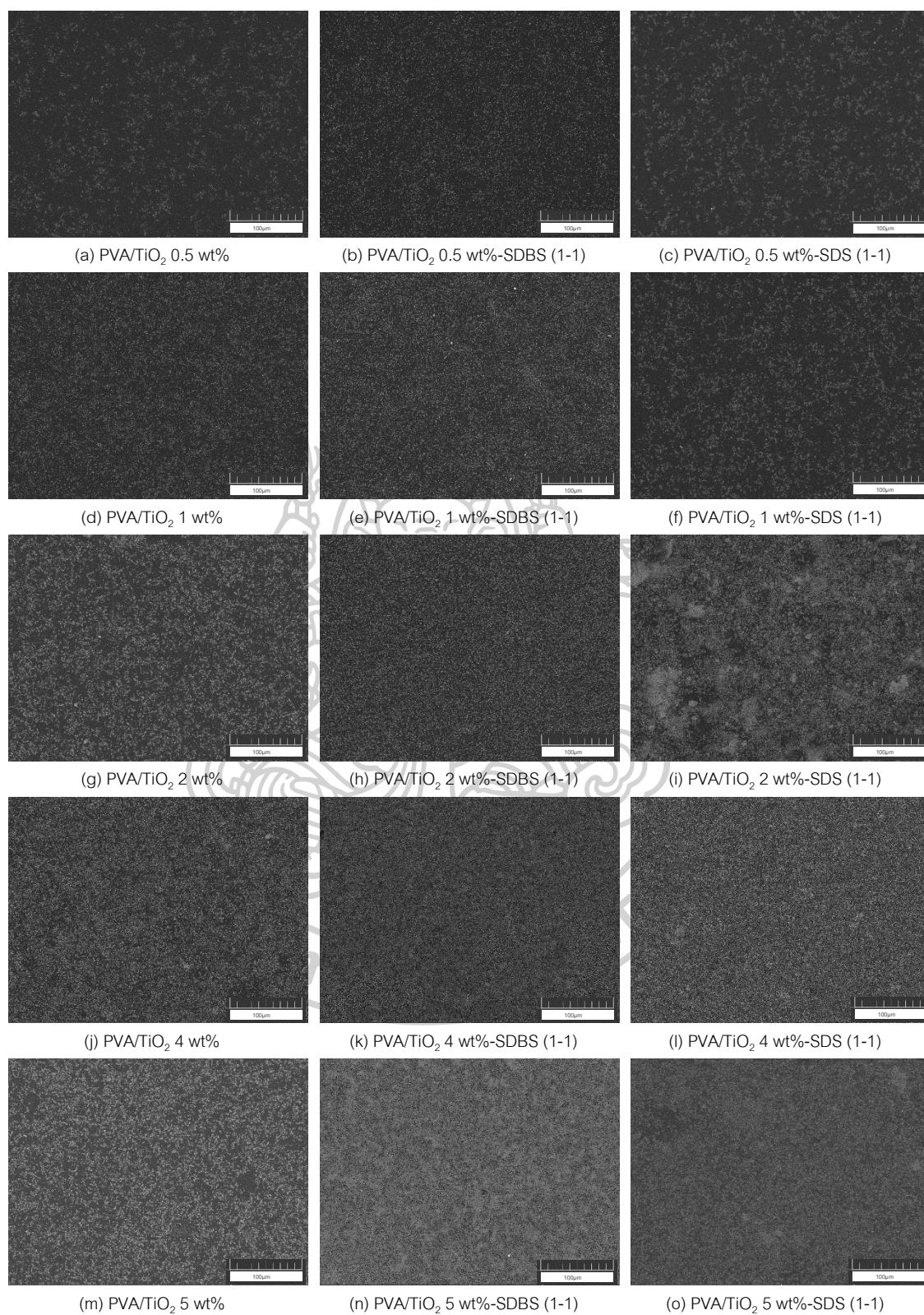


Figure 61 SEM images with BSE of PVA/TiO<sub>2</sub> nanocomposite films without and with surfactant at magnitude 500X.



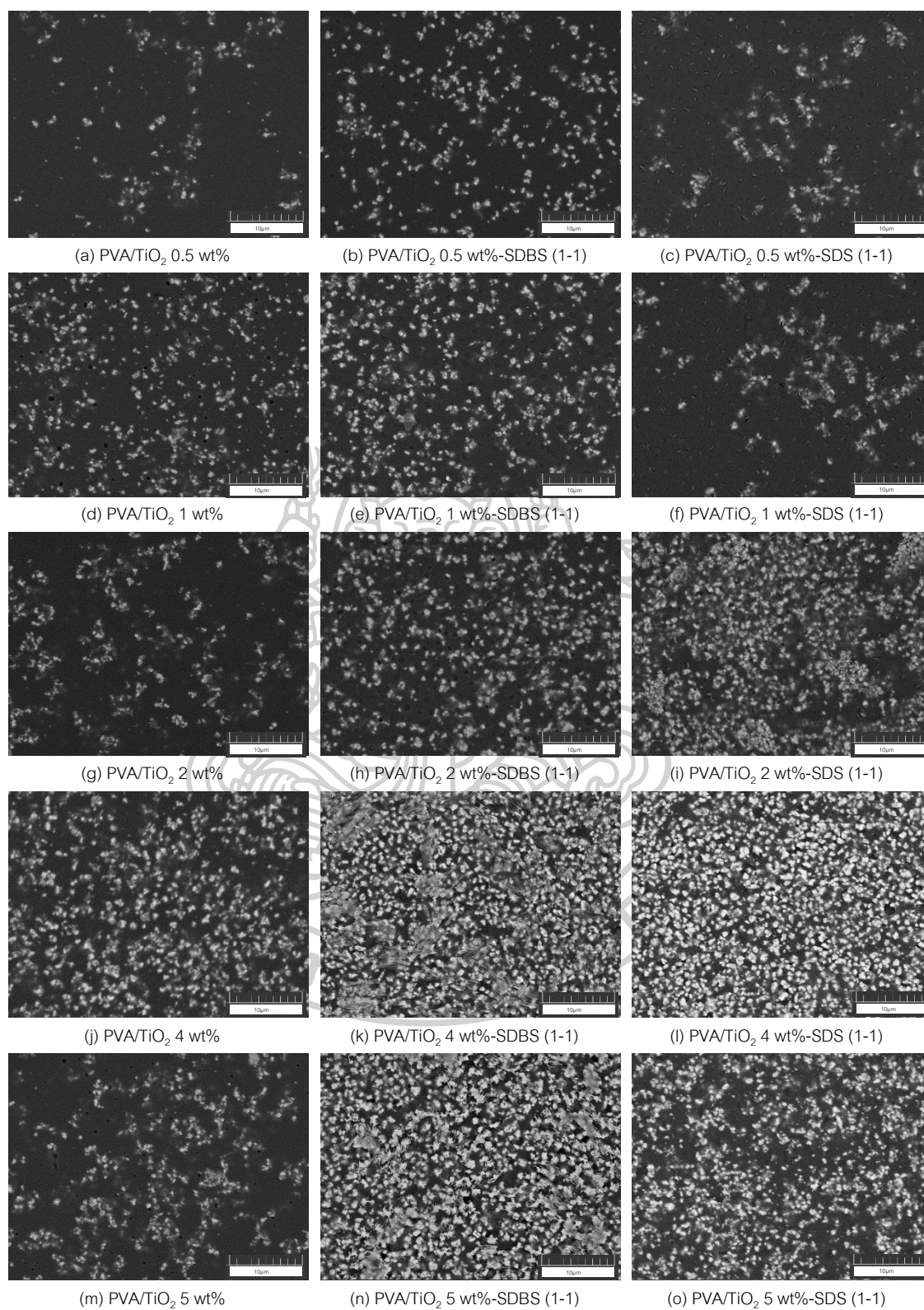


Figure 62 SEM images with BSE of PVA/TiO<sub>2</sub> nanocomposite films without and with surfactant at magnitude 5000X.

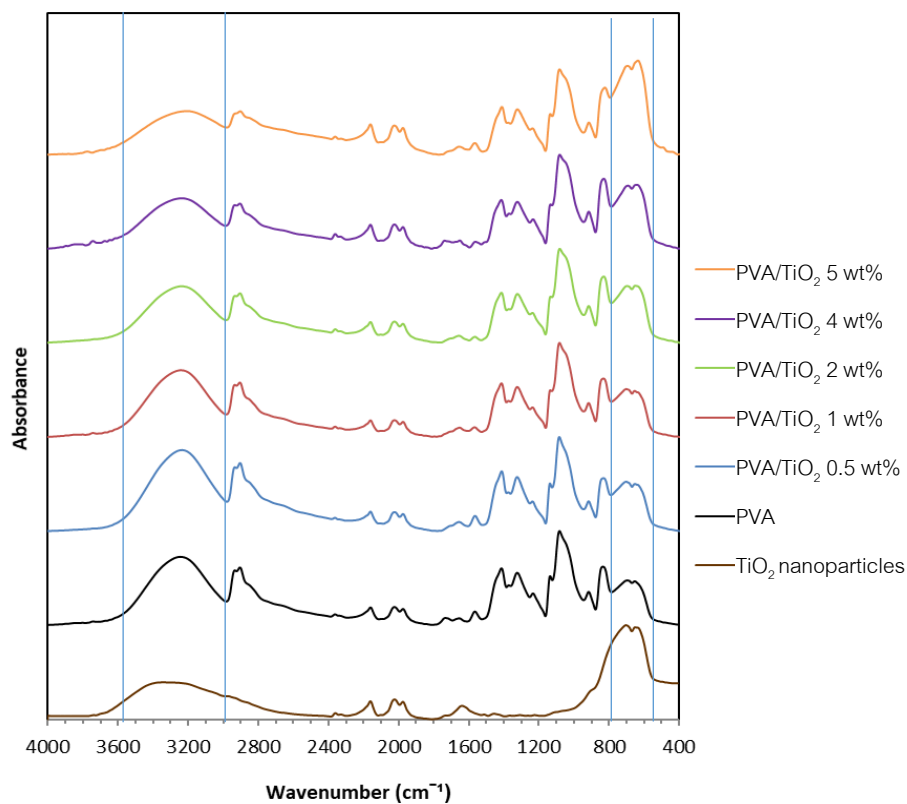


Figure 63 Infrared spectra of TiO<sub>2</sub> nanoparticles, PVA film and PVA/TiO<sub>2</sub> nanocomposite films.

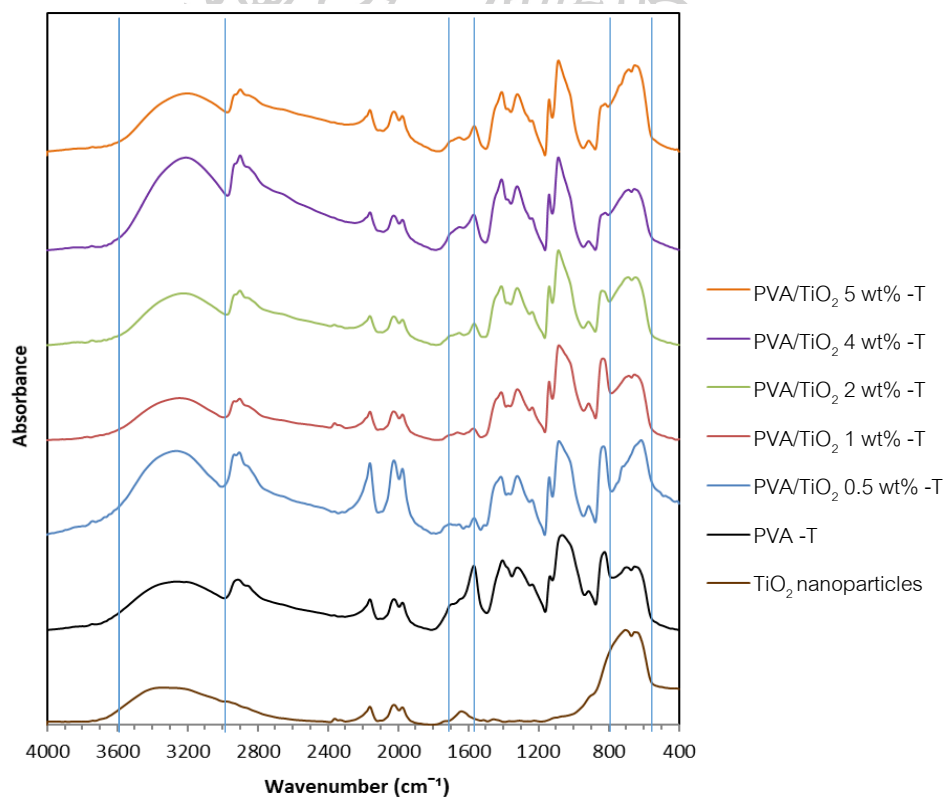


Figure 64 Infrared spectra of TiO<sub>2</sub> nanoparticles, PVA film and PVA/TiO<sub>2</sub> nanocomposite films after thermal treatment.

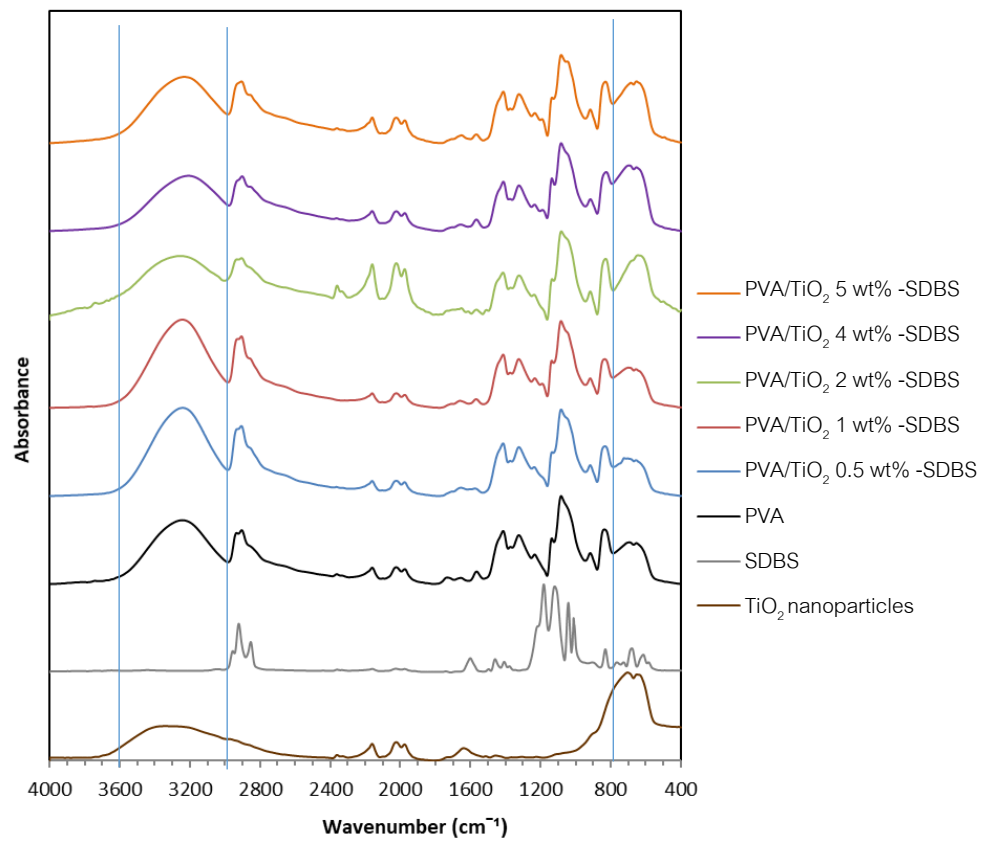


Figure 65 Infrared spectra of TiO<sub>2</sub> nanoparticles, SDBS, PVA film and PVA/TiO<sub>2</sub>-SDBS nanocomposite films.



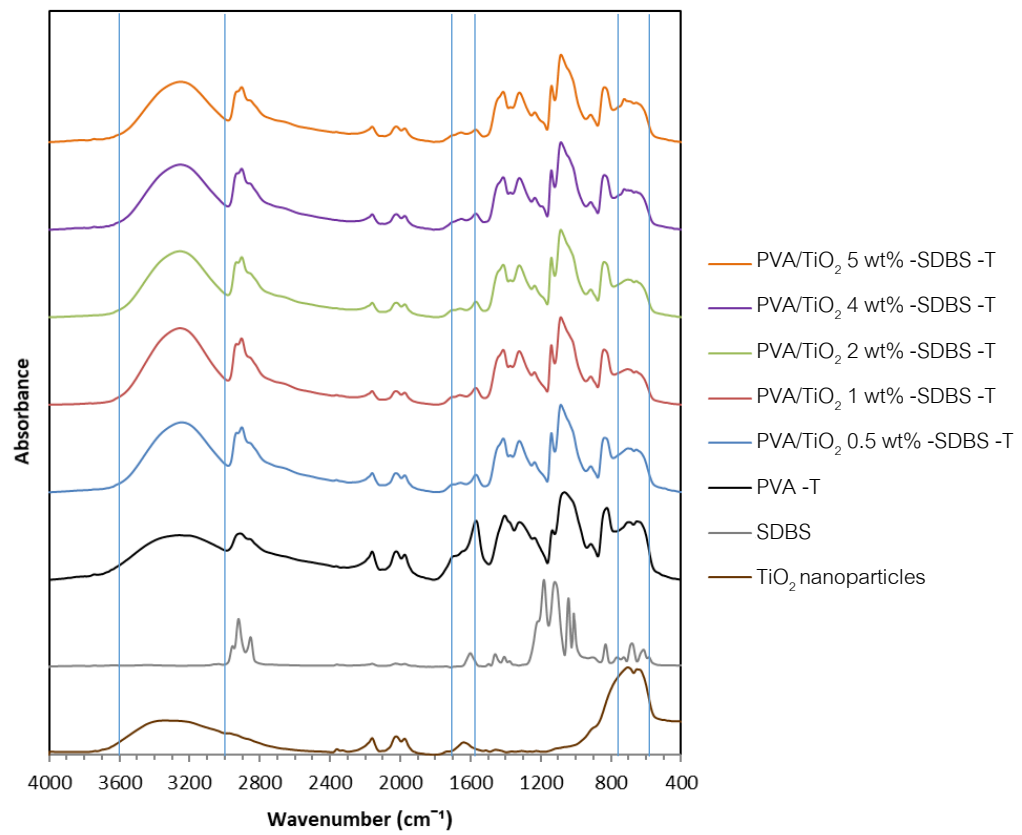
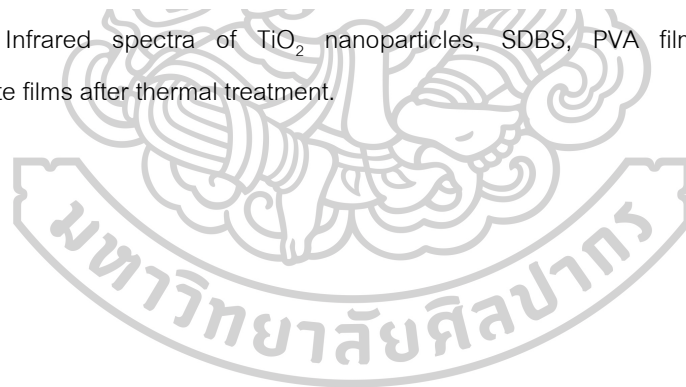


Figure 66 Infrared spectra of TiO<sub>2</sub> nanoparticles, SDBS, PVA film and PVA/TiO<sub>2</sub>-SDBS nanocomposite films after thermal treatment.



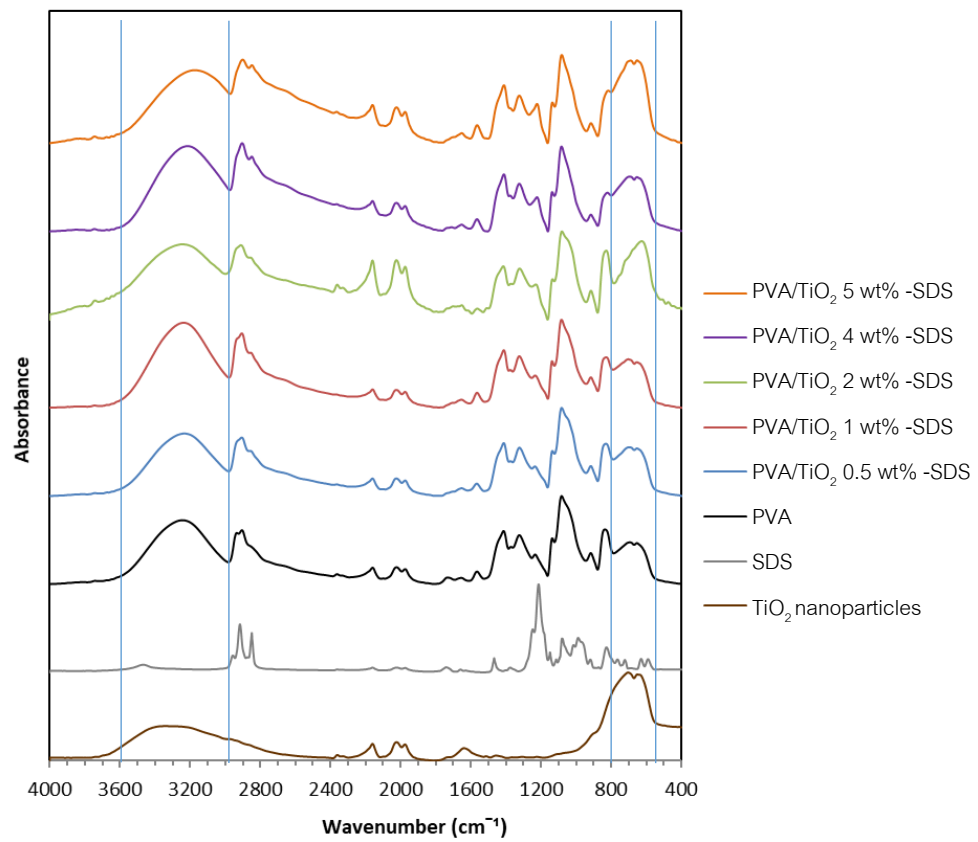
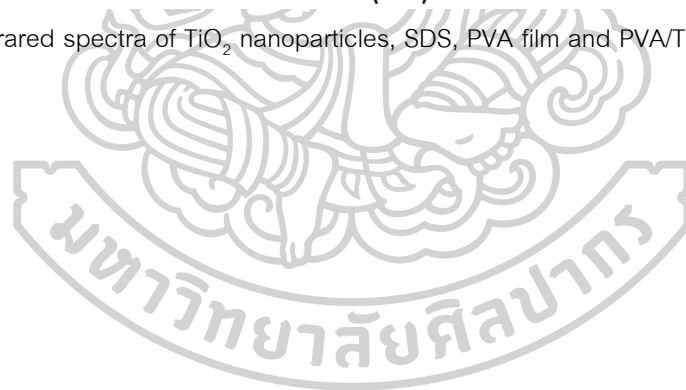


Figure 67 Infrared spectra of TiO<sub>2</sub> nanoparticles, SDS, PVA film and PVA/TiO<sub>2</sub>-SDS nanocomposite films.





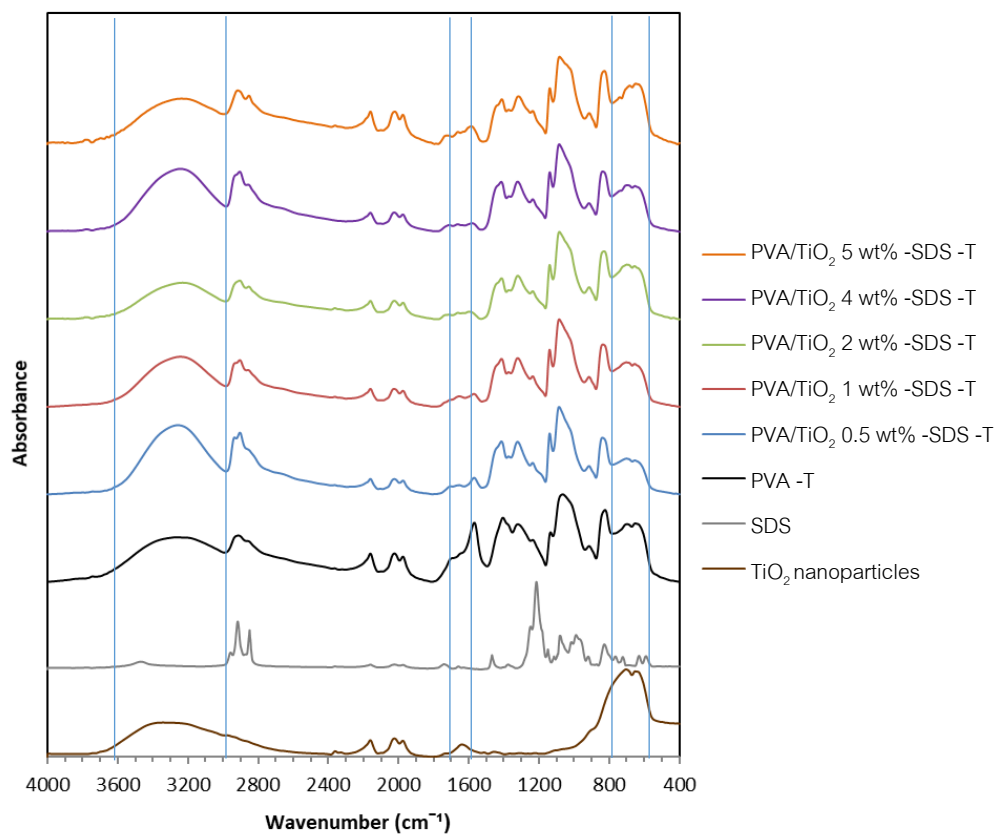


Figure 68 Infrared spectra of TiO<sub>2</sub> nanoparticles, SDS, PVA film and PVA/TiO<sub>2</sub>-SDS nanocomposite films after thermal treatment.



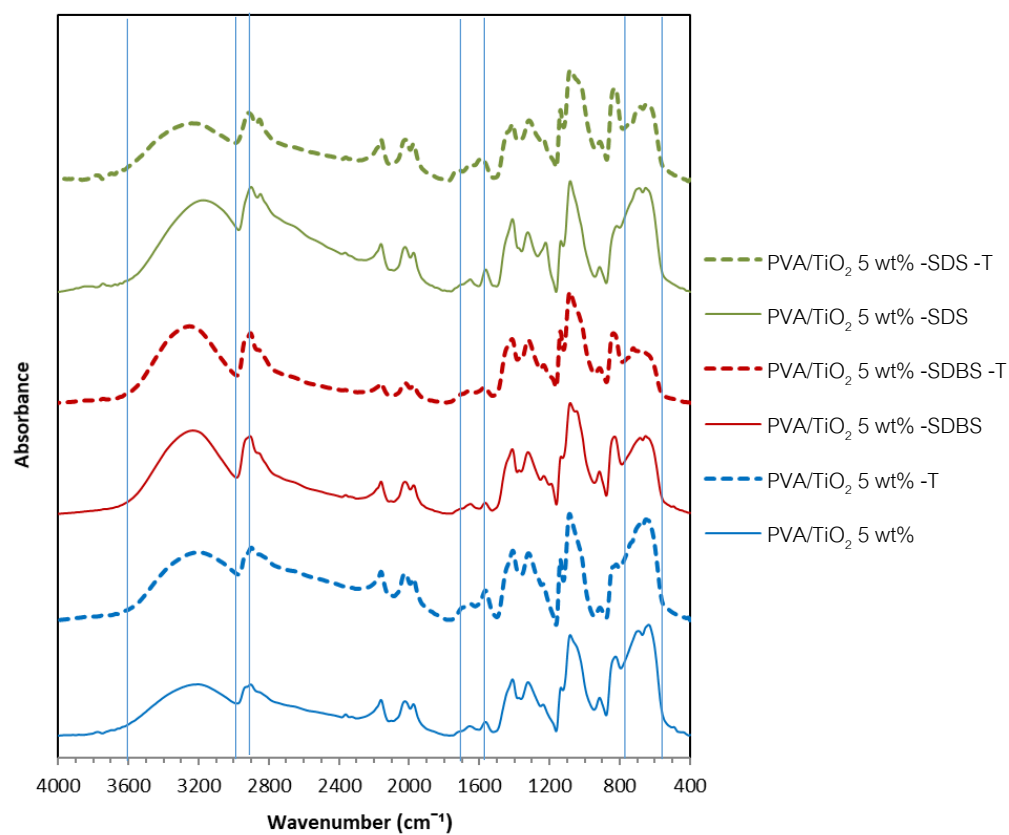


Figure 69 Infrared spectra of PVA film, PVA/TiO<sub>2</sub> nanocomposite films at 5 wt% of TiO<sub>2</sub> without and with surfactants, before and after thermal treatment.

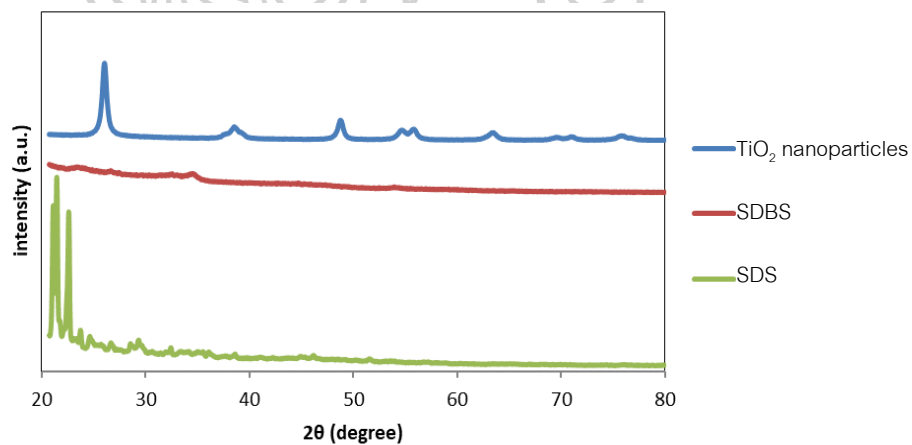
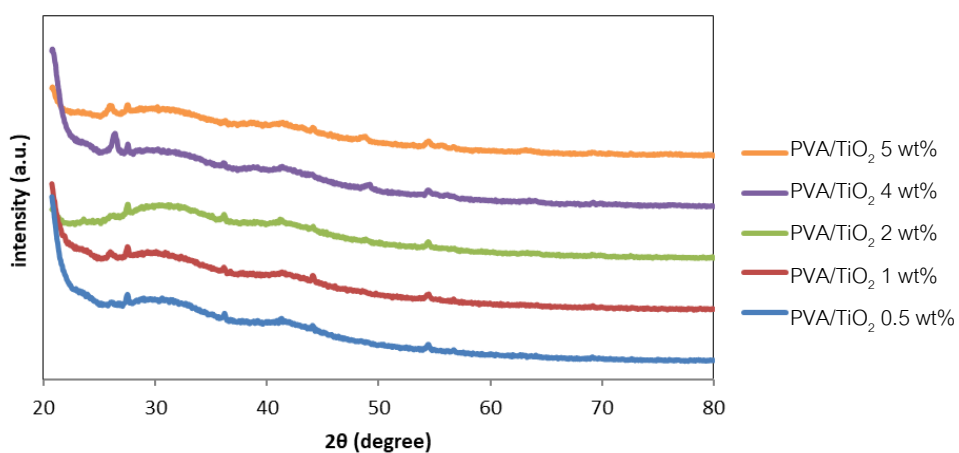
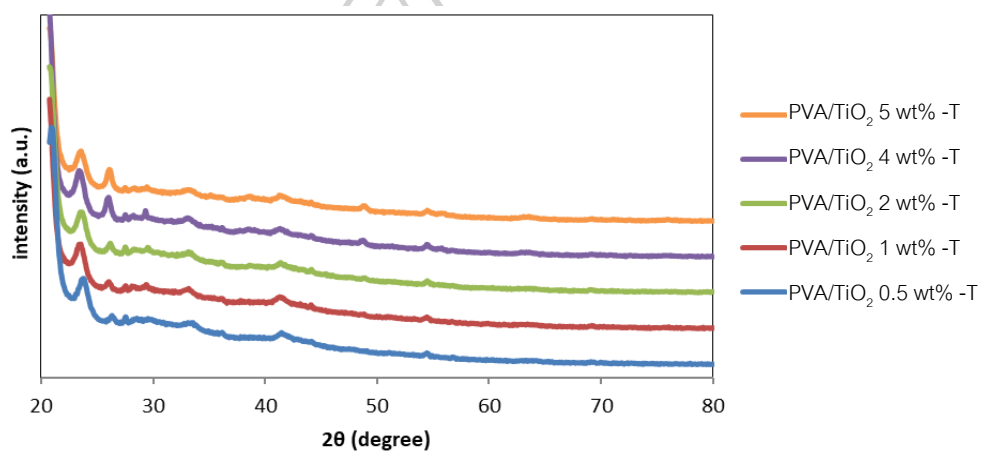
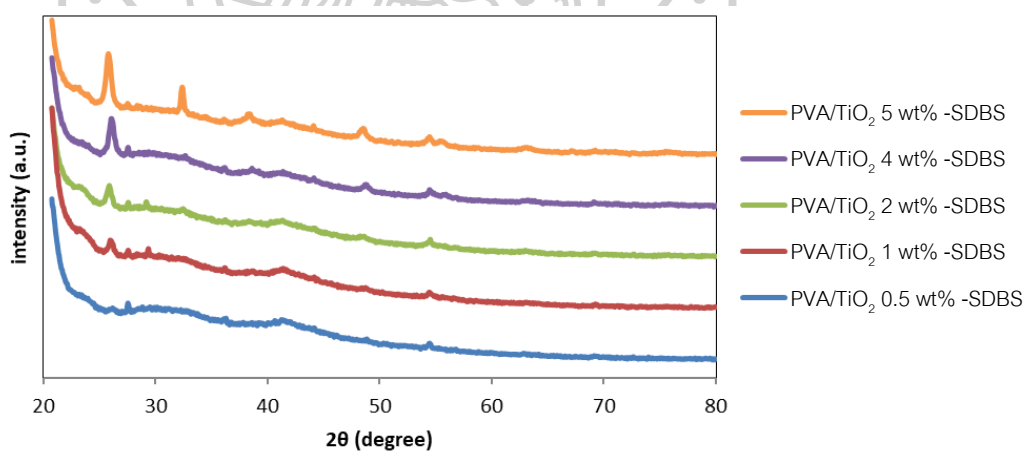


Figure 70 XRD patterns of TiO<sub>2</sub> nanoparticles, SDBS and SDS.



Figure 71 XRD pattern of PVA/TiO<sub>2</sub> nanocomposite films.Figure 72 XRD pattern of PVA/TiO<sub>2</sub> nanocomposite films after thermal treatment.Figure 73 XRD pattern of PVA/TiO<sub>2</sub>-SDBS nanocomposite films.

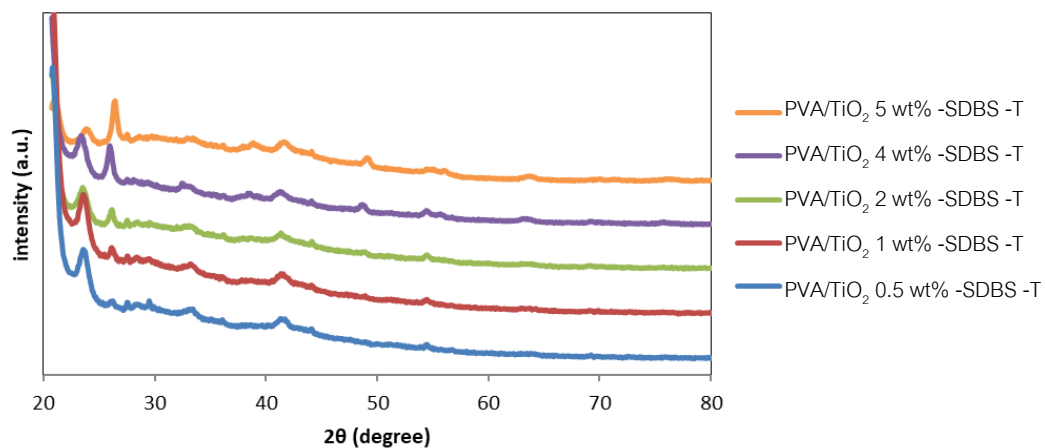


Figure 74 XRD pattern of PVA/TiO<sub>2</sub>-SDBS nanocomposite films after thermal treatment.

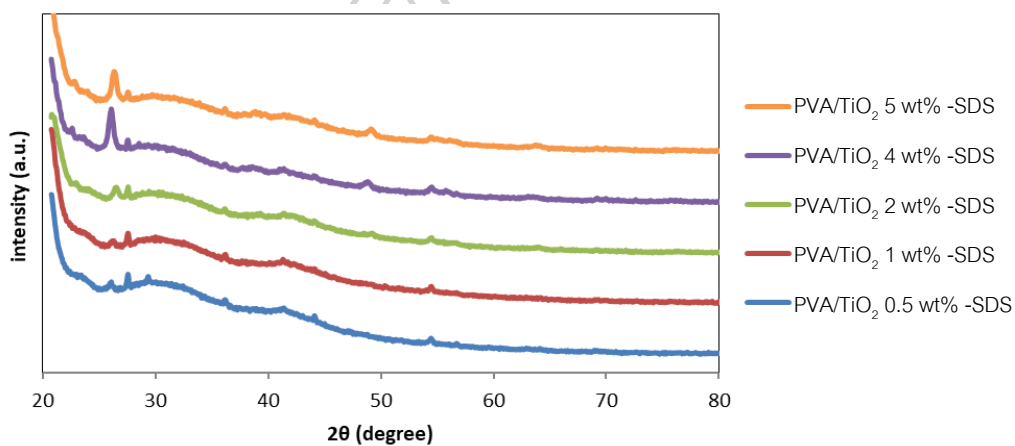


Figure 75 XRD pattern of PVA/TiO<sub>2</sub>-SDS nanocomposite films.

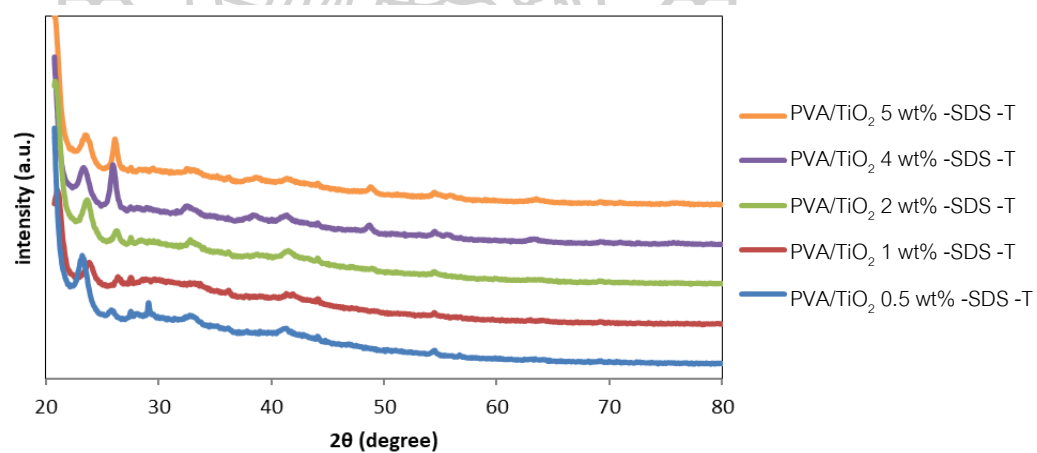


Figure 76 XRD pattern of PVA/TiO<sub>2</sub>-SDS nanocomposite films after thermal treatment.

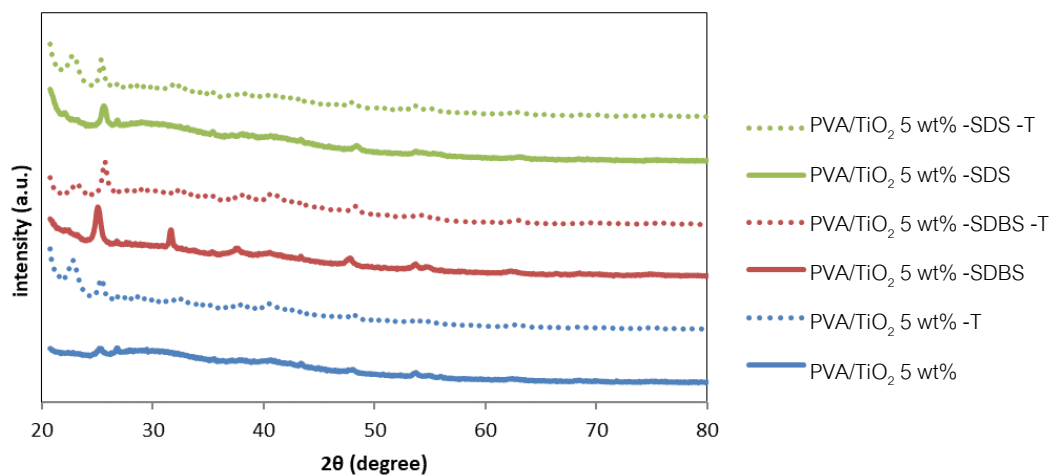


Figure 77 XRD pattern of PVA/TiO<sub>2</sub> nanocomposite films at 5wt% of TiO<sub>2</sub> without and with surfactants, before and after thermal treatment.

#### 5.3.4 Mechanical properties

Table 9 and Figure 78 show the tensile strength, Table 10 and Figure 79 show the strain at break and Table 11 and Figure 80 show the Young's modulus of PVA film, PVA/TiO<sub>2</sub>, PVA/TiO<sub>2</sub>-SDBS and PVA/TiO<sub>2</sub>-SDS nanocomposite films before and after thermal treatment. The addition of TiO<sub>2</sub>, SDBS and SDS did not improved the mechanical properties of PVA/TiO<sub>2</sub> nanocomposite films. However, the films with TiO<sub>2</sub> nanoparticles showed better mechanical properties after thermal treatment, which differed from those observed for the films with TiO<sub>2</sub> microparticles.



Table 9 The tensile Strength of PVA film, PVA/TiO<sub>2</sub>, PVA/TiO<sub>2</sub>-SDBS and PVA/TiO<sub>2</sub>-SDS nanocomposite films before and after thermal treatment.

| Sample                           | Tensile Strength (MPa)   |                         |
|----------------------------------|--------------------------|-------------------------|
|                                  | Before thermal treatment | After thermal treatment |
| PVA                              | 107.1 ± 7.4              | 141.3 ± 23.7            |
| PVA/TiO <sub>2</sub> 0.5wt%      | 106.8 ± 9.2              | 130.0 ± 4.6             |
| PVA/TiO <sub>2</sub> 1wt%        | 107.2 ± 6.8              | 128.4 ± 13.6            |
| PVA/TiO <sub>2</sub> 2wt%        | 98.5 ± 13.1              | 125.5 ± 5.9             |
| PVA/TiO <sub>2</sub> 4wt%        | 113.7 ± 1.5              | 124.9 ± 9.5             |
| PVA/TiO <sub>2</sub> 5wt%        | 111.9 ± 7.9              | 133.5 ± 3.5             |
| PVA/TiO <sub>2</sub> 0.5wt%-SDBS | 111.7 ± 9.3              | 128.0 ± 6.8             |
| PVA/TiO <sub>2</sub> 1wt%-SDBS   | 111.1 ± 9.8              | 90.8 ± 17.2             |
| PVA/TiO <sub>2</sub> 2wt%-SDBS   | 77.0 ± 6.9               | 84.9 ± 5.1              |
| PVA/TiO <sub>2</sub> 4wt%-SDBS   | 73.3 ± 3.9               | 76.9 ± 6.0              |
| PVA/TiO <sub>2</sub> 5wt%-SDBS   | 97.0 ± 13.5              | 111.1 ± 28.1            |
| PVA/TiO <sub>2</sub> 0.5wt%-SDS  | 108.4 ± 4.2              | 99.9 ± 17.1             |
| PVA/TiO <sub>2</sub> 1wt%-SDS    | 106.3 ± 10.8             | 82.0 ± 14.5             |
| PVA/TiO <sub>2</sub> 2wt%-SDS    | 97.7 ± 9.1               | 114.6 ± 4.6             |
| PVA/TiO <sub>2</sub> 4wt%-SDS    | 75.2 ± 5.8               | 82.6 ± 3.7              |
| PVA/TiO <sub>2</sub> 5wt%-SDS    | 88.0 ± 5.9               | 81.9 ± 14.1             |

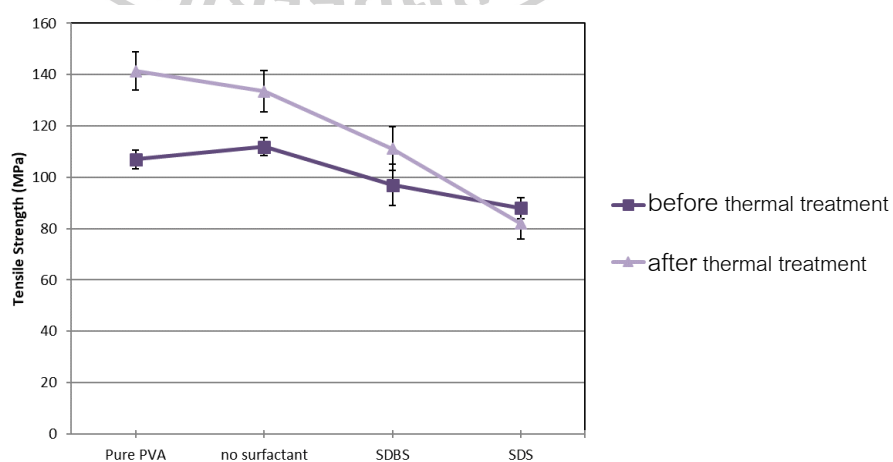


Figure 78 Tensile strength of PVA film and PVA/TiO<sub>2</sub> nanocomposite films at 5wt% of TiO<sub>2</sub> without and with surfactants, before and after thermal treatment.

Table 10 The strain at break of PVA film, PVA/TiO<sub>2</sub>, PVA/TiO<sub>2</sub>-SDBS and PVA/TiO<sub>2</sub>-SDS nanocomposite films before and after thermal treatment.

| Sample                           | Strain at break (%)      |                         |
|----------------------------------|--------------------------|-------------------------|
|                                  | Before thermal treatment | After thermal treatment |
| PVA                              | 2.73 ± 0.31              | 2.39 ± 0.66             |
| PVA/TiO <sub>2</sub> 0.5wt%      | 2.77 ± 0.36              | 3.27 ± 0.22             |
| PVA/TiO <sub>2</sub> 1wt%        | 2.57 ± 0.32              | 2.69 ± 0.72             |
| PVA/TiO <sub>2</sub> 2wt%        | 2.46 ± 0.58              | 2.82 ± 0.27             |
| PVA/TiO <sub>2</sub> 4wt%        | 2.68 ± 0.17              | 3.05 ± 0.31             |
| PVA/TiO <sub>2</sub> 5wt%        | 2.37 ± 0.18              | 2.58 ± 0.47             |
| PVA/TiO <sub>2</sub> 0.5wt%-SDBS | 2.37 ± 0.26              | 2.18 ± 0.23             |
| PVA/TiO <sub>2</sub> 1wt%-SDBS   | 2.21 ± 0.35              | 1.82 ± 0.52             |
| PVA/TiO <sub>2</sub> 2wt%-SDBS   | 2.08 ± 0.25              | 1.93 ± 0.18             |
| PVA/TiO <sub>2</sub> 4wt%-SDBS   | 1.94 ± 0.40              | 1.61 ± 0.18             |
| PVA/TiO <sub>2</sub> 5wt%-SDBS   | 1.80 ± 0.42              | 1.94 ± 0.32             |
| PVA/TiO <sub>2</sub> 0.5wt%-SDS  | 2.44 ± 0.20              | 1.89 ± 0.55             |
| PVA/TiO <sub>2</sub> 1wt%-SDS    | 2.70 ± 0.30              | 1.67 ± 0.36             |
| PVA/TiO <sub>2</sub> 2wt%-SDS    | 1.92 ± 0.26              | 2.24 ± 0.21             |
| PVA/TiO <sub>2</sub> 4wt%-SDS    | 2.11 ± 0.18              | 2.07 ± 0.19             |
| PVA/TiO <sub>2</sub> 5wt%-SDS    | 1.74 ± 0.15              | 2.00 ± 0.56             |

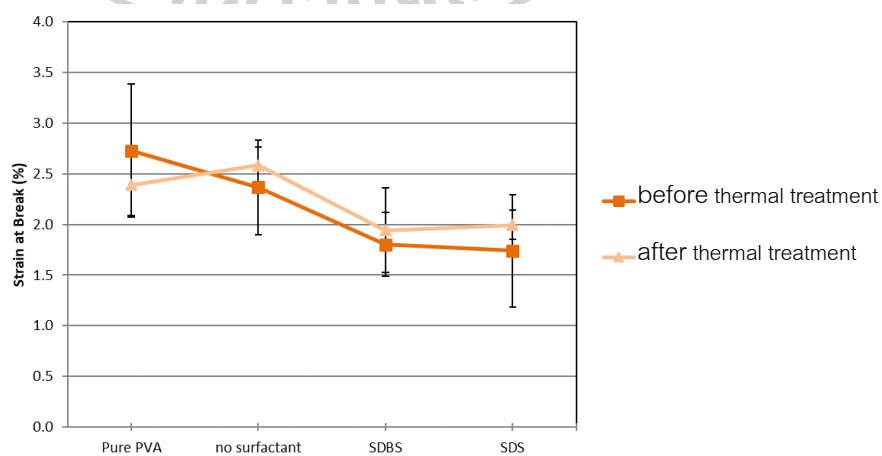


Figure 79 The strain at break of PVA film and PVA/TiO<sub>2</sub> nanocomposite films at 5 wt% of TiO<sub>2</sub> without and with surfactants, before and after thermal treatment.

Table 11 Young's modulus of PVA film, PVA/TiO<sub>2</sub>, PVA/TiO<sub>2</sub>-SDBS and PVA/TiO<sub>2</sub>-SDS nanocomposite films before and after thermal treatment.

| Sample                           | Young's Modulus (MPa)    |                         |
|----------------------------------|--------------------------|-------------------------|
|                                  | Before thermal treatment | After thermal treatment |
| PVA                              | 6883.6 ± 143.3           | 9183.8 ± 282.9          |
| PVA/TiO <sub>2</sub> 0.5wt%      | 6639.2 ± 301.9           | 7072.0 ± 258.8          |
| PVA/TiO <sub>2</sub> 1wt%        | 7113.8 ± 179.3           | 7813.3 ± 408.7          |
| PVA/TiO <sub>2</sub> 2wt%        | 6651.5 ± 232.0           | 7468.0 ± 483.5          |
| PVA/TiO <sub>2</sub> 4wt%        | 7185.8 ± 123.3           | 7301.9 ± 183.9          |
| PVA/TiO <sub>2</sub> 5wt%        | 7489.4 ± 176.8           | 8543.8 ± 646.2          |
| PVA/TiO <sub>2</sub> 0.5wt%-SDBS | 6705.7 ± 280.7           | 8101.4 ± 351.0          |
| PVA/TiO <sub>2</sub> 1wt%-SDBS   | 7187.9 ± 265.0           | 6874.2 ± 419.4          |
| PVA/TiO <sub>2</sub> 2wt%-SDBS   | 5073.2 ± 207.7           | 5852.6 ± 245.9          |
| PVA/TiO <sub>2</sub> 4wt%-SDBS   | 5859.5 ± 254.7           | 6257.1 ± 115.2          |
| PVA/TiO <sub>2</sub> 5wt%-SDBS   | 8273.1 ± 99.9            | 8513.5 ± 444.8          |
| PVA/TiO <sub>2</sub> 0.5wt%-SDS  | 6965.5 ± 142.3           | 7484.9 ± 173.3          |
| PVA/TiO <sub>2</sub> 1wt%-SDS    | 6074.4 ± 347.8           | 6513.4 ± 414.8          |
| PVA/TiO <sub>2</sub> 2wt%-SDS    | 6990.6 ± 204.5           | 7257.8 ± 89.2           |
| PVA/TiO <sub>2</sub> 4wt%-SDS    | 5106.0 ± 232.5           | 5800.0 ± 171.0          |
| PVA/TiO <sub>2</sub> 5wt%-SDS    | 7135.1 ± 182.4           | 6624.1 ± 488.4          |

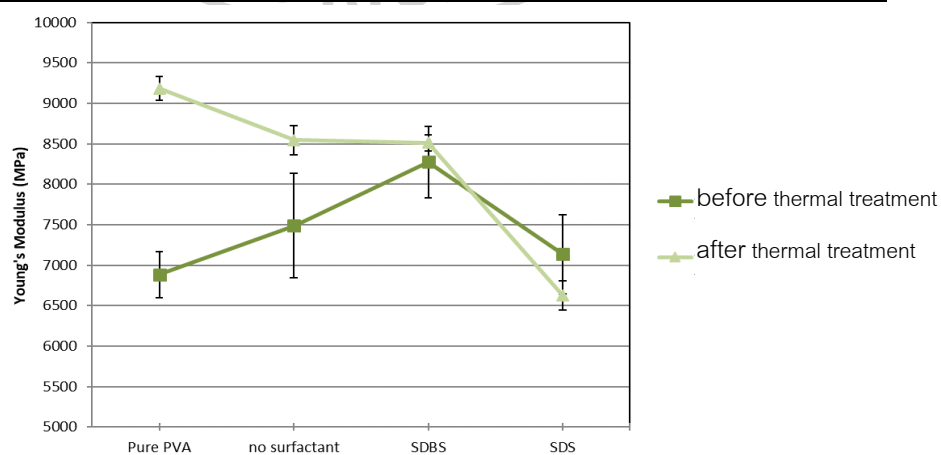


Figure 80 Young's modulus of PVA film and PVA/TiO<sub>2</sub> nanocomposite films 5 wt% of TiO<sub>2</sub> without and with surfactants, before and after thermal treatment.

### 5.3.5 TGA analysis

Figures 81-86 show the thermal degradation of PVA/TiO<sub>2</sub> nanocomposite films without and with surfactants, before and after thermal treatment. The degradation of the films was proceeded by three steps as mentioned earlier. The addition of TiO<sub>2</sub> and surfactants, as well as thermal treatment delayed the thermal degradation process of the nanocomposite films with as previously observed for the PVA/TiO<sub>2</sub> composite films. The effect was more pronounced with SDS addition as clearly seen the shift of the predominant degradation step toward higher temperature as shown in Figure 87. The results were in accordance with the decomposition temperature at 50% weight loss ( $T_{d50}$ ) in Table 12, in which  $T_{d50}$  increased with TiO<sub>2</sub> and surfactant addition, and also increased after thermal treatment. Table 13 shows the remaining weight at temperature 600°C of PVA film and PVA/TiO<sub>2</sub> nanocomposite films without and with surfactant, before and after thermal treatment. The remaining weight enhanced after thermal treatment by thermal treatment.

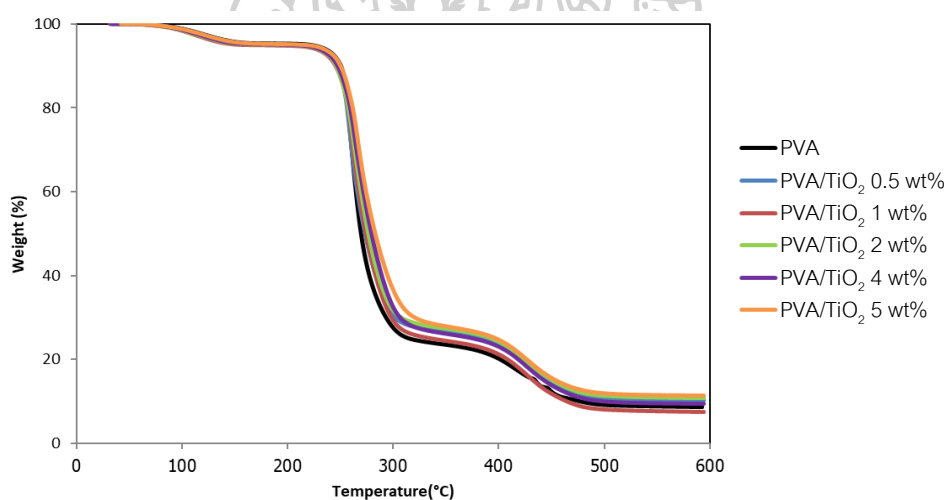


Figure 81 TGA analyses of PVA film and PVA/TiO<sub>2</sub> nanocomposite films.

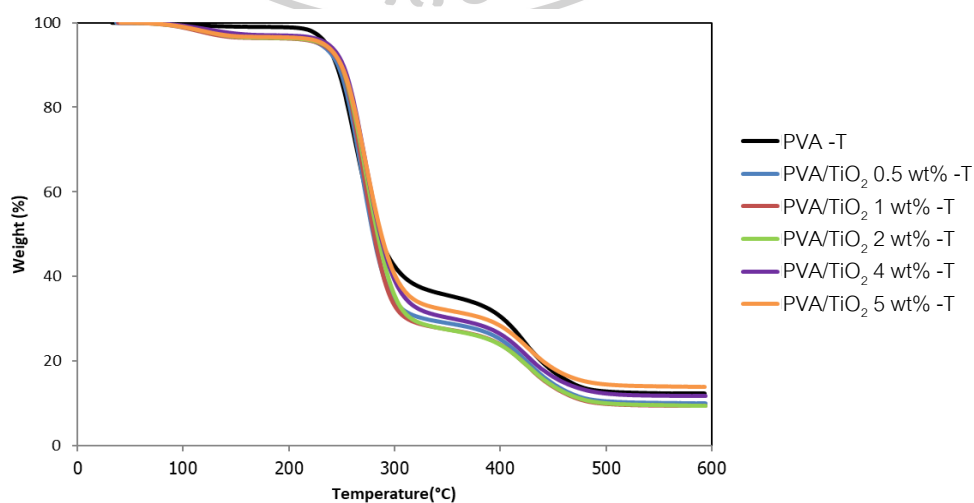


Figure 82 TGA analyses of PVA film and PVA/TiO<sub>2</sub> nanocomposite films after thermal treatment.

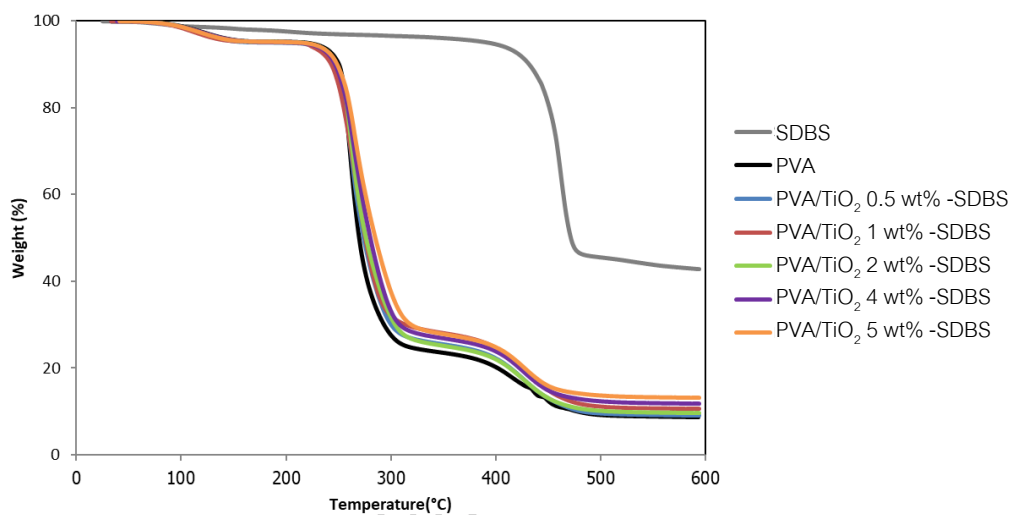


Figure 83 TGA analyses of SDBS particles, PVA film and PVATiO<sub>2</sub>-SDBS nanocomposite films.

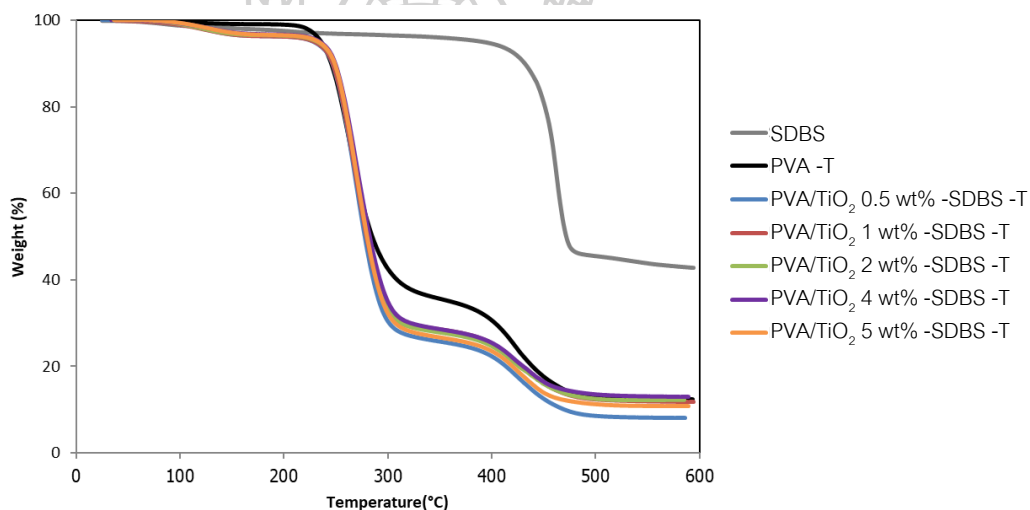


Figure 84 TGA analyses of SDBS particles, PVA film and PVATiO<sub>2</sub>-SDBS nanocomposite films after thermal treatment.

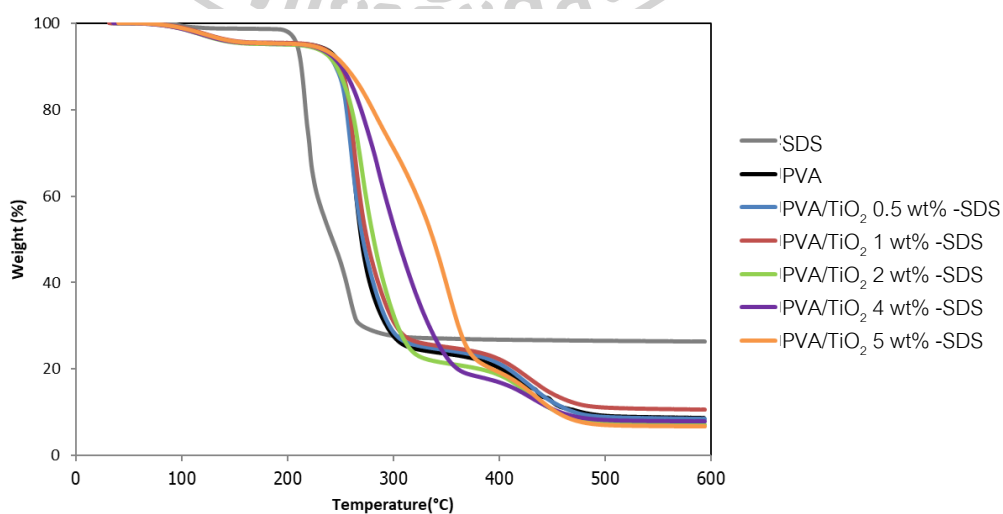


Figure 85 TGA analyses of SDS particles, PVA film and PVATiO<sub>2</sub>-SDS nanocomposite films.



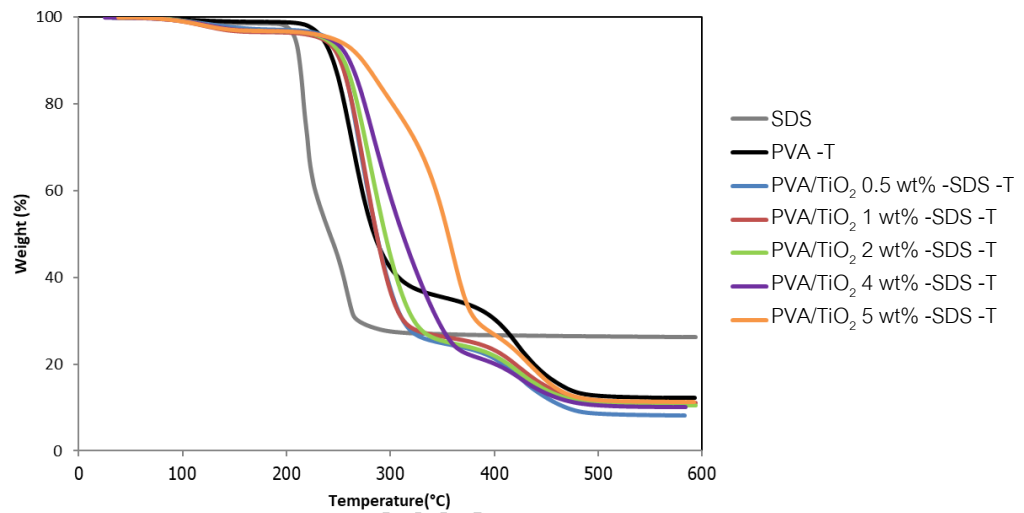


Figure 86 TGA analyses of SDS particles, PVA film and PVA/TiO<sub>2</sub>-SDS nanocomposite films after thermal treatment.

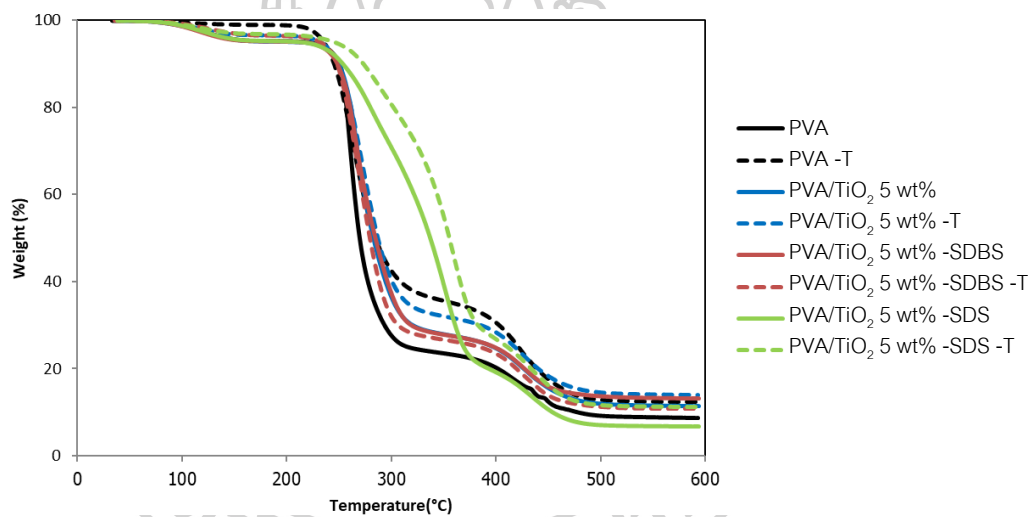


Figure 87 TGA analyses of PVA film and PVA/TiO<sub>2</sub> nanocomposite films at 5wt% of TiO<sub>2</sub> without and with surfactants, before and after thermal treatment.

Table 12 Decomposition temperature of SDBS, SDS particles, PVA film, PVA/TiO<sub>2</sub>, PVA/TiO<sub>2</sub>-SDBS and PVA/TiO<sub>2</sub>-SDS nanocomposite films before and after thermal treatment.

| Sample                           | T <sub>d50</sub> (°C)    |                         |
|----------------------------------|--------------------------|-------------------------|
|                                  | Before thermal treatment | After thermal treatment |
| SDBS                             | 471.7                    | -                       |
| SDS                              | 212.4                    | -                       |
| PVA                              | 269.6                    | 284.6                   |
| PVA/TiO <sub>2</sub> 0.5wt%      | 273.2                    | 279.9                   |
| PVA/TiO <sub>2</sub> 1wt%        | 274.1                    | 280.4                   |
| PVA/TiO <sub>2</sub> 2wt%        | 276.5                    | 284.1                   |
| PVA/TiO <sub>2</sub> 4wt%        | 279.5                    | 286.5                   |
| PVA/TiO <sub>2</sub> 5wt%        | 282.8                    | 287.4                   |
| PVA/TiO <sub>2</sub> 0.5wt%-SDBS | 274.0                    | 277.7                   |
| PVA/TiO <sub>2</sub> 1wt%-SDBS   | 275.5                    | 279.5                   |
| PVA/TiO <sub>2</sub> 2wt%-SDBS   | 276.5                    | 280.8                   |
| PVA/TiO <sub>2</sub> 4wt%-SDBS   | 280.5                    | 282.4                   |
| PVA/TiO <sub>2</sub> 5wt%-SDBS   | 285.1                    | 279.6                   |
| PVA/TiO <sub>2</sub> 0.5wt%-SDS  | 271.0                    | 286.8                   |
| PVA/TiO <sub>2</sub> 1wt%-SDS    | 274.7                    | 286.9                   |
| PVA/TiO <sub>2</sub> 2wt%-SDS    | 281.2                    | 295.3                   |
| PVA/TiO <sub>2</sub> 4wt%-SDS    | 303.8                    | 311.7                   |
| PVA/TiO <sub>2</sub> 5wt%-SDS    | 337.4                    | 355.3                   |

Table 13 The char yield of SDBS, SDS particles, PVA film, PVA/TiO<sub>2</sub>, PVA/TiO<sub>2</sub>-SDBS and PVA/TiO<sub>2</sub>-SDS nanocomposite films before and after thermal treatment.

| Sample                           | Char yield (%)           |                         |
|----------------------------------|--------------------------|-------------------------|
|                                  | Before thermal treatment | After thermal treatment |
| SDBS                             | 42.9                     | -                       |
| SDS                              | 26.3                     | -                       |
| PVA                              | 8.7                      | 12.3                    |
| PVA/TiO <sub>2</sub> 0.5wt%      | 10.1                     | 10.1                    |
| PVA/TiO <sub>2</sub> 1wt%        | 7.5                      | 9.4                     |
| PVA/TiO <sub>2</sub> 2wt%        | 10.7                     | 9.4                     |
| PVA/TiO <sub>2</sub> 4wt%        | 9.5                      | 11.7                    |
| PVA/TiO <sub>2</sub> 5wt%        | 11.3                     | 14.0                    |
| PVA/TiO <sub>2</sub> 0.5wt%-SDBS | 9.0                      | 8.0                     |
| PVA/TiO <sub>2</sub> 1wt%-SDBS   | 10.6                     | 11.9                    |
| PVA/TiO <sub>2</sub> 2wt%-SDBS   | 9.6                      | 12.2                    |
| PVA/TiO <sub>2</sub> 4wt%-SDBS   | 11.7                     | 12.9                    |
| PVA/TiO <sub>2</sub> 5wt%-SDBS   | 13.2                     | 10.8                    |
| PVA/TiO <sub>2</sub> 0.5wt%-SDS  | 8.6                      | 8.1                     |
| PVA/TiO <sub>2</sub> 1wt%-SDS    | 10.7                     | 11.0                    |
| PVA/TiO <sub>2</sub> 2wt%-SDS    | 7.1                      | 10.6                    |
| PVA/TiO <sub>2</sub> 4wt%-SDS    | 8.0                      | 10.1                    |
| PVA/TiO <sub>2</sub> 5wt%-SDS    | 6.8                      | 11.2                    |

### 5.3.6 DSC analysis

The melting point temperature ( $T_m$ ) of PVA film, PVA/TiO<sub>2</sub>, PVA/TiO<sub>2</sub>-SDBS, and PVA/TiO<sub>2</sub>-SDS nanocomposite films before and after thermal treatment are shown in Table 14. The results showed no significant change between the melting point temperature of PVA/TiO<sub>2</sub> nanocomposite films without and with surfactants, before and after thermal treatment, as previously observed for the PVA/TiO<sub>2</sub> composite films. Table 15 shows the crystallinity of PVA film, PVA/TiO<sub>2</sub> nanocomposite films without and with surfactants, before and after thermal treatment. The thermal treatment decreased

crystallinity of PVA, whereas the addition of SDBS and SDS remained crystallinity of PVA/TiO<sub>2</sub> nanocomposite films nearby before thermal treatment.

Table 14 Melting point temperature ( $T_m$ ) of PVA film, PVA/TiO<sub>2</sub>, PVA/TiO<sub>2</sub>-SDBS and PVA/TiO<sub>2</sub>-SDS nanocomposite films before and after thermal treatment.

| Sample                            | $T_m$ (°C)               |                         |
|-----------------------------------|--------------------------|-------------------------|
|                                   | Before thermal treatment | After thermal treatment |
| PVA                               | 224.5                    | 223.1                   |
| PVA/TiO <sub>2</sub> 0.5 wt%      | 223.0                    | 222.8                   |
| PVA/TiO <sub>2</sub> 1 wt%        | 223.2                    | 222.1                   |
| PVA/TiO <sub>2</sub> 2 wt%        | 223.1                    | 222.9                   |
| PVA/TiO <sub>2</sub> 4 wt%        | 223.9                    | 222.9                   |
| PVA/TiO <sub>2</sub> 5 wt%        | 224.5                    | 222.9                   |
| PVA/TiO <sub>2</sub> 0.5 wt%-SDBS | 223.4                    | 223.1                   |
| PVA/TiO <sub>2</sub> 1 wt%-SDBS   | 222.7                    | 222.3                   |
| PVA/TiO <sub>2</sub> 2 wt%-SDBS   | 223.4                    | 222.4                   |
| PVA/TiO <sub>2</sub> 4 wt%-SDBS   | 222.2                    | 222.1                   |
| PVA/TiO <sub>2</sub> 5 wt%-SDBS   | 222.9                    | 221.9                   |
| PVA/TiO <sub>2</sub> 0.5 wt%-SDS  | 222.7                    | 222.7                   |
| PVA/TiO <sub>2</sub> 1 wt%-SDS    | 223.1                    | 223.2                   |
| PVA/TiO <sub>2</sub> 2 wt%-SDS    | 222.7                    | 223.9                   |
| PVA/TiO <sub>2</sub> 4 wt%-SDS    | 222.7                    | 224.4                   |
| PVA/TiO <sub>2</sub> 5 wt%-SDS    | 222.7                    | 225.3                   |

Table 15 Crystallinity of PVA film, PVA/TiO<sub>2</sub>, PVA/TiO<sub>2</sub>-SDBS and PVA/TiO<sub>2</sub>-SDS nanocomposite films before and after thermal treatment.

| Sample                            | Crystallinity (%)        |                         |
|-----------------------------------|--------------------------|-------------------------|
|                                   | Before thermal treatment | After thermal treatment |
| PVA                               | 30.4                     | 22.3                    |
| PVA/TiO <sub>2</sub> 0.5 wt%      | 25.4                     | 23.4                    |
| PVA/TiO <sub>2</sub> 1 wt%        | 23.1                     | 24.4                    |
| PVA/TiO <sub>2</sub> 2 wt%        | 22.8                     | 25.3                    |
| PVA/TiO <sub>2</sub> 4 wt%        | 23.9                     | 22.7                    |
| PVA/TiO <sub>2</sub> 5 wt%        | 24.8                     | 21.6                    |
| PVA/TiO <sub>2</sub> 0.5 wt%-SDBS | 23.7                     | 21.6                    |
| PVA/TiO <sub>2</sub> 1 wt%-SDBS   | 18.9                     | 21.8                    |
| PVA/TiO <sub>2</sub> 2 wt%-SDBS   | 25.1                     | 22.8                    |
| PVA/TiO <sub>2</sub> 4 wt%-SDBS   | 22.2                     | 21.5                    |
| PVA/TiO <sub>2</sub> 5 wt%-SDBS   | 21.8                     | 21.8                    |
| PVA/TiO <sub>2</sub> 0.5 wt%-SDS  | 23.7                     | 26.7                    |
| PVA/TiO <sub>2</sub> 1 wt%-SDS    | 25.2                     | 25.9                    |
| PVA/TiO <sub>2</sub> 2 wt%-SDS    | 24.1                     | 25.0                    |
| PVA/TiO <sub>2</sub> 4 wt%-SDS    | 26.0                     | 27.2                    |
| PVA/TiO <sub>2</sub> 5 wt%-SDS    | 27.9                     | 31.4                    |

### 5.3.7 UV absorption

Figures 88-93 show the UV absorption spectra of TiO<sub>2</sub> nanoparticles, PVA film, and PVA/TiO<sub>2</sub> nanocomposite films without and with surfactant before and after thermal treatment. The absorption spectra of the films varying TiO<sub>2</sub> contents, before and after thermal treatment were similar to those previously observed for PVA/TiO<sub>2</sub> composite films. The comparison between absorption spectra of PVA film and PVA/TiO<sub>2</sub> nanocomposite films at 5 wt% of TiO<sub>2</sub> without and with SDBS or SDS, before and after thermal treatment is shown in Figure 94. The intensity of TiO<sub>2</sub> absorption band of PVA/TiO<sub>2</sub> nanocomposite film was the highest, following by PVA/TiO<sub>2</sub> with SDBS and SDS, respectively, both before and after thermal treatment.

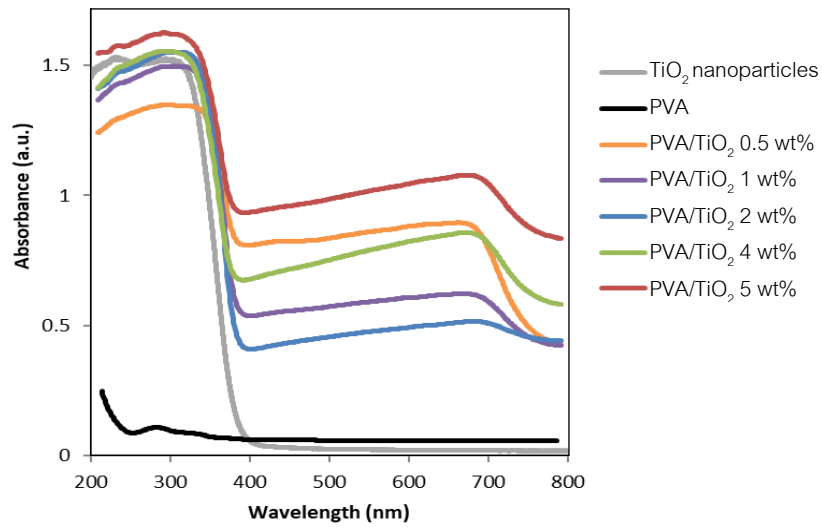


Figure 88 UV-visible absorption spectra for PVA film and PVA/TiO<sub>2</sub> nanocomposite films.

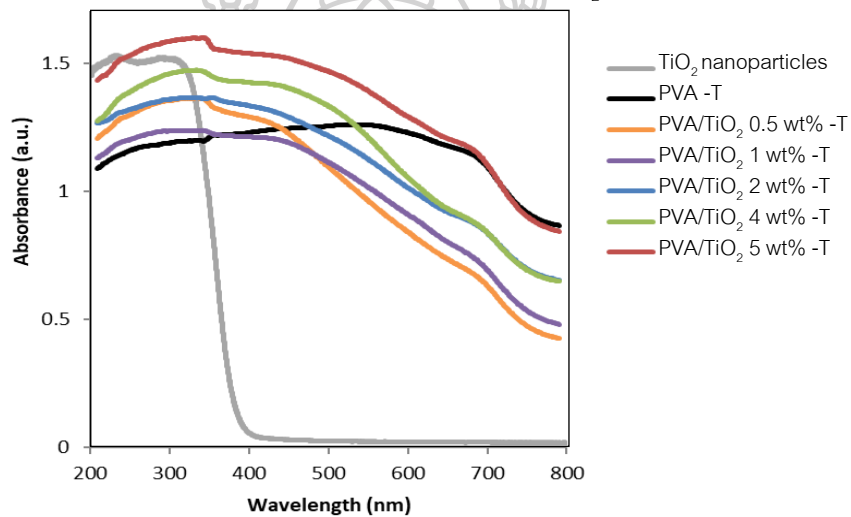


Figure 89 UV-visible absorption spectra for PVA film and PVA/TiO<sub>2</sub> nanocomposite films after thermal treatment.

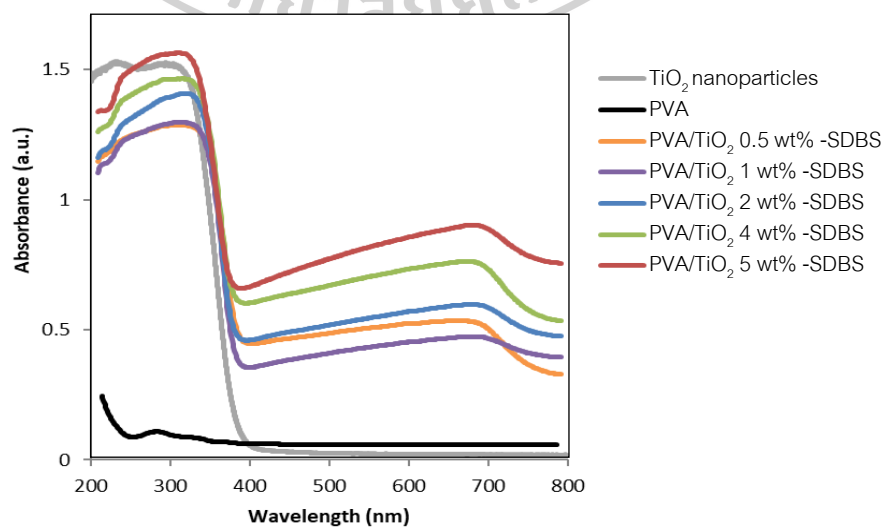


Figure 90 UV-visible absorption spectra for PVA film and PVA/TiO<sub>2</sub>-SDBS nanocomposite films.

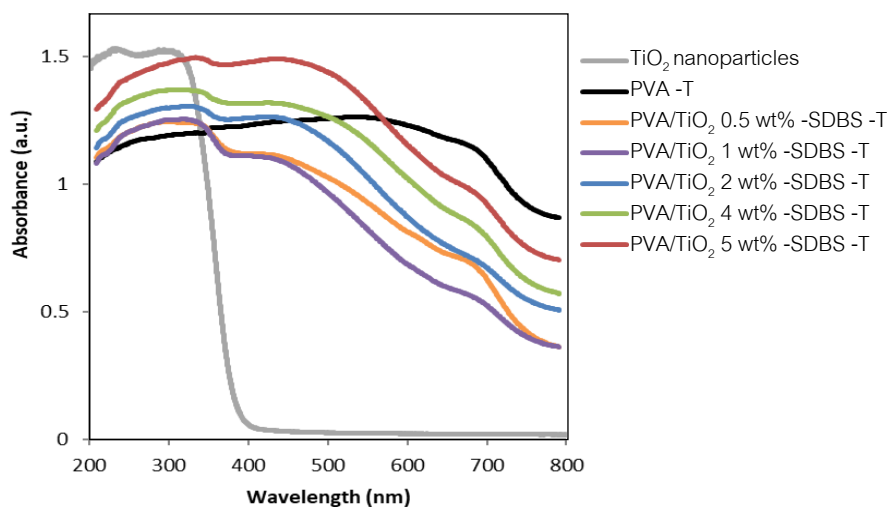


Figure 91 UV-visible absorption spectra for PVA film and PVA/TiO<sub>2</sub>-SDBS nanocomposite films after thermal treatment.

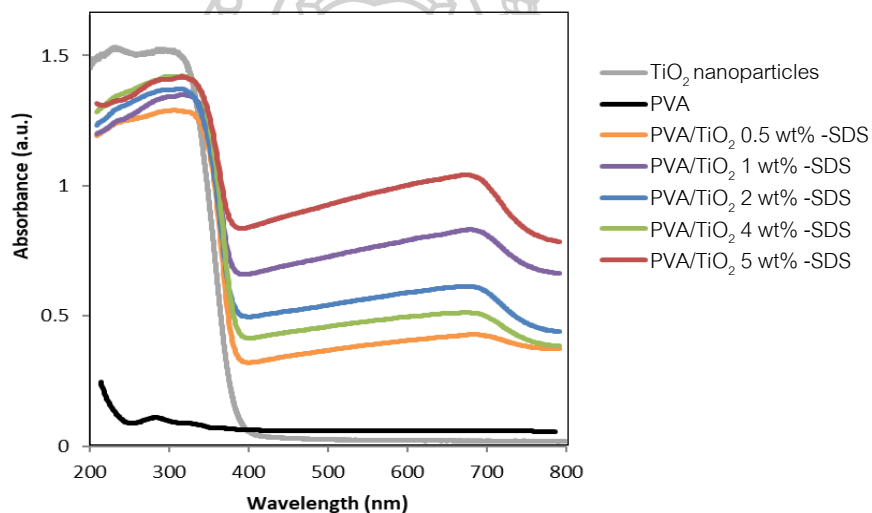


Figure 92 UV-visible absorption spectra for PVA film and PVA/TiO<sub>2</sub>-SDS nanocomposite films.

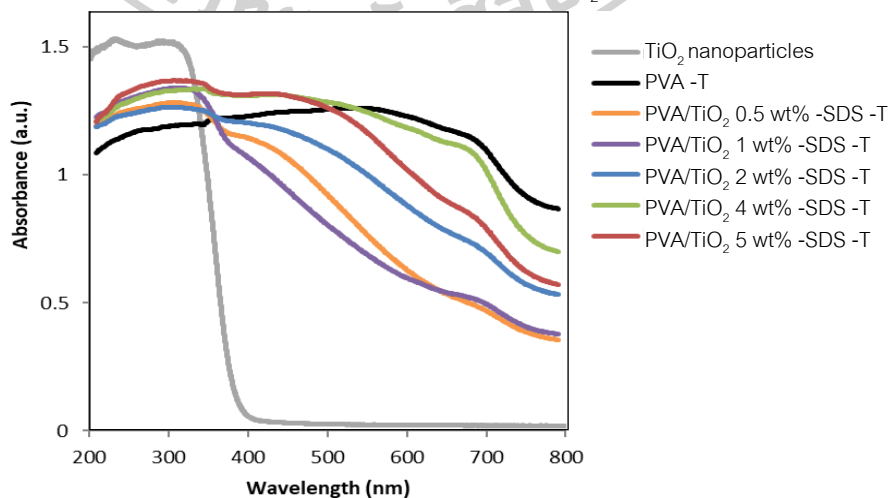


Figure 93 UV-visible absorption spectra for PVA film and PVA/TiO<sub>2</sub>-SDS nanocomposite films after thermal treatment.



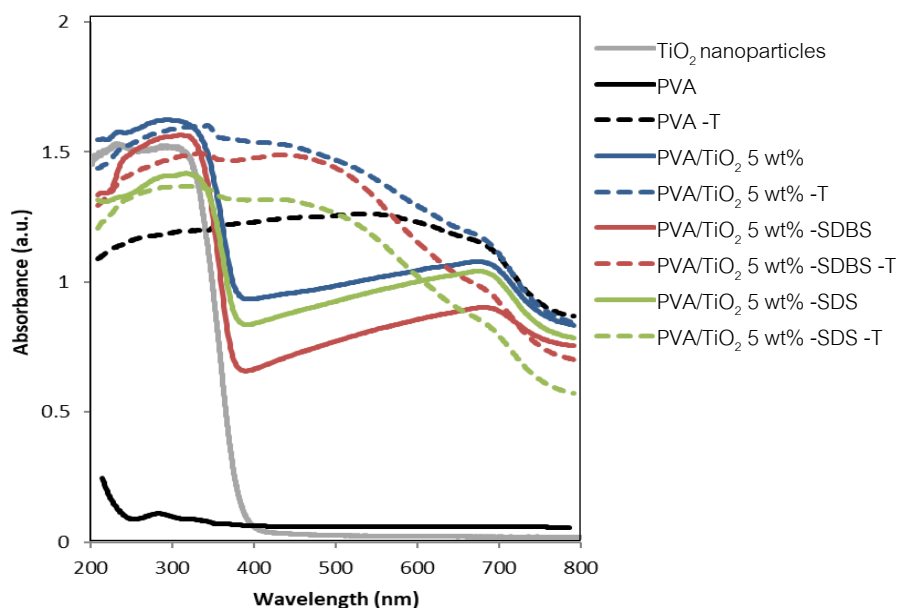


Figure 94 UV-visible absorption spectra for PVA film and PVA/TiO<sub>2</sub> nanocomposite films at 5 wt% of TiO<sub>2</sub> without and with surfactants, before and after thermal treatment.

### 5.3.8 Photocatalytic activity

Figure 95 and 96 show MB removal efficiency of the TiO<sub>2</sub> nanoparticles, PVA film and PVA/TiO<sub>2</sub> nanocomposite films without and with surfactant, before and after thermal treatment. The immobilization of TiO<sub>2</sub> in the PVA matrix increased MB removal efficiency in comparison with TiO<sub>2</sub> nanoparticles, which MB removal efficiency of TiO<sub>2</sub> nanoparticles was a result of only photocatalysis whereas PVA/TiO<sub>2</sub> nanocomposite films was a result of adsorption. The PVA/TiO<sub>2</sub> nanocomposite films without and with surfactant, both before and after thermal treatment exhibited the similar MB removal efficiency as observed for the PVA/TiO<sub>2</sub> composite films. The comparison between MB removal of PVA/TiO<sub>2</sub>-SDBS and PVA/TiO<sub>2</sub>-SDS nanocomposite films at 5 wt% of TiO<sub>2</sub> before and after thermal treatment is shown in Figure 97. The surfactant addition improved MB removal both before and after thermal treatment due to the characteristics of anionic surfactant. PVA/TiO<sub>2</sub>-SDBS showed a higher MB removal than PVA/TiO<sub>2</sub>-SDS both before and after thermal treatment.

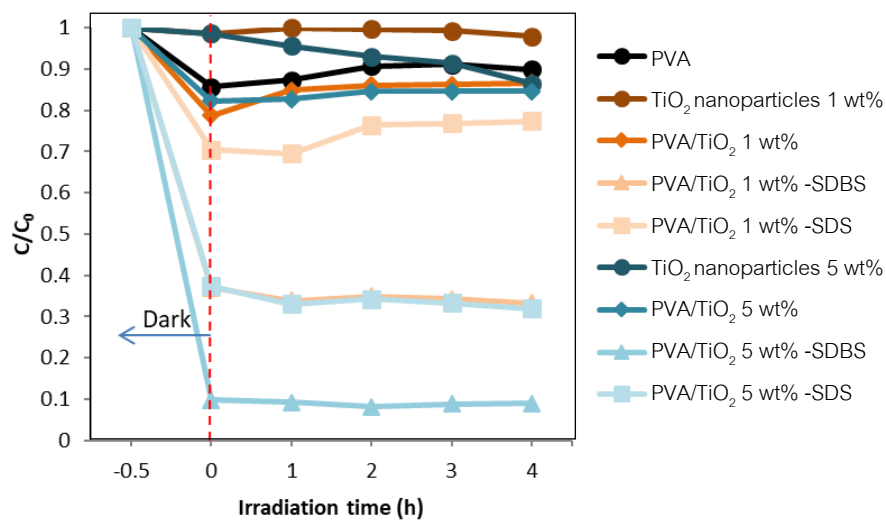


Figure 95 Extent of MB removal of PVA film, PVATiO<sub>2</sub>, PVATiO<sub>2</sub>-SDBS and PVA/TiO<sub>2</sub>-SDS nanocomposite films.

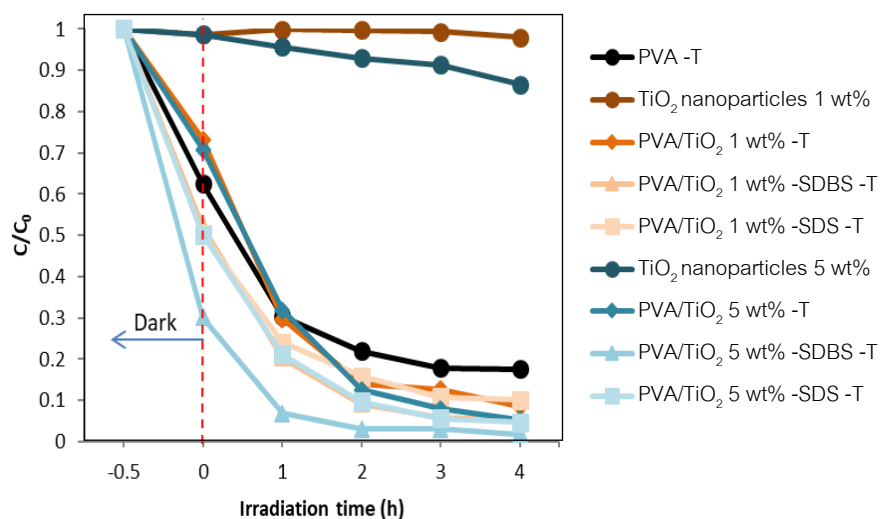


Figure 96 Extent of MB removal of PVA film, PVATiO<sub>2</sub>, PVATiO<sub>2</sub>-SDBS and PVA/TiO<sub>2</sub>-SDS nanocomposite films after thermal treatment.

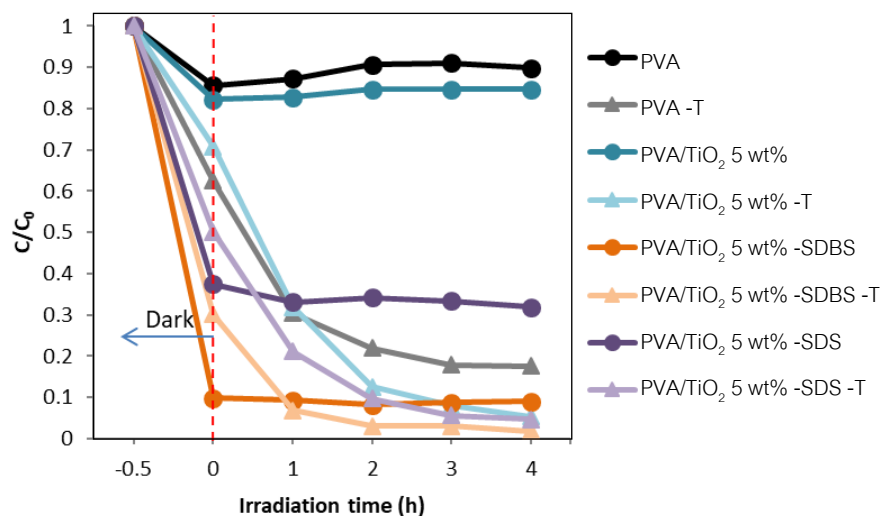


Figure 97 Extent of MB removal of PVA film and PVA/TiO<sub>2</sub> nanocomposite films 5wt% of TiO<sub>2</sub> without and with surfactants, before and after thermal treatment.

### 5.3.9 Antimicrobial activity

The antimicrobial activity of PVA/TiO<sub>2</sub> and PVA/TiO<sub>2</sub>-SDBS nanocomposite films at 5 wt% of TiO<sub>2</sub> were tested against *E. coli* and *S. aureus* and presented with the percentage of bacterial reduction as shown in Table 16. After 24 h contact, *E. coli* and *S. aureus* were reduced, respectively, to 4.5% and 7% for PVA/TiO<sub>2</sub> nanocomposite film, and 18.3% and 15.1% for PVA/TiO<sub>2</sub>-SDBS nanocomposite film. The addition of SDBS has been shown to improve antimicrobial activity [71]. In our study, insignificant bacterial reduction of PVA/TiO<sub>2</sub>-SDBS nanocomposite film was observed, which was in agreement with its high photocatalytic activity. The assessment of antimicrobial activity was not performed under UV light. As a result, the antimicrobial ability could not be fully activated, leading to the poor antimicrobial activity of the film.

Table 16 The antibacterial activity of PVA/TiO<sub>2</sub> and PVA/TiO<sub>2</sub>-SDBS nanocomposite films at 5 wt% of TiO<sub>2</sub>.

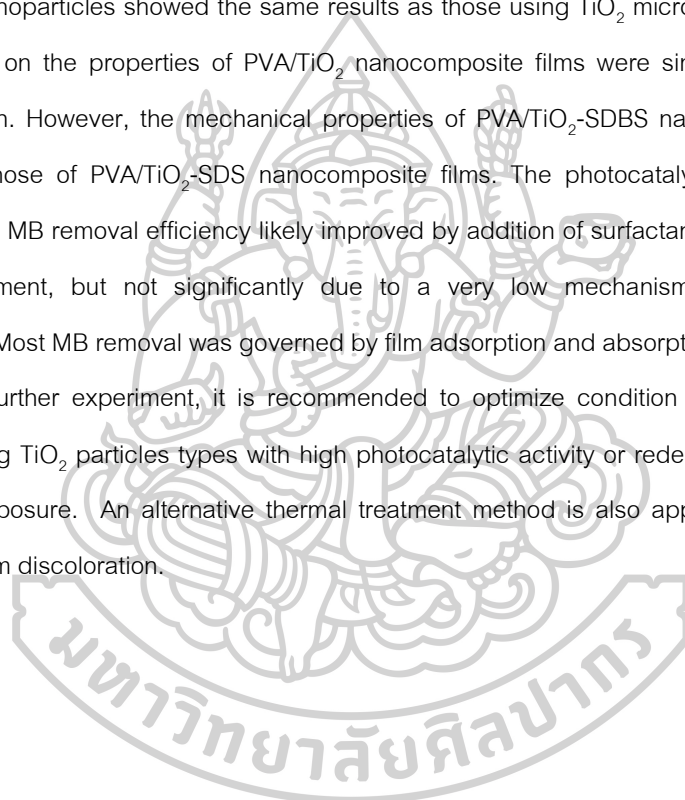
| Sample                     | <i>E. coli</i> |                                       | <i>S. aureus</i> |                                       |
|----------------------------|----------------|---------------------------------------|------------------|---------------------------------------|
|                            | Reduction (%)  | Log <sub>10</sub> Bacterial reduction | Reduction (%)    | Log <sub>10</sub> Bacterial reduction |
| PVA/TiO <sub>2</sub>       | 4.5            | 0                                     | 7                | 0                                     |
| PVA/TiO <sub>2</sub> -SDBS | 18.3           | 0.1                                   | 15.1             | 0.1                                   |

## CHAPTER 6

### CONCLUSIONS

The dispersion of  $\text{TiO}_2$  particles in  $\text{PVA/TiO}_2$  composite films presented agglomeration at high  $\text{TiO}_2$  content. However, the SDBS addition at  $\text{TiO}_2$ :SDBS (1:1) could improve the dispersion stability of  $\text{TiO}_2$  in the  $\text{PVA/TiO}_2$  composite films, hence improved the film properties. The addition of SDBS inhibited dehydration of PVA in thermal treatment, retarded thermal decomposition of the  $\text{PVA/TiO}_2$  composite films, but decreased mechanical properties. The  $\text{PVA/TiO}_2$  composite films using  $\text{TiO}_2$  nanoparticles showed the same results as those using  $\text{TiO}_2$  microparticles. The effects of SDS addition on the properties of  $\text{PVA/TiO}_2$  nanocomposite films were similar to those films with SDBS addition. However, the mechanical properties of  $\text{PVA/TiO}_2$ -SDBS nanocomposite films were better than those of  $\text{PVA/TiO}_2$ -SDS nanocomposite films. The photocatalytic activity of the films detected from MB removal efficiency likely improved by addition of surfactant, especially SDBS, and thermal treatment, but not significantly due to a very low mechanism of photocatalytic MB degradation. Most MB removal was governed by film adsorption and absorption mechanisms.

For further experiment, it is recommended to optimize condition for MB removal testing either by using  $\text{TiO}_2$  particles types with high photocatalytic activity or redesigning UV reactor for a better film exposure. An alternative thermal treatment method is also appreciated for preventing aggressive film discoloration.



## REFERENCES

- [1] U. G. Akpan and B. H. Hameed, "Parameters affecting the photocatalytic degradation of dyes using TiO<sub>2</sub>-based photocatalysts: A review," *Journal of Hazardous Materials*, vol. 170, no. 2, pp. 520-529, 2009/10/30/ 2009, doi: <https://doi.org/10.1016/j.jhazmat.2009.05.039>.
- [2] S. Singh, H. Mahalingam, and P. K. Singh, "Polymer-supported titanium dioxide photocatalysts for environmental remediation: A review," *Applied Catalysis A: General*, vol. 462-463, pp. 178-195, 2013/07/10/ 2013, doi: <https://doi.org/10.1016/j.apcata.2013.04.039>.
- [3] X. Zhao, L. Lv, B. Pan, W. Zhang, S. Zhang, and Q. Zhang, "Polymer-supported nanocomposites for environmental application: A review," *Chemical Engineering Journal*, vol. 170, no. 2, pp. 381-394, 2011/06/01/ 2011, doi: <https://doi.org/10.1016/j.cej.2011.02.071>.
- [4] P. Lei, F. Wang, X. Gao, Y. Ding, S. Zhang, J. Zhao, S. Liu, and M. Yang, "Immobilization of TiO<sub>2</sub> nanoparticles in polymeric substrates by chemical bonding for multi-cycle photodegradation of organic pollutants," *Journal of Hazardous Materials*, vol. 227-228, pp. 185-194, 2012/08/15/ 2012, doi: <https://doi.org/10.1016/j.jhazmat.2012.05.029>.
- [5] W. Yan, Q. Chen, X. Meng, and B. Wang, "Multicycle photocatalytic reduction of Cr(VI) over transparent PVA/TiO<sub>2</sub> nanocomposite films under visible light," *Science China Materials*, vol. 60, no. 5, pp. 449-460, 2017/05/01 2017, doi: 10.1007/s40843-017-9024-9.
- [6] H. D. Jang, S.-K. Kim, and S.-J. Kim, "Effect of particle size and phase composition of titanium dioxide nanoparticles on the photocatalytic properties," *Journal of Nanoparticle Research*, vol. 3, no. 2, pp. 141-147, 2001/06/01 2001, doi: 10.1023/A:1017948330363.
- [7] Y. Geng, M. Y. Liu, J. Li, X. M. Shi, and J. K. Kim, "Effects of surfactant treatment on mechanical and electrical properties of CNT/epoxy nanocomposites," *Composites Part A: Applied Science and Manufacturing*, vol. 39, no. 12, pp. 1876-1883, 2008/12/01/ 2008, doi: <https://doi.org/10.1016/j.compositesa.2008.09.009>.
- [8] K. Satoh, S. Kobayashi and K. Müllen Eds, "Poly(vinyl alcohol) (PVA)," in *Encyclopedia of Polymeric Nanomaterials*,: Springer Berlin Heidelberg, 2014, pp. 1-6.
- [9] M. I. Baker, S. P. Walsh, Z. Schwartz, and B. D. Boyan, "A review of polyvinyl alcohol and its uses in cartilage and orthopedic applications," *Journal of Biomedical Materials Research Part B: Applied Biomaterials*, vol. 100B, no. 5, pp. 1451-1457, 2012, doi: 10.1002/jbm.b.32694.
- [10] C. C. DeMerlis and D. R. Schoneker, "Review of the oral toxicity of polyvinyl alcohol (PVA)," *Food and Chemical Toxicology*, vol. 41, no. 3, pp. 319-326, 2003/03/01/ 2003, doi: [https://doi.org/10.1016/S0278-6915\(02\)00258-2](https://doi.org/10.1016/S0278-6915(02)00258-2).

- [11] S. T. Gaaz, B. A. Sulong, N. M. Akhtar, A. A. Kadhum, B. A. Mohamad, and A. A. Al-Amiery, "Properties and applications of polyvinyl alcohol, halloysite nanotubes and their nanocomposites," *Molecules*, vol. 20, no. 12, 2015, doi: 10.3390/molecules201219884.
- [12] X. Chen and S. S. Mao, "Titanium dioxide nanomaterials: synthesis, properties, modifications, and applications," *Chemical reviews*, vol. 107, no. 7, pp. 2891-2959, 2007.
- [13] S. M. Gupta and M. Tripathi, "A review of TiO<sub>2</sub> nanoparticles," *Chinese Science Bulletin*, vol. 56, no. 16, p. 1639, 2011.
- [14] M. Pelaez, N. T. Nolan, S. C. Pillai, M. K. Seery, P. Falaras, A. G. Kontos, P. S. Dunlop, and W. J. Jeremy Byrne, "A review on the visible light active titanium dioxide photocatalysts for environmental applications," *Applied Catalysis B: Environmental*, vol. 125, pp. 331-349, 2012.
- [15] Q. Guo, C. Zhou, Z. Ma, Z. Ren, H. Fan, and X. Yang, "Fundamental processes in surface photocatalysis on TiO<sub>2</sub>," in *Heterogeneous Photocatalysis*: Springer, 2016, pp. 361-416.
- [16] A. Wold, "Photocatalytic properties of titanium dioxide (TiO<sub>2</sub>)," *Chemistry of Materials*, vol. 5, no. 3, pp. 280-283, 1993.
- [17] D. Myers, *Surfactant science and technology*. John Wiley & Sons, 2005.
- [18] S. J. Woltornist, "Pristine graphene as a two-dimensional surfactant," 2016.
- [19] G. W. Ware, L. A. Albert, D. G. Crosby, P. Voogt, O. Hutzinger, J. B. Knaak, F. L. Mayer, D. P. Morgan, D. L. Park, and R. S. Tjeerdema, *Reviews of environmental contamination and toxicology*. Springer, 2006.
- [20] W. AA, "Current trends and future application of sodium dodecyl sulphate in biotechnology and surfactant chemistry," *Research and Reviews*, vol. 1, no. 1, 2012.
- [21] D. K. Tripathy and B. P. Sahoo, *Properties and Applications of Polymer Nanocomposites: Clay and Carbon Based Polymer Nanocomposites*. Springer, 2017.
- [22] D. R. Paul and L. M. Robeson, "Polymer nanotechnology: nanocomposites," *Polymer*, vol. 49, no. 15, pp. 3187-3204, 2008.
- [23] S. Roy and N. R. Singha, "Polymeric nanocomposite membranes for next generation pervaporation process: strategies, challenges and future prospects," *Membranes*, vol. 7, no. 3, p. 53, 2017.
- [24] U. Siemann, "Solvent cast technology—a versatile tool for thin film production," in *Scattering Methods and the Properties of Polymer Materials*: Springer, 2005, pp. 1-14.
- [25] J. R. Davis, *Tensile testing*. ASM international, 2004.
- [26] G. W. H. Höhne, W. Hemminger, and H. J. Flammersheim, "Differential Scanning Calorimetry," Springer, 1996.
- [27] C. Schick, "Differential scanning calorimetry (DSC) of semicrystalline polymers," *Analytical and*



- bioanalytical chemistry*, vol. 395, no. 6, p. 1589, 2009.
- [28] J. D. Menczel and R. B. Prime, *Thermal analysis of polymers: fundamentals and applications*. John Wiley & Sons, 2014.
- [29] P. Gabbott, *Principles and applications of thermal analysis*. John Wiley & Sons, 2008.
- [30] O. C. Microbiology, "Microbiology," *OpenStax-CNX* <https://legacy.cnx.org/content/col12087/1.4/>, 2016.
- [31] L. Reimer, *Scanning electron microscopy: physics of image formation and microanalysis*. Springer, 2013.
- [32] Q. Guo, *Polymer morphology: principles, characterization, and processing*. John Wiley & Sons, 2016.
- [33] T. Owen, *Fundamentals of UV-visible spectroscopy: a primer*. Hewlett-Packard, 1996.
- [34] R. E. Dinnebier and S. J. L. Billinge, *Powder diffraction: theory and practice*. Royal Society of Chemistry, 2008.
- [35] B. C. Smith, *Fundamentals of Fourier transform infrared spectroscopy*. CRC press, 2011.
- [36] J. C. C. Quintero and Y. J. Xu, "Heterogeneous photocatalysis: from fundamentals to green applications," ed: Springer Google Scholar, 2015.
- [37] M. Umar and H. A. Aziz, "Photocatalytic degradation of organic pollutants in water," in *Organic Pollutants-Monitoring, Risk and Treatment*. InTech, 2013.
- [38] N. Beyth, Y. Hour-Haddad, A. Domb, W. Khan, and R. Hazan, "Alternative antimicrobial approach: nano-antimicrobial materials," (in eng), *Evid Based Complement Alternat Med*, vol. 2015, pp. 246012-246012, 2015, doi: 10.1155/2015/246012.
- [39] G. Li, L. Chen, M. Graham, and K. Gray, "A comparison of mixed phase titania photocatalysts prepared by physical and chemical methods: The importance of the solid–solid interface," *Journal of Molecular Catalysis A: Chemical*, vol. 275, pp. 30-35, 09/01 2007, doi: 10.1016/j.molcata.2007.05.017.
- [40] N. Xu, Z. Shi, Y. Fan, J. Dong, J. Shi, and M. Z. C. Hu, "Effects of particle size of TiO<sub>2</sub> on photocatalytic degradation of methylene blue in aqueous suspensions," *Industrial & Engineering Chemistry Research*, vol. 38, no. 2, pp. 373-379, 1999/02/01 1999, doi: 10.1021/ie980378u.
- [41] A. Han and R. Bai, "Buoyant photocatalyst with greatly enhanced visible-light activity prepared through a low temperature hydrothermal method," *Ind. Eng. Chem. Res.*, vol. 48, 03/18 2009, doi: 10.1021/ie801362a.
- [42] S. Surah, S. Sirohi, R. Nain, and G. Kumar, *Antimicrobial activity of TiO<sub>2</sub> nanostructures synthesized by hydrothermal method*. 2018, p. 030038.



- [43] A. M. Shehap and D. S. Akil, "Structural and optical properties of TiO<sub>2</sub> nanoparticles/PVA for different composites thin films," *International Journal of Nanoelectronics & Materials*, vol. 9, no. 1, 2016.
- [44] S. Cho and W. Choi, "Solid-phase photocatalytic degradation of PVC–TiO<sub>2</sub> polymer composites," *Journal of Photochemistry and Photobiology A: Chemistry*, vol. 143, pp. 221-228, 10/01 2001, doi: 10.1016/S1010-6030(01)00499-3.
- [45] F. Wang and S. X. Min, "TiO<sub>2</sub>/polyaniline composites: an efficient photocatalyst for the degradation of methylene blue under natural light," *Chinese Chemical Letters*, vol. 18, no. 10, pp. 1273-1277, 2007.
- [46] S. Ameen, M. S. Akhtar, Y. S. Kim, and H. S. Shin, "Nanocomposites of poly (1-naphthylamine)/SiO<sub>2</sub> and poly (1-naphthylamine)/TiO<sub>2</sub>: comparative photocatalytic activity evaluation towards methylene blue dye," *Applied Catalysis B: Environmental*, vol. 103, no. 1-2, pp. 136-142, 2011.
- [47] N. Sridewi, L. T. Tan, and K. Sudesh, "Solar photocatalytic decolorization and detoxification of industrial batik dye wastewater using P(3HB)-TiO<sub>2</sub> nanocomposite films," *Clean–Soil, Air, Water*, vol. 39, no. 3, pp. 265-273, 2011.
- [48] J. A. Byrne, B. R. Eggins, N. M. D. Brown, B. McKinney, and M. Rouse, "Immobilisation of TiO<sub>2</sub> powder for the treatment of polluted water," *Applied Catalysis B: Environmental*, vol. 17, no. 1, pp. 25-36, 1998/06/30/ 1998, doi: [https://doi.org/10.1016/S0926-3373\(97\)00101-X](https://doi.org/10.1016/S0926-3373(97)00101-X).
- [49] J. Krýsa, G. Waldner, H. Měšťánková, J. Jirkovský, and G. Grabner, "Photocatalytic degradation of model organic pollutants on an immobilized particulate TiO<sub>2</sub> layer," *Applied Catalysis B: Environmental*, vol. 64, pp. 290-301, 05/02 2006, doi: 10.1016/j.apcatb.2005.11.007.
- [50] A. M. Shehap and D. S. Akil, "Structural and optical properties of TiO<sub>2</sub> nanoparticles/PVA for different composites thin films," *International Journal of Nanoelectronics & Materials*, vol. 9, no. 1, 2016.
- [51] E. Filippo, C. Carlucci, A. L. Capodilupo, P. Perulli, F. Conciauro, G. A. Corrente, G. Gigli, and G. Ciccarella, "Facile preparation of TiO<sub>2</sub>-polyvinyl alcohol hybrid nanoparticles with improved visible light photocatalytic activity," *Applied Surface Science*, vol. 331, pp. 292-298, 2015.
- [52] X. Liu, Q. Chen, L. Lv, X. Feng, and X. Meng, "Preparation of transparent PVA/TiO<sub>2</sub> nanocomposite films with enhanced visible-light photocatalytic activity," *Catalysis Communications*, vol. 58, pp. 30-33, 2015.
- [53] P. Hegedűs, E. Szabó-Bárdos, O. Horváth, P. Szabó, and K. Horváth, "Investigation of a TiO<sub>2</sub>

- photocatalyst immobilized with poly (vinyl alcohol)," *Catalysis Today*, vol. 284, pp. 179-186, 2017.
- [54] Y. Wang, M. Zhong, F. Chen, and J. Yang, "Visible light photocatalytic activity of TiO<sub>2</sub>/D-PVA for MO degradation," *Applied Catalysis B: Environmental*, vol. 90, no. 1-2, pp. 249-254, 2009.
- [55] T. F. Moghadam and S. Azizian, "Effect of ZnO nanoparticles on the interfacial behavior of anionic surfactant at liquid/liquid interfaces," *Colloids and Surfaces A: Physicochemical and Engineering Aspects*, vol. 457, pp. 333-339, 2014.
- [56] R. Chadha, R. Sharma, N. Maiti, A. Ballal, and S. Kapoor, "Effect of SDS concentration on colloidal suspensions of Ag and Au nanoparticles," *Spectrochimica Acta Part A: Molecular and Biomolecular Spectroscopy*, vol. 150, pp. 664-670, 2015.
- [57] Y. Song, H. Lee, J. Ko, J. Ryu, M. Kim, and D. Sohn, "Preparation and characterization of surfactant-exfoliated graphene," (in En), *Bulletin of the Korean Chemical Society*, vol. 35, pp. 2009-2012, 07/20 2014, doi: 10.5012/BKCS.2014.35.7.2009.
- [58] L. D. L. Miranda, C. R. Bellato, J. L. Milagres, L. G. Moura, A. H. Munteer, and M. F. de Almeida, "Hydrotalcite-TiO<sub>2</sub> magnetic iron oxide intercalated with the anionic surfactant dodecylsulfate in the photocatalytic degradation of methylene blue dye," *Journal of Environmental Management*, vol. 156, pp. 225-235, 2015/06/01/ 2015, doi: <https://doi.org/10.1016/j.jenvman.2015.03.051>.
- [59] P. Zhang, I. Lo, D. O'Connor, S. Pehkonen, H. Cheng, and D. Hou, "High efficiency removal of methylene blue using SDS surface-modified ZnFe<sub>2</sub>O<sub>4</sub> nanoparticles," *Journal of Colloid and Interface Science*, vol. 508, pp. 39-48, 2017/12/15/ 2017, doi: <https://doi.org/10.1016/j.jcis.2017.08.025>.
- [60] M. S. Enayati, T. Behzad, P. Sajkiewicz, R. Bagheri, L. Ghasemi-Mobarakeh, W. Lojkowski, Z. Pahlevanneshan, M. Ahmadi, "Crystallinity study of electrospun poly (vinyl alcohol) nanofibers: effect of electrospinning, filler incorporation, and heat treatment," *Iranian Polymer Journal*, vol. 25, no. 7, pp. 647-659, 2016/07/01 2016, doi: 10.1007/s13726-016-0455-3.
- [61] D. Yu, L. M. Zhu, C. Branford-White, J. Yang, X. Wang, Y. li, and W. Qian, "Solid dispersions in the form of electrospun core-sheath nanofibers," *International journal of nanomedicine*, vol. 6, pp. 3271-80, 12/13 2011, doi: 10.2147/IJN.S27468.
- [62] A. T. Tyowua, S. Yiase, and R. Wuana, "Manipulation of concentration-conductivity data of sodium dodecyl sulphate and sodium dodecylbenzene sulfonate in KCl solution in relation to micellization parameters," *Chem. Sci. J.*, vol. 79, pp. 1-9, 01/01 2012.
- [63] T. Akahane, M. Ueda, S. Tsuchiya, and H. Nakayasu, "Discoloration of poly (vinyl alcohol) and ethylene-vinyl alcohol copolymers by heat treatment," *kobunshi ronbunshu*, vol. 37, no. 8, pp.

- 521-525, 1980, doi: 10.1295/koron.37.521.
- [64] S. Mallakpour and A. Barati, "Efficient preparation of hybrid nanocomposite coatings based on poly(vinyl alcohol) and silane coupling agent modified TiO<sub>2</sub> nanoparticles," *Progress in Organic Coatings*, vol. 71, no. 4, pp. 391-398, 2011/08/01/ 2011, doi: <https://doi.org/10.1016/j.porgcoat.2011.04.010>.
- [65] V. Stengl, V. Houšková, N. Murafa, and S. Bakardjieva, "Synthesis of mesoporous titania by homogeneous hydrolysis of titania oxo-sulfate in the presence of cationic and anionic," vol. 54, pp. 368-378, 01/01 2010.
- [66] K. Wong, M. Zinke-Allmang, and W. Wan, "Effect of annealing on aqueous stability and elastic modulus of electrospun poly(vinyl alcohol) fibers," *Journal of Materials Science*, vol. 45, pp. 2456-2465, 05/01 2010, doi: 10.1007/s10853-010-4217-1.
- [67] J. Ahmad, K. Deshmukh, M. Habib, and M.-B. Hägg, "Influence of TiO<sub>2</sub> nanoparticles on the morphological, thermal and solution properties of PVA/TiO<sub>2</sub> nanocomposite membranes," *Arabian Journal for Science and Engineering*, vol. 39, 10/01 2014, doi: 10.1007/s13369-014-1287-0.
- [68] Y. Song, J. Zhang, H. Yang, S. Xu, L. Jiang, and Y. Dan, "Preparation and visible light-induced photo-catalytic activity of H-PVA/TiO<sub>2</sub> composite loaded on glass via sol-gel method," *Applied Surface Science*, vol. 292, 01/31 2014, doi: 10.1016/j.apsusc.2013.12.090.
- [69] L. V. Smirnov, N. V. Platonova, and K. R. Popov, "Color change of poly(vinyl alcohol) during heat treatment (dehydration and formation of polyene fractions)," *Journal of Applied Spectroscopy*, vol. 7, no. 1, pp. 71-74, 1967/07/01 1967, doi: 10.1007/BF00714709.
- [70] E. Fundador, G. Lagmay, A. de Cadiz, T. Iwata, and N. Fundador, "Photocatalytic and antibacterial studies on poly (hydroxybutyrate-co-hydroxyhexanoate)/titanium dioxide composites," *Banwa B*, vol. 12, 2017.
- [71] L. Dong, A. Henderson, and C. Field, "Antimicrobial activity of single-walled carbon nanotubes suspended in different surfactants," *Journal of Nanotechnology*, vol. 2012, 01/01 2012, doi: 10.1155/2012/928924.



## VITA

NAME Miss Sirinan Ratchawong

DATE OF BIRTH 11 Febuary 1993

PLACE OF BIRTH Suphan Buri, Thailand, 72180

HOME ADDRESS 245 M.4 T.Nong Makha Mong A.Dan Chang, Suphan Buri, Thailand,  
72180

